Spring 5-2013

Relationships Between Cure Kinetics, Network Architecture, and Fluid Sensitivity in Glassy Epoxies

Katherine Lea Frank
University of Southern Mississippi

The University of Southern Mississippi

RELATIONSHIPS BETWEEN CURE KINETICS, NETWORK ARCHITECTURE, AND FLUID SENSITIVITY IN GLASSY EPOXIES

by

Katherine Lea Frank

Abstract of a Dissertation
Submitted to the Graduate School
of The University of Southern Mississippi
in Partial Fulfillment of the Requirements
for the Degree of Doctor of Philosophy

May 2013

ABSTRACT

RELATIONSHIPS BETWEEN CURE KINETICS, NETWORK ARCHITECTURE, AND FLUID SENSITIVITY IN GLASSY EPOXIES

by Katherine Lea Frank

May 2013

Relationships between chemical structure, cure kinetics, network morphology and free volume have been correlated with fluid ingress for glassy epoxy network blends. Polymers synthesized from diglycidyl ether of bisphenol-A (DGEBA) and diglycidyl ether of bisphenol-F (DGEBF) were blended with varying amounts of triglycidyl-*m*-aminophenol (TGAP), tetraglycidyl-4,4-diaminodiphenylmethane (TGMP), napthylamine (NA), adamantylamine (AA), and aminopropylisobutyl polyhedral oliogmericsilsesquioxane (AI-POSS) and cured with 3,3'- and 4,4'-diaminodiphenylsulfone (DDS) to control fractional free volume, average hole size and morphology.

Varying curing profiles introduced morphological changes resulting in differences in network architectures. Epoxy with 10% NA had a smaller V_h (71 $Å^3$) than with 10% AA (74 $Å^3$); the decrease was due to pi-pi stacking and growth kinetics of the 10% NA network. Architecture was a key determinant of moisture and solvent ingress in blends and off-stoichiometry epoxies. Hole size decreased with increasing crosslink density, from 75 $Å^3$ (DGEBA-33DDS) to 48 $Å^3$ (m-TGAP-33DDS). Fractional free volume increased with increasing crosslink density. Equilibrium water uptake increased with FFV, from 2.9% to 7.3% (DGEBA-33DDS and m-TGAP, respectively). Solvent uptake

was almost completely inhibited in the epoxy blends when the V_h of the epoxies decreased below the size of the solvent molecule.

In networks formulated with excess epoxy, the importance of chain packing on solvent ingress was clarified. The excess-epoxy networks had lower crosslink densities than the on-stoichiometry benchmarks; however, they exhibited lower hole sizes. Equilibrium water uptake decreased from 2.9% to 2.0% and MEK uptake rate decreased from 3.3×10^{-3} to 2.1×10^{-3} weight percent h^{-1} between DGEBA-33DDS and $DGEBA_{XS}$-33DDS. The improved resistance to fluid was attributed to improved packing by the longer chain segments in the off-stoichiometry networks.

Dispersion of pendant POSS was improved by pre-reacting amine-functionalized POSS with an excess of epoxy. In later experiments, using an improved POSS pre-reaction product, two separate morphologies were identified for unmodified and pre-reacted POSS at loading levels of 0-2.5 weight percent. Unmodified POSS exhibited crystallites in a neat epoxy matrix, whereas pre-reacted POSS exhibited a weakly crystalline POSS-rich phase and an epoxy-rich phase. Fluid ingress in the epoxies was not affected by POSS loading.

The University of Southern Mississippi

RELATIONSHIPS BETWEEN CURE KINETICS, NETWORK ARCHITECTURE, AND FLUID SENSITIVITY IN GLASSY EPOXIES

by

Katherine Lea Frank

A Dissertation
Submitted to the Graduate School
of The University of Southern Mississippi
in Partial Fulfillment of the Requirements
for the Degree of Doctor of Philosophy

Approved:

Jeffrey Wiggins
Director

Sarah Morgan

Derek Patton

Sergei Nazarenko

James Rawlins

Susan A. Siltanen
Dean of the Graduate School

May 2013

DEDICATION

To Alma Frank for the brains

And Jerry Stine for the panache

ACKNOWLEDGMENTS

I would like to acknowledge my advisor, Dr. Jeffrey S. Wiggins, for his constant support and encouragement. Dr. Wiggins has provided me with countless opportunities over the last four years to grow and challenge myself as a scientist and team member. I would also like to acknowledge my committee members: Dr. Sarah Morgan, Dr. Sergei Nazarenko, Dr. Derek Patton, and Dr. James Rawlins. Thanks as well to Steve Christensen, Steve Ward, Rob Maskell, and Joe Lichtenhan for their insight and guidance on my research.

Contributions from several other researchers made this dissertation possible. I would like to acknowledge Dr. David Gidley (PALS), Sarah Exley (TEM), Christopher Childers (PVT), and Sukhendu Hait (POSS synthesis) for their invaluable assistance.

Finally I would like to thank all the members of the Wiggins Research Group, especially Matthew Jackson and Sam Tucker for teaching me to be a researcher and Chris Childers and Travis Thornell for supporting me so I could conduct my research.

TABLE OF CONTENTS

LIST OF TABLES

Table

LIST OF ILLUSTRATIONS

Figure

CHAPTER I

INTRODUCTION

Composite materials represent a new frontier in materials engineering. Composites can have lighter weights, higher stiffnesses, and improved strength-to-weight ratios than the metals traditionally used in high-performance applications. Therefore composites are an appealing candidate to replace metals in applications where engineering designs are limited by the constraints of traditional materials. The foremost example of this situation is the aerospace industry. Small improvements in strength-to-weight ratio can result in large gains in fuel economy and aircraft performance. Large improvements in strength-to-weight ratio can result in designs that that revolutionize the aerospace industry, as the Boeing 787 Dreamliner is currently demonstrating.

Aerospace Composites

Fiber-reinforced polymer composites have been used in a variety of aerospace applications since the 1960s.[1] Composites were first used for primary structure in the 1980s, in the form of carbon-fiber-reinforced epoxy.[2] Primary structure comprises the essential load-bearing components of an airframe. Therefore the polymer matrix for a structural composite must have high strength, high stiffness, and a high glass transition temperature (T_g) as well as a low coefficient of thermal expansion (CTE) and low cure shrinkage. Furthermore, these properties must be achieved at price and processability envelopes that are acceptable to the aerospace industry.[3] Amine-cured epoxies meet all these requirements and are therefore the dominant matrix material for structural composites.

In order to achieve the mechanical and thermal properties necessitated by aerospace applications, the epoxies and amine curatives used for these materials are generally highly aromatic, low-molecular-weight monomers that produce densely-crosslinked glassy polymer networks. The inherent drawback of these networks is their brittleness. To alleviate this problem, rubber or thermoplastic toughening are commonly added to the epoxy.[3] These additives complicate material processing and evaluation. Therefore it is desirable to design epoxies that are inherently tougher without sacrificing stiffness or T_g.

High-Distortion Resins

One approach to improving inherent toughness involves distortional capabilities. When a force is applied to a polymer, the polymer can deform via dilation or distortion. Dilational deformation, which results in volume expansion, is the dominant failure mode for glassy epoxies. Dilation occurs when the applied force overcomes the cohesive interatomic forces in the polymer, resulting in cavitation.[4] Cavitations can coalesce and ultimately precipitate catastrophic brittle failure.[5] Distortional deformation, on the other hand, does not result in a volume change. Instead, the applied energy is dissipated by volume-conserving torsional motions on the molecular-level.[6] In this case, no covalent bonds are broken. Intermolecular forces may be disrupted during the deformation event, but they can be re-established in recovery. Polymer chain segments between crosslinks are thought to be responsible for distortional response, with the greatest capability for distortion exhibited by materials whose chain segments can access a broad range of molecular motions and relaxations. Theoretically, the toughness of glassy epoxies could be improved by designing materials with increased distortional capabilities.

Researchers at the Boeing Company, the Commonwealth Scientific and Industrial Organisation (CSIRO), and other institutions have successfully designed, synthesized, and tested several potential high-distortion resins. However, these resins were extremely susceptible to solvent ingress. The fluid sensitivity of standard epoxies was already a known issue; susceptibility to moisture and organic solvents limits the use and performance of standard epoxies.[7,8,9] One promising high-distortion material based on the diglycidyl ether of bisphenol-M (DGEBM) nearly disintegrated after 24 hours of exposure to methyl ethyl ketone (MEK), while the benchmark resin was unchanged (Figure 1).[10]

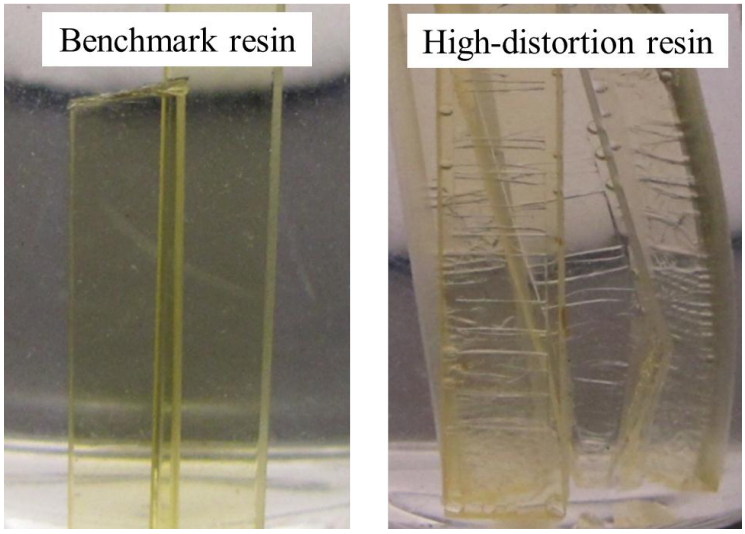

Figure 1. Epoxies after 24 h in MEK. Reproduced from reference with permission.[10]

Attempts to understand the increased fluid sensitivity of the high-distortion epoxy were stymied by the paucity of research correlating fluid uptake to fundamental structure-property relationships in amine-cured epoxies. The three-dimensional architecture of the glassy network is determined by a variety of factors including epoxide equivalent weight (EEW), amine reactivity ratio, monomer functionality, and cure temperature. Changes in any of these variables result in appreciable differences in the epoxy network architecture.

Fluid resistance and performance confidence could be improved if the relationships between network chemistry, network architecture, and solvent susceptibility were fully resolved.

Epoxy Network Architecture

Architecture is defined by Mirriam-Webster as "a unifying or coherent form or structure."[11] In thermoset matrix science, the term "architecture" is used to describe the three-dimensional way in which a polymer network is arranged in space. Changes in network architecture are manifested by changes in mechanical properties, T_g, free volume characteristics, and fluid sensitivity. Monomers with different chemical structures and functionalities give rise to networks with different architectures and therefore different properties. The kinetics of network formation change based on these variables, which further influences network architecture.

The epoxy network develops through crosslinking reactions between epoxides and amine hydrogens. In the first phase of the reaction, the primary amine ring-opens the epoxide via nucleophilic attack on the oxirane ring (Figure 2a). This reaction generates a hydroxypropylether linkage and a secondary amine. In the second phase of the reaction, the secondary amine reacts with another oxirane to complete the crosslink, forming a tertiary amine (Figure 2b). Under certain conditions (such as high temperatures or an excess of epoxide), the hydroxyl groups produced by the epoxy-amine reaction can also ring-open an oxirane ring, resulting in an ether-based crosslink (Figure 2c).[12,13] This reaction is known as etherification.

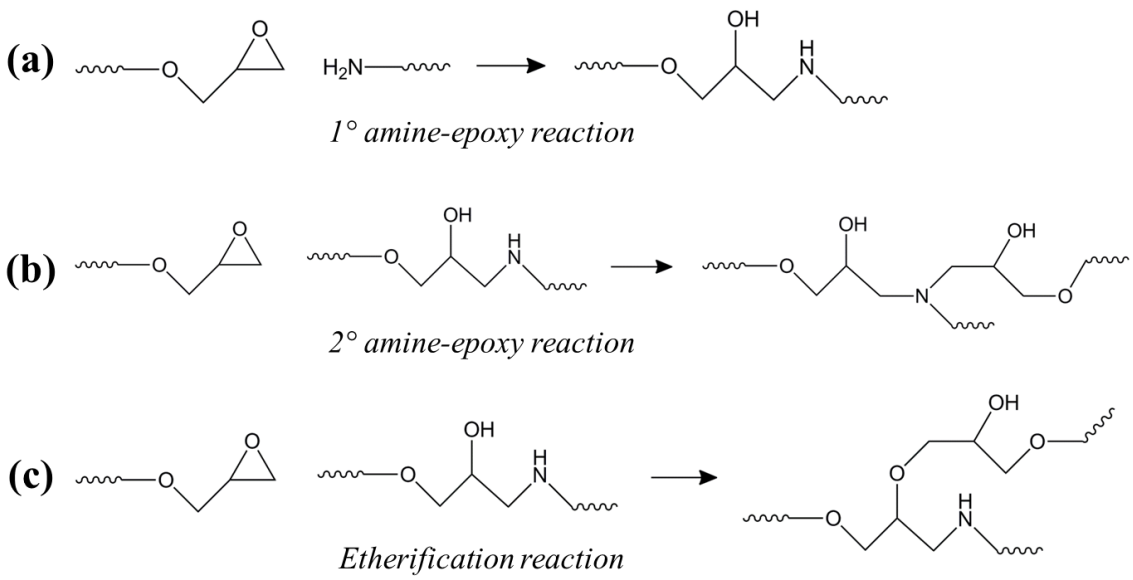

Figure 2. Possible amine-epoxy and etherification reactions: (a) epoxy-1° amine reaction, (b) epoxy-2° amine reaction, and (c) etherification.

As these curing reactions proceed, the physical state of the system progresses from a liquid to a gel to a glassy solid. The monomers in the liquid state react until the molecular weight of the growing network becomes infinite; this is defined as the gelation point.[14] The amines and epoxides continue to react until the T_g of the network exceeds the temperature of the environment (the cure temperature). This phenomenon is known as vitrification. After vitrification, chain motions are severely hindered. Unreacted epoxides and amines may remain in the system, but they are too constrained to collide and continue reacting. The network architecture is effectively "frozen" in the configuration it had at the onset of vitrification. Some vitreous-state curing occurs after vitrification, but its impact on architecture is minimal.

The free volume characteristics of the epoxy are determined by network architecture. Free volume exists in polymers in the form of holes that are distributed throughout the material.[15] Free volume is described in terms of the average size of those

holes (V_h) as well as their relative fraction of the polymer's volume (fractional free volume, FFV). V_h is measured by positron annihilation lifetime spectroscopy (PALS). FFV is measured directly by pressure-volume-temperature (PVT) dilatometry or indirectly using PALS data. Free volume is the dominant factor governing fluid uptake in glassy epoxies.[16] It is necessary to fully understand the relationships between network architecture, free volume, and fluid ingress in order to improve the fluid resistance of high-distortion epoxy systems.

Epoxy networks structures are difficult to characterize directly because these materials are, by definition, insoluble. Traditional polymer characterization techniques such as solution nuclear magnetic resonance (NMR) and size exclusion chromatography (SEC) are not feasible. Hence, network architecture is investigated by characterizing the cure process of the final cured material. When characterizing the cure process, techniques such as infrared (IR) spectroscopy, dynamic scanning calorimetry (DSC), and broadband dielectric resonance spectroscopy (DRS) show how the network is developing. The architecture of the cured network is inferred from the information about its development. When characterizing the final cured material, insights into network architecture are gleaned from dynamical mechanical analysis (DMA) or free volume data. Both approaches require that inferences be made between final properties or cure kinetics, which are objectively measured, and the network architecture, which cannot be directly observed. The ultimate network architecture is a function of the chemical structure and average functionality of the starting materials, as well as the kinetics of their cure reactions.

Effect of Chemical Structure

At first glance, the differences in chemical structure between many common aerospace epoxides and amines may seem minimal. However, subtle variations in structure are responsible for significant variations in material properties. For example, the diglycidyl ethers of bisphenol-A (DGEBA) and bisphenol-F (DGEBF) are near-identical diepoxide resins (Figure 3). DGEBA has an isopropyl moiety at the center of the molecule, while DGEBF has a methylene group in that position. That methylene group disrupts chain packing and hinders chain rotation.[17,18] Networks based on DGEBA has higher stiffness and T_g than networks based on DGEBF, due to the constraints on chain motion. However, the decreased packing efficiency of the DGEBA segments results in a higher V_h and FFV for those networks. [16,19]

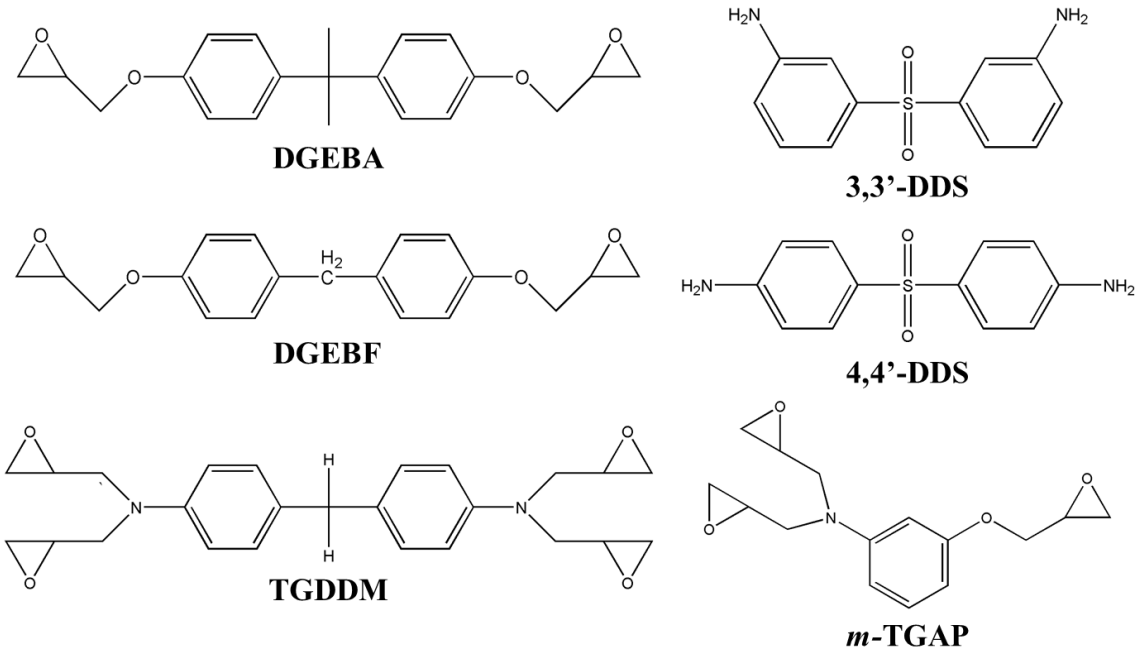

Figure 3. Chemical structures of common aerospace epoxies and amines.

Structural isomerism also has an impact on network architecture. Two isomers of an aromatic diamine, diaminodiphenylsulfone (DDS), are often used in high-performance

applications (Figure 3). The meta-substituted isomer, 3,'3-DDS, has more conformational mobility than the para-substitued isomer, 4,4'-DDS. As a result, epoxies cured with 3,3'-DDS exhibit lower stiffness, T_g's, V_h's, and FFV's than epoxies cured with 4,4'-DDS.[20,21]

Effect of Functionality

The average functionality of an epoxide resin is an important determinant of the properties of the cured material. DGEBA and DGEBF are difunctional, whereas triglycidyl-*m*-aminophenol (*m*-TGAP) is tri-functional and tetraglycidyl-4,4'-diaminodiphenylmethane (TGDDM) is tetrafunctional (Figure 3). The higher functionality of *m*-TGAP- or TGDDM-based systems affects network architecture by increasing the crosslink density and the time to vitrification of the epoxies.

Crosslink density increases with increasing functionality. Crosslink density can be determined experimentally from the following equation, derived from classical theories of rubber elasticity:

$$\nu = \frac{E'}{3RT}$$

where ν is crosslink density in mol m^{-3}, E' is storage modulus in the rubbery plateau in Pa, and T is temperature in K.[15] An increase in crosslink density is generally accompanied by an increase in strength, stiffness, and T_g.[22,23] Higher crosslink densities reduce hole size, with smaller V_h values reported for networks based on multifunctional rather than difunctional epoxides.[24]

Increasing functionality shortens the time to vitrification in epoxy systems.[25] The high-functionality monomers experience rapid growth in molecular weight, and the high crosslink density constrains molecular motion in the growing network. Consequently

networks with multifunctional epoxies vitrify at lower conversions than their difunctional analogues. The rate of epoxy-amine reaction is severely reduced after vitrification.[26] Cured multifunctional resins exhibit heterogeneous network architectures, incorporating densely-crosslinked and lightly-crosslinked regions. The lightly-crosslinked regions correspond to network segments that were not fully reacted at the onset of vitrification. The heterogenous architecture is evinced by DMA results, which show a broad bimodal T_g peak for epoxies based on *m*-TGAP and TGDDM (Figure 4). T_g broadening indicates a continuum of cooperative motions and is representative of architectural heterogeneity.[27,28]

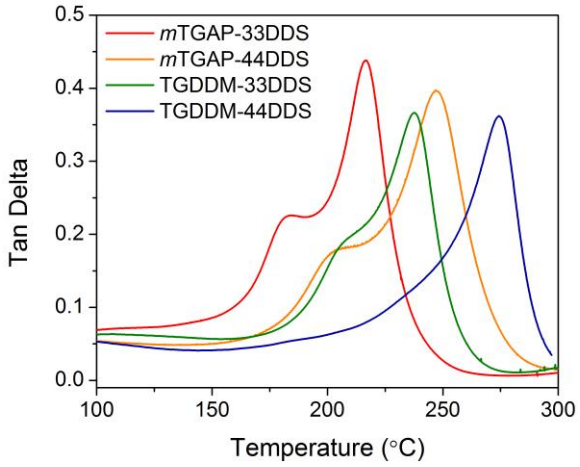

Figure 4. Tan delta curves for multifunctional epoxies. Reproduced from reference with permission.[10]

Effect of Stoichiometry

The epoxide-amine stoichiometry of an epoxy system also affects its architecture and therefore its final properties. Epoxies formulated with a 1:1 ratio of epoxide to amine active hydrogen are considered "stoichiometric" networks. Because epoxy-amine crosslinking is an AA-BB step-growth polymerization, complete conversion is only achieved with 1:1 stoichiometry.[14] In theory, any deviation from 1:1 stoichiometry results

in a decrease in crosslink density and an increase in molecular weight between crosslinks and dangling chain ends. This theory has been validated experimentally by several researchers, who measured decreased crosslinked density for off-stoichiometry epoxies.[12,29] The longer, more flexible chain segements in off-stoichiometry networks may be able to pack more efficiently than the shorter, more rigid segments in on-stoichiometry networks. Increased packing efficiency results in decreased free volume. A decrease in T_g has been noted for excess-epoxy materials, and it was ascribed to decreased free volume in those samples.[30]

Networks cured with excess epoxy have improved moisture resistance as compared to on-stoichiometry networks. Excess-epoxy materials have demonstrated reduced equilibrium water uptake and uptake rate.[31,32] The decrease in water ingress has been attributed to lower free volume and to development of a two-phase microstructure wherein a high-density phase limited diffusion.

Effect of Network Growth Kinetics

The chemical structure, functionality, and stoichiometry of epoxy and amine monomers are inherently related to network architecture; the manner in which these molecules come together to form the network also affects the final structure. The amine group on a curative undergoes two reactions: the primary amine reacts and becomes a secondary amine, and the secondary amine reacts and becomes a tertiary amine. The relative rate of secondary versus primary amine reaction has significant implications for network architecture.

Epoxy network growth can be illustrated by two extreme examples: linear-type growth and microgel-type growth. Linear-type growth occurs when the primary amine is

much more reactive than the secondary amine. Because the amine is less reactive after the first addition reaction, it exhibits a negative substitution effect in its reactivity. In this scenario, the primary amines react fully at the beginning of the reaction, creating linear oligomers. Next, the secondary amines react, crosslinking the linear segments together.[25] This growth mechanism is thought to produce more homogenous networks with lower free volume, due to the tendency of the linear segments to pack efficiently before crosslinking.

Microgel-type growth occurs when the primary amine and secondary amine are equally reactive. In this scenario, primary and secondary amines react simultaneously, creating regions of high crosslink density. The material is fully cured when these regions impinge on one another.[30] Microgel-type growth is thought to produce more heterogenous networks with higher free volume.

Reactivity ratio is governed by steric hindrance, chemical structure, and cure temperature. When the monomers are bulky or rigid, the secondary amine is sterically hindered and the reactivity ratio is low. When the monomers are less bulky or more flexible, the reactivity ratio is higher. Primary amine reaction affects the basicity, conjugation, and nucleophilicity of the amine, impacting reactivity ratio.[33,34,35]

Reactivity ratio changes with cure temperature, with different effects operating in different temperature windows. These relationships have been studied using near-IR spectroscopy, which allows for direct measurement of epoxide, primary amine, and secondary amine concentrations throughout the cure process.[36,37] During linear-type growth, the secondary amine concentration first increases (as primary amines convert to secondary amines) and then decreases (as secondary amines convert to tertiary amines).

In contrast, secondary amine concentration is more constant during microgel-type growth, as secondary amine is produced and consumed simultaneously. DGEBF cured with 3,3'-DDS and 4,4'-DDS at 180 °C exhibits linear-type network growth, as illustrated by the secondary amine concentrations in the IR cure profiles in Figure 5.

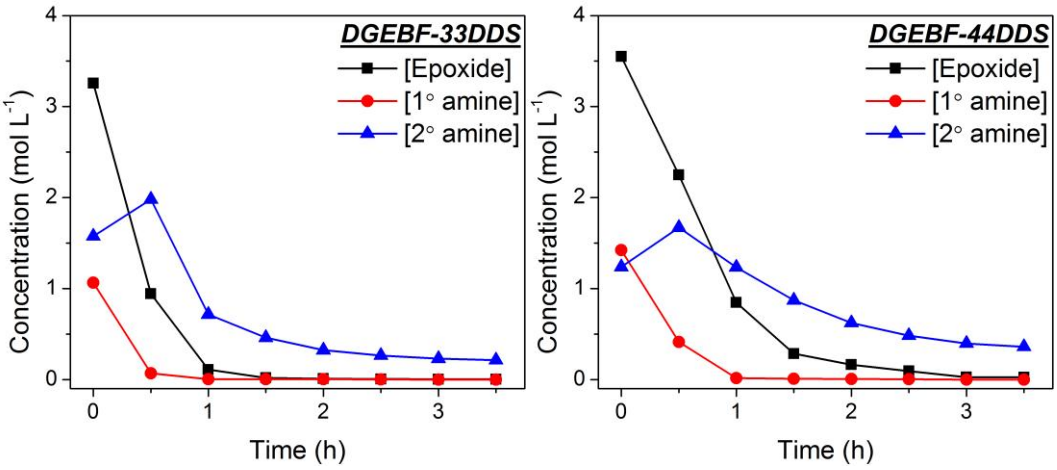

Figure 5. IR cure profiles for epoxy cured at 180 °C. Reproduced from reference with permission.[10]

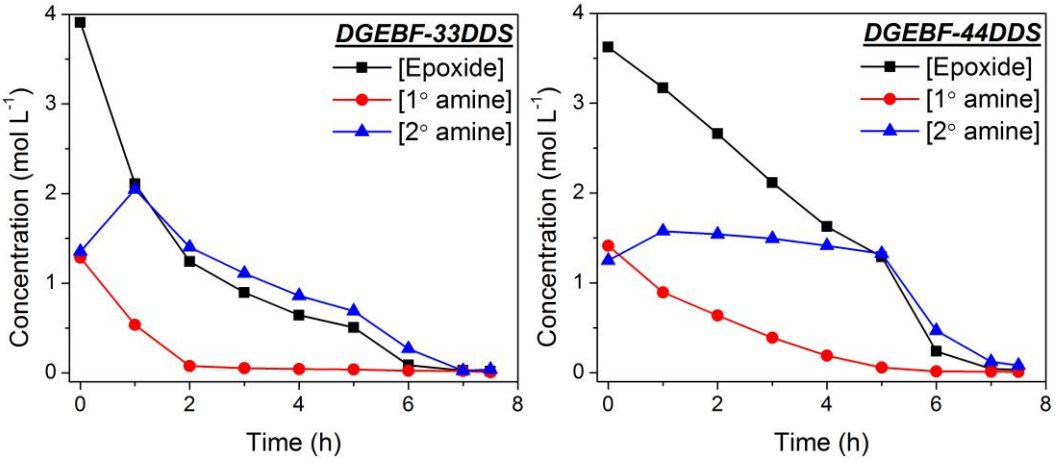

Figure 6. IR cure profiles for epoxy cured at 125 °C and postcured at 200 °C. Reproduced from reference with permission.[10]

IR profiles for the same epoxies cured at 125 °C and post-cured at 200 °C show somewhat different results (Figure 6). The profile for DGEBF/3,3'-DDS is largely unchanged. The cure profile for DGEBF/4,4'-DDS exhibits microgel-type growth at this

temperature, in contrast to the linear-type growth apparent at 180 °C. The shift in cure kinetics for the para-substituted amine was attributed to hydrogen bonding. Hydrogen bonding is stronger at lower temperatures, and most of the network development occurred at 125 °C. Hydrogen-bonded complexes can lower the activation energy (E_a) of the secondary amine-epoxy reaction, promoting microgel-type growth.[38] This effect was not observed for 3,3'-DDS because the steric hindrance associated with meta substitution has a greater impact than hydrogen bonding on secondary amine reactivity.

Network growth kinetics can also affect final architecture via etherification reactions. Etherification occurs when an epoxide moiety reacts with a hydroxyl group. An ether-based crosslink and a new hydroxyl group are generated. The E_a of the etherification reaction is higher than the E_a of the epoxy-amine reaction, and therefore the epoxy-amine reaction is favored under normal conditions.[39] However, when excess epoxide is present or reaction temperature is very high, etherification can become a competitive reaction. Networks with a high degree of etherification are expected to have different architectures and consequently different properties than their non-etherified analogues.

Several techniques have been developed to characterize epoxy network growth as it occurs. IR spectroscopy (discussed above),[25,35,36,37,40] dielectric resonance spectroscopy (DRS),[41,42,43,44] and dynamic scanning calorimetry (DSC)[45,46,47] have all been used to follow the epoxy-amine cure process. Each of these techniques measure different variables that are expected to change throughout network development. They can be used alone or together to develop an understanding of network growth, and through that understanding, a prediction of final network architecture.

Fluid Ingress

A thorough understanding of chemical structure and network architecture is necessary to understand and predict fluid ingress in epoxies. An aerospace epoxy is exposed to a variety of aggressive solvents in its service lifetime, including water, paint remover (methyl ethyl ketone, MEK), hydraulic fluid, and jet fuel. Exposure to these fluids can precipitate an increase in weight and a decrease in key mechanical properties of the matrix. The limitations imposed on aerospace epoxies by fluid ingress are twofold: composite parts must be over-designed to account for the loss in T_g or stiffness due to fluid uptake in the epoxy, and many promising epoxy systems must be disregarded entirely because they do not pass preliminary fluid resistance tests.[48] High-distortion resins are an extreme example of the latter category. If the mechanisms governing fluid uptake in glassy networks were fully understood, it would be possible to design high-distortion materials with improved fluid resistance. Unfortunately, traditional approaches to fluid uptake have been unable to explain why two seemingly similar epoxies absorb moisture or organic solvents at different rates.

Chemical structure has long been regarded as the primary determinant of fluid susceptibility in polymers. Chemical approaches to fluid susceptibility, including analyses of solubility parameters and polar groups, have proven effective for predicting trends in fluid uptake rate and equilibrium uptake level for linear polymers.[49] Chemistry alone does not explain the fluid absorption patterns observed in crosslinked epoxies. When the same epoxide is cured with 3,3'-DDS and 4,4'-DDS, the resulting networks are chemically identical except for the structural isomerism in the DDS segments. However, the 3,3'-DDS network absorbs water and MEK more slowly than the 4,4'-DDS

network.[16] IR data showed that the two DDS isomers promote different network growth schemes, ultimately resulting in different network architectures. It is clear that network architecture and its related physical descriptors (free volume characteristics, chain packing efficiency, etc.) have a significant impact on moisture and organic solvent ingress in epoxy networks.

Moisture Ingress

Moisture diffusion has been well characterized for linear and crosslinked polymer glasses. Diffusion of water through polymeric glasses has been extensively studied and shown to follow classic Fickian behavior, in which uptake rate depends on concentration gradient.[50,51] Fickian diffusion is described by the following equation:

$$\frac{\partial \varphi}{\partial t} = D \frac{\partial^2 \varphi}{\partial x^2}$$

whereφ is moisture concentration, t is time, and x is position.[52] These diffusion kinetics give rise to concentration profiles like those shown schematically in Figure 7, with moisture gradually diffusing through the material until an equilibrium saturation is reached.

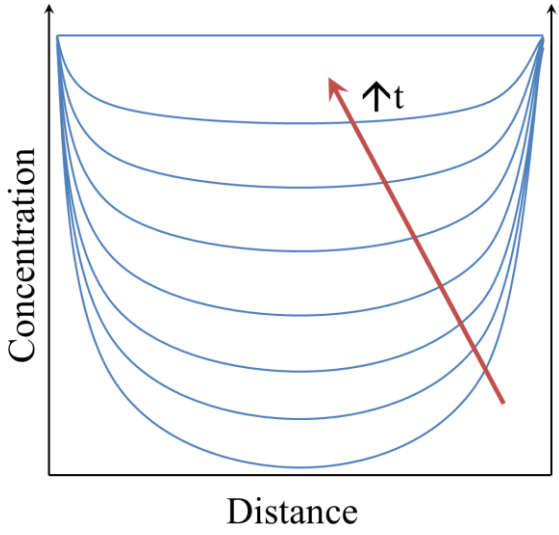

Figure 7. Schematic of Fickian diffusion profiles over time.

Absorbed moisture in epoxies has traditionally been characterized as "free" (moisture that has accumulated in free volume sites in the epoxies) or "bound" (moisture that bound to the network by hydrogen bonds).[53] The amounts of free and bound moisture have been estimated from changes in hydrogen-bond related signals in IR[54] and solid-state NMR[55,56] and from changes in molecular motion associated with hydrogen bonding in DRS.[54,57] Bound and free fractions have also been predicted from molecular dynamics (MD) simulations.[58] Researchers have attempted to relate equilibrium moisture uptake and uptake rate in epoxies primarily to polarity and hydrogen bonding in the material.[8,59,60,61,62] While it is clear from that research that hydrogen bonding plays an important role in water uptake in epoxies, this consideration alone does not explain why similar epoxies can have markedly different moisture uptake kinetics.

Organic Solvent Ingress

Reports on the diffusion of organic solvents through glassy polymers are less common than analyses of moisture diffusion. Transport of organic solvents through polymer glasses has been shown to follow non-Fickian kinetics; specifically, Case II

diffusion is observed.[63] Case II diffusion occurs when the ingressing solvent molecules plasticize the glassy polymer. As some solvent molecules diffuse into the polymer, additional free volume is created, and more solvent molecules are absorbed. This behavior results in a constantly moving well-defined flow front between the swollen and glassy regions. An unperturbed glassy region persists in the center of the sample until equilibrium. The concentration profiles that result from Case II diffusion are shown schematically in Figure 8. Case II diffusion can result in solvent absorption greater than 25 weight percent in many epoxy samples (compared to <10 weight percent for water in the same systems).[64]

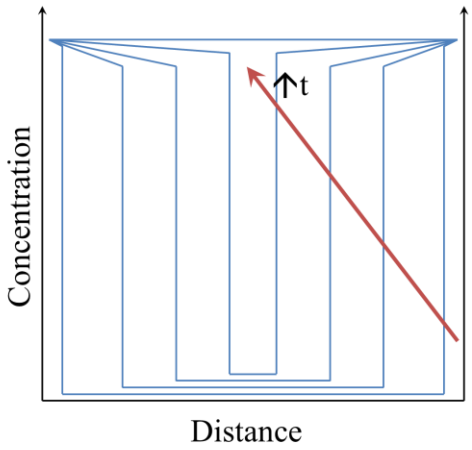

Figure 8. Schematic of Case II diffusion profiles.

The extreme difference between Fickian and Case II diffusion kinetics has been attributed to relaxation mechanisms active in Case II diffusion.[65] Fickian diffusion occurs when the rate of diffusion is much less than the rate of polymer segemental motion, whereas Case II diffusion occurs when the rate of diffusion is much greater than segmental motion.[51,66] In the latter case, diffusion rate is limited by swelling kinetics. Attempts to predict Case II diffusion behavior have relied on a model first introduced by Thomas and Windle.[67] The original model and elaborations on it have employed

constants associated with viscosity to describe the uptake profiles. These models have been used successfully to predict Case II diffusion in linear polymer systems.[68,69] However, prediction of Case II diffusion behavior is difficult for crosslinked materials because the rheological environment in the crosslinked glass is very different from that of a linear polymer and the viscosity coefficient has limited relevance.

Free Volume Approach

While the kinetics of moisture and solvent ingress in epoxy networks have been well-reported, a comprehensive understanding of why different epoxies have different fluid uptake characteristics has been lacking. Recently, researchers have attempted to explain water ingress in epoxies in terms of free volume hole size (V_h) and fractional free volume (FFV). Ramesh et al. published a review article describing free-volume approaches to diffusivity theory for polymer glasses.[70] Soles and co-workers studied the effects of fractional free volume on moisture uptake and concluded that FFV played a significant role.[53,60] The nature of water absorption in epoxies, e.g., moderate water uptake with no change in sample dimensions, is consistent with a free volume explanation. In this scenario, ingressing water molecules gradually fill free volume holes. When all holes are full, ingress stops and the sample is considered equilibrated. VanLandingham et al. concurred, postulating a free volume explanation for changes in water absorption for epoxies with different stoichiometries.[32]

Recently, free volume arguments have also been used to explain the ingress of organic solvents in glassy polymers in terms of the size of the penetrant molecule. A relationship between molecular size and diffusion rate in non-polymer systems was observed as early as 1964. Then, Tricklebank et al. studied ionic diffusion and calculated

much higher activation energies for that process when the size of the ion was larger than the V_h of the diffusion medium.[71] Gall[68] and Sahlin[64] observed relationships between penetrant size and uptake rate for various solvents and glassy polymers; however, the free volume characteristics of the polymer were not considered. Shantarovich investigated diffusion in glassy polymers characterized by PALS and hypothesized that the relationship between polymer V_h and solvent size is the primary factor governing diffusion rate.[72]

Previous work by the Wiggins Research Group applied the free volume approach to a series of glassy epoxy matrix materials whose free volume properties were comprehensively characterized via PALS and PVT (Table 1).[16] The epoxides DGEBA and DGEBF were cured with 3,3'-DDS and 4,4'-DDS and submerged in water and a variety of organic solvents. The water uptake results exhibited different equilibrium uptake values and different diffusivities for the four networks, despite their chemical similarities (Figure 9). The equilibrium uptake correlated well to FFV data. Therefore Jackson et al. concluded that FFV is the major determinant for equilibrium water uptake.[16] According to this line of reasoning, water diffuses into the material until all free volume sites are filled and equilibrium is reached. It was also hypothesized that diffusivity is independent of FFV and dependent on V_h. However, this hypothesis was difficult to validate because those variables were linked in many of the systems studied. The material with the highest V_h had the highest FFV. It was not possible to resolve the separate effects of FFV and V_h on moisture uptake in these epoxies.

Table 1

Free Volume Characteristics of Common Epoxy System.

Epoxy System	FFV (%)	V_h (Å^3)
DGEBF-33DDS	3.8	67
DGEBF-44DDS	4.2	76
DGEBA-33DDS	4.6	77
DGEBA-44DDS	4.8	82

Reproduced from reference with permission.[16]

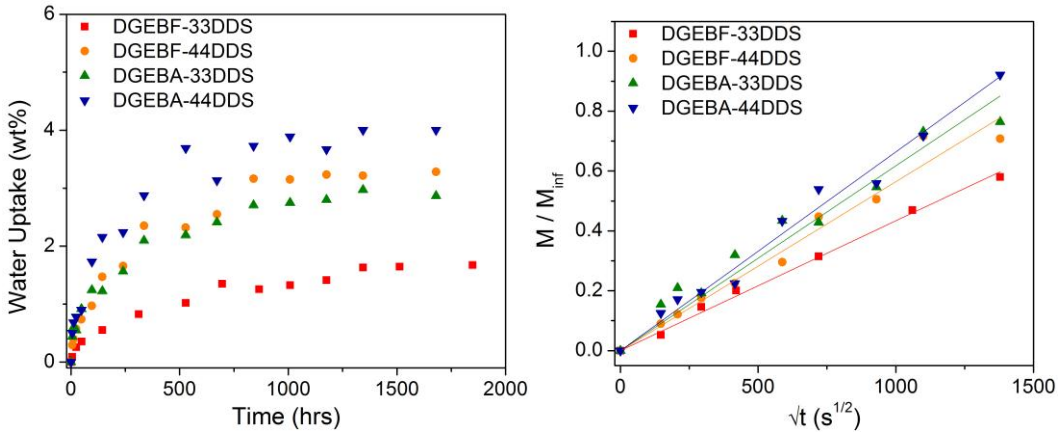

Figure 9. Water uptake vs. time and M_t/M_{inf} vs. $t^{1/2}$ for common epoxy systems. Reproduced with permission from references.[10,16]

The free volume approach was also used to gain new understanding of organic solvent ingress in glassy epoxies. When the same four epoxy networks were exposed to a variety of solvents, a division was apparent between networks that absorbed solvent quickly and networks that absorbed solvent slowly (Figure 10). The explanation for the divide became apparent when solvent hydrodynamic sizes were considered. The van der

Waals volume of each solvent molecule was estimated using molecular dynamics simulations (Table 2). Solvent uptake was rapid in systems where the solvent volume was smaller than the average V_h, and uptake was slow in systems where solvent volume was larger than V_h. The significance of V_h for Case II diffusion rate was confirmed by experiments using MEK. The four epoxies absorbed MEK at different rates, with uptake rate increasing with V_h (Figure 11).

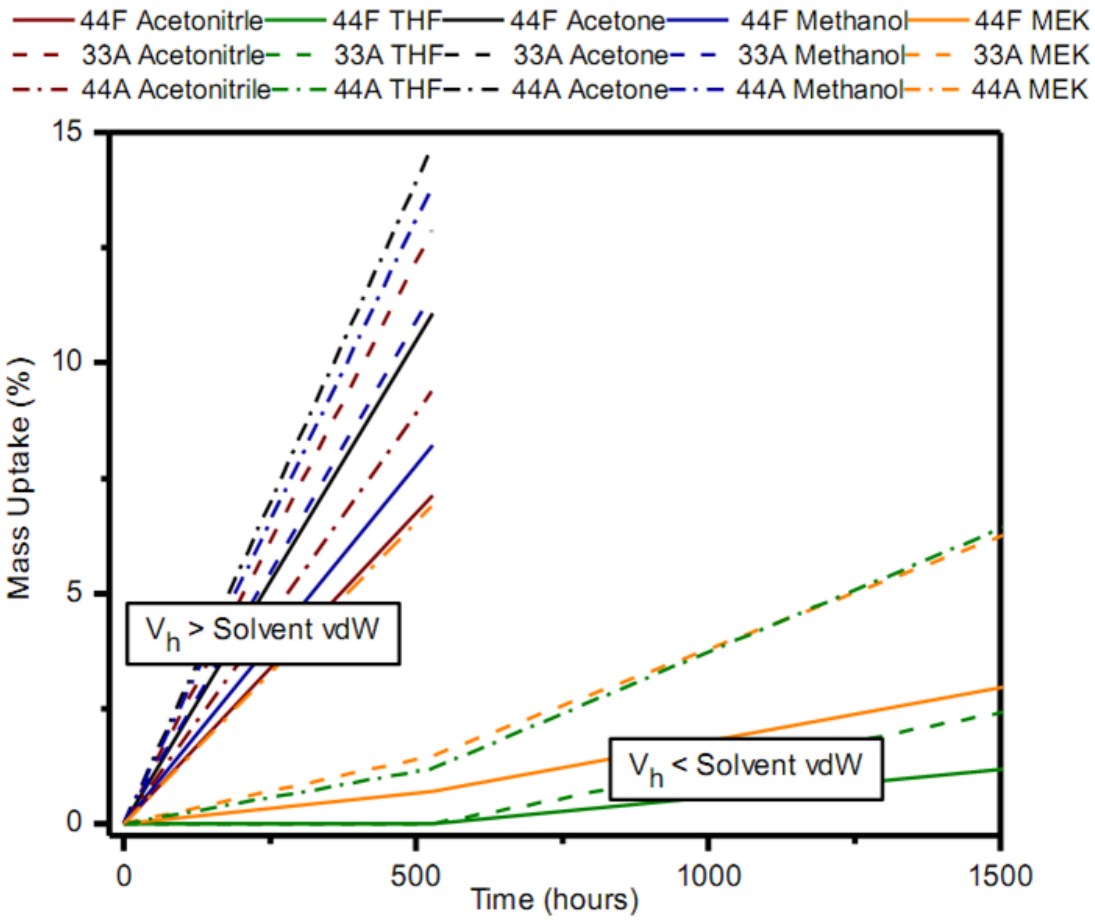

Figure 10. Mass uptake for common epoxies and solvents.Reproduced from reference with permission.[10]

Table 2

Solvent van der Waals Volumes

Solvent	vdW Volume ($Å^3$)
Water	19.5
Methanol	36.8
Acetonitrile	45.7
Acetone	65.9
THF	77.4
MEK	81.5

Reproduced from reference with permission.[16]

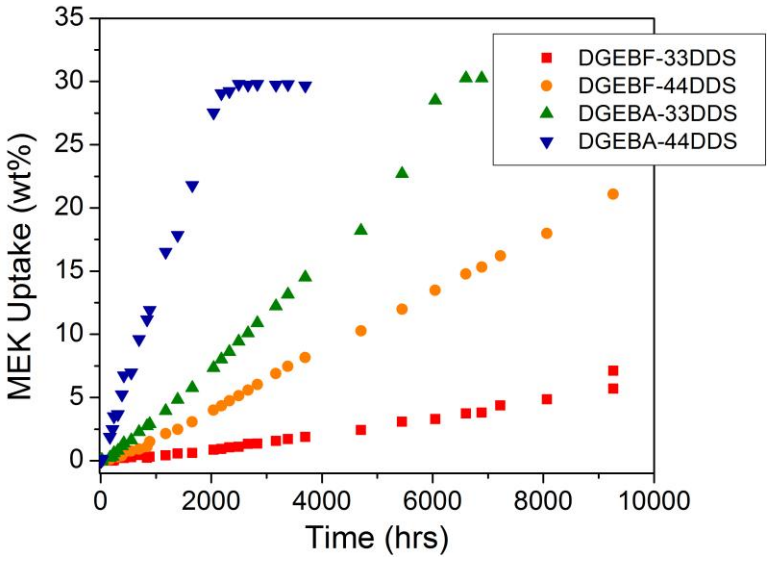

Figure 11. MEK uptake vs. time for common epoxy systems. Reproduced from reference with permission.[16]

An understanding of fluid ingress in glassy matrix materials is crucial to further development of high-distortion epoxy resins. Widespread use of high-distortion resins is currently limited by the poor fluid resistance of these materials. If the mechanisms governing distortional capabilities and fluid sensitivity are resolved, researchers may be able to design high-distortion resins with solvent and moisture resistance.

POSS-Modified Epoxies

One potential route towards developing new high-distortion resins involves polyhedral oliogmericsilsesquioxane (POSS). POSS, shown in Figure 12, is a hybrid organic-inorganic material that can be functionalized with up to eight reactive groups. When the Wiggins Research Group simulated an epoxy network with pendant POSS moieties, the resulting material had an 80% increase in von Mises strain (a parameter related to yield strain) with no loss in stiffness or T_g. The improvement in properties was attributed to new molecular motions and relaxations introduced by the POSS cage, or to free volume created by the pendant group. Both of these mechanisms could be very detrimental to fluid resistance of the material. To fully evaluate the POSS-containing nanocomposite as a high-distortion material, the fluid absorption behavior of the epoxy must be characterized.

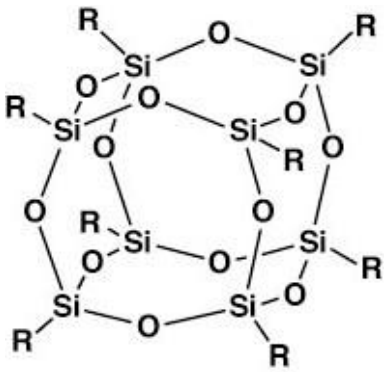

Figure 12. POSS structure.

POSS Incorporation in Epoxies

Synthesis of epoxy networks with pendant POSS has presented a considerable challenge. To obtain these networks, molecular-level dispersion of monofunctional POSS must be achieved. Monofunctional POSS is much less dispersible in epoxy precursors than multifunctional POSS. Octaepoxide POSS can be readily mixed with common epoxy-amine systems to give clear, homogeneous nanocomposites. Researchers have cured octaepoxide POSS with Jeffamine-type aliphatic amines,[73,74,75] aromatic amines,[76,77,78] cycloaliphatic amines,[79] and dicyandiamide.[80] In these systems, the POSS moiety served as a junction point in the network architecture. As such, it reinforced the networks by increasing crosslink density (because of its eight reactive sites) and constraining molecular motion in the rigid region around the inorganic POSS unit. The resulting networks were stiffer and more brittle than unmodified thermosets.

Pendant POSS moieties could have an entirely different effect on the mechanical properties of epoxy networks. The POSS units could introduce new modes of molecular relaxation or increase free volume. POSS as a pendant group is achieved using monofunctional POSS, which has one reactive substituent and seven nonreactive inorganic substituents. These structure-property relationships for epoxies modified with pendant POSS have not been elucidated because of the difficulty in dispersing monofunctional POSS in an epoxy network.

Unlike octafunctional POSS, monofunctional POSS has an overwhelming tendency to aggregate and crystallize in these systems. Monofunctional POSS compounds are less soluble in epoxy precursors. Even when reacted into the network, the pendant POSS units are not completely constrained. Therefore they can aggregate. The

result is a phase-segregated structure with POSS crystals in an epoxy matrix. Early research on epoxies modified with monofunctional POSS showed mechanical property changes consistent with aggregation.[81] Strachota and Matejka used microscopy techniques to relate observed property changes to morphology.[73,74] Matejka observed aggregation for monoepoxide POSS mixed with the diglycidyl ether of bisphenol-A (DGEBA) and cured with Jeffamine.[73] Bocek reported phase segregation for monoepoxide POSS mixed with DGEBA and cured with a cycloaliphatic amine.[79] Xu observed a heterogeneous morphology when anhydride-functionalized POSS was mixed with DGEBA and cured with an anhydride.[82]

Several researchers have reported improved dispersion by pre-reacting POSS with epoxy precursors. Liu mixed amine-functionalized POSS with DGEBA in THF, then evaporated the solvent and conducted the pre-reaction in the POSS/DGEBA residue at 160 °C.[83] This reaction likely produced many POSS/DGEBA oligomers. A similar approach was employed by Zucchi, using a monoepoxide POSS and an aromatic amine in the pre-reaction.[84] Matejka conducted the pre-reaction in solvent and noted improved dispersion in a rubbery epoxy network.[85] For all of these systems, some aggregation was still observed. To the best of our knowledge, molecular-level dispersion of monofunctional POSS in an epoxy-amine network, with the POSS units serving as pendant groups, has not yet been achieved.

Modifications to the curing prescription can also be considered as a route towards improved POSS dispersion. Previous studies have found that monofunctional POSS reacts more slowly than standard network formers.[73,84] The bulky inorganic silsesquioxane cage reduces molecular mobility and promotes aggregation. It has been

speculated that any modification to the POSS-epoxy system that increases the rate of POSS reaction will improve dispersion by making POSS reaction into the growing network more competitive with phase segregation.[86] Increasing the reaction temperature could enhance POSS dispersion by increasing the reaction rate.

POSS Effects on Epoxy Properties

The effect of POSS on material properties strongly depends on loading level and interaction with the matrix. Because POSS is a hybrid organic-inorganic material, it has the potential to interact with the polymer matrix in more complex ways than other nanoscale additives. Under some circumstances the POSS cage plasticizes the polymer by disrupting intermolecular bonding and creating free volume. The result is a decrease in T_g and stiffness. When the POSS cage constrains chain motion, however, the overall effect is fortifying and increases in T_g and stiffness are observed. This plasticizing/fortifying duality has been observed for POSS in polycarbonate,[87,88] DGEBA cured with Jeffamines,[85,89] and DGEBA cured with cycloaliphatic amines.[79] Recently, researchers have successfully predicted plasticizing or reinforcing effects in POSS-polymer nanocomposites using Hansen solubility parameters.[90,91]

The nature of POSS interaction with a polymer matrix is also a function of loading level. A complex relationship between nanofiller loading level and material properties has been observed for all nanocomposites, including those based on carbon nanotubes[92,93] and halloysite nanotubes[94] as well as POSS.[95,96] At low concentrations the POSS acts as a plasticizer (usually denoted by a decrease in T_g).[97] At higher concentrations, the POSS fortifies the material, lengthening relaxation times and increasing the T_g.[98] This trend has been attributed to aggregation and physical

crosslinking. As POSS content increases, the size or number of POSS aggregates increases as well. The aggregates act as microscale fillers and reinforce the material. Physical crosslinking between POSS aggregates or moieties can also produce a reinforcing effect.

The relationships between POSS loading level, dispersion, free volume architecture, and mechanical and thermal properties determine the utility of specific POSS-epoxy nanocomposites for high-performance applications. The effect of these characteristics on distortional behavior and fluid sensitivity determines whether epoxies with pendant POSS are a viable candidate for the next generation of high-distortion materials.

Research Overview

The purpose of this dissertation is to investigate the fundamental structure-property relationships between network architecture and fluid ingress in glassy epoxies. Previous work by the Wiggins Research Group in the area of amine-cured epoxies elucidated the effects of chemical structure, functionality, and network growth kinetics on ultimate network architecture in benchmark two-part epoxy systems. Foundational fluid ingress research conducted in this laboratory examined moisture and organic solvent ingress in those benchmark epoxies and correlated the observed results to free volume characteristics.

The present work expands on previous research by evaluating fluid uptake in more complex epoxy systems. This research is motivated by growing scientific and industrial interest in high-distortion resin systems. High-distortion epoxies have the potential to dramatically improve performance of aerospace epoxy materials. However,

these high-distortion systems are plagued by debilitating fluid sensitivity. Their fluid resistance could be improved if the relationships between distortional properties, network architecture, and fluid ingress were better understood.

This dissertation examines structure-property relationships in epoxy systems relevant to high-distortion materials. In Chapter III, cure kinetics are evaluated by three complementary techniques for epoxies modified with bulky amines. This analysis demonstrates the connection between cure kinetics, network architecture, and network properties. In Chapter IV, free volume trends and fluid uptake are characterized in blends of difunctional and multifunctional epoxides. The water and solvent ingress are interpreted in light of V_h and FFV measurements. Blending with multifunctional epoxides is demonstrated to be an effective method for inhibiting solvent uptake in epoxies. Chapter V extends the analysis of fluid sensitivity to networks formulated with excess epoxide. The excess-epoxy treatment is shown to reduce fluid uptake due to increased chain packing. Distortional resins are introduced in Chapter VI, which considers POSS-modified epoxy, a material predicted to be high-distortion by MD simulations. A pre-reaction and elevated cure temperature are evaluated as routes towards improved POSS dispersion in epoxy. In Chapter VII, the fluid sensitivity of POSS-modified epoxies is investigated as a function of pre-reaction state and loading level.

CHAPTER II

EXPERIMENTAL

Materials

The following materials were used as received: diglycidyl ether of bisphenol-F (DGEBF, EPON862, EEW = 169, Momentive), diglycidyl ether of bisphenol-A (DGEBA, EPON825, EEW = 177.5, Momentive), N,N,N',N'-tetraglycidyl-4,4'-diaminodiphenylmethane (TGDDM, MY721, EEW = 113, Huntsman), *p*-trigylcidylaminophenol (*p*TGAP, MY0510, EEW = 101, Huntsman), *m*-trigylcidylaminophenol (*m*TGAP, MY0610, EEW = 101, Huntsman), 3,3'-diaminodiphenylsulfone (3,3'-DDS, Royce Chemical Corp., >99% pure, 4 μm particle size), and 4,4'-diaminodiphenylsulfone (4,4'-DDS, Royce Chemical Corp., >99% pure, 4 μm particle size). Their structures are shown in non-chain-extended form in Figures 13-15.

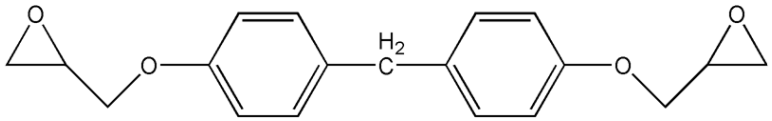

DGEBF

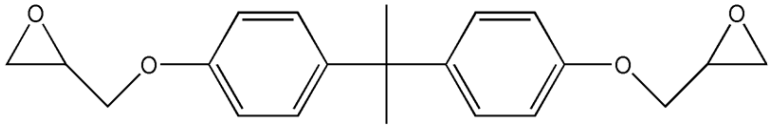

DGEBA

Figure 13. Difunctional epoxide structures.

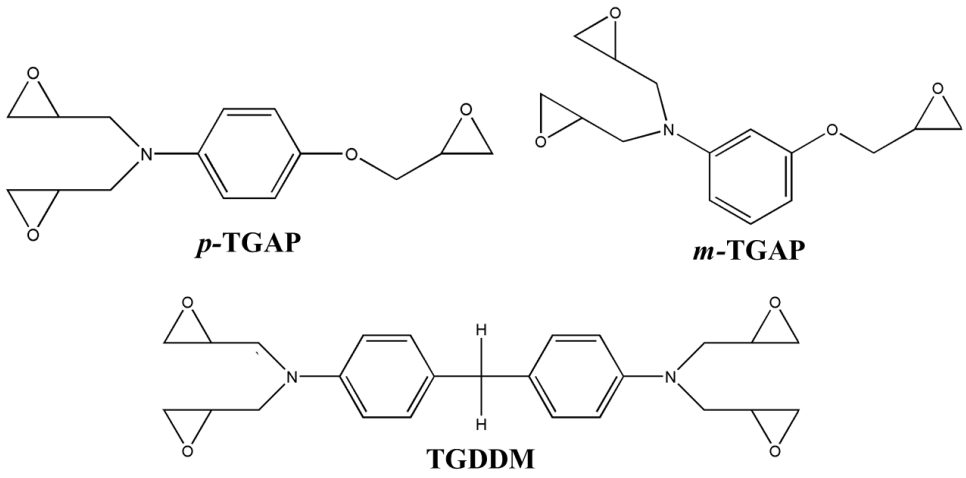

Figure 14. Multifunctional epoxide structures.

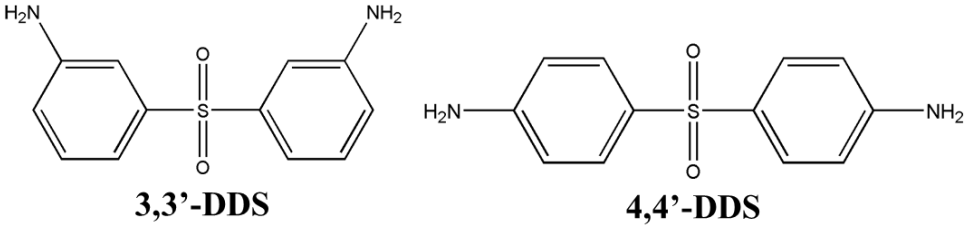

Figure 15. DDS structures.

The bulky amines 1-naphthylamine (NA) and 1-adamantylamine (AA) were supplied by Aldrich and used as received. Their structures are shown in Figure 16.

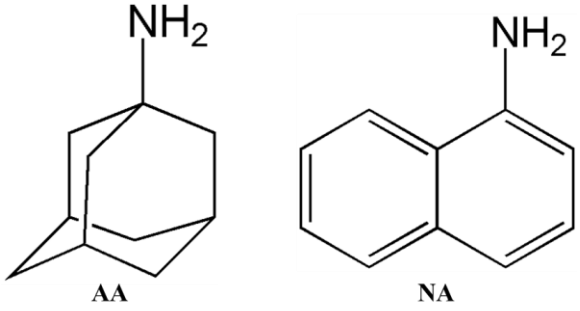

Figure 16. Bulky amine structures.

Aminopropylisobutyl POSS (AI-POSS, AM0265) was supplied by Hybrid Plastics and used as received. Two POSS pre-reaction product are evaluated in this dissertation. One pre-reaction product based on DGEBA and AI-POSS was synthesized by the Wiggins Research Group using the method described in in the "POSS pre-reaction" section of this chapter. Another pre-reaction product based on DGEBF and AI-POSS was synthesized by Hybrid Plastics. That product, denoted as the POSS trimer ($POSS_{trimer}$), was used as received. Its structure is shown in Figure 17.

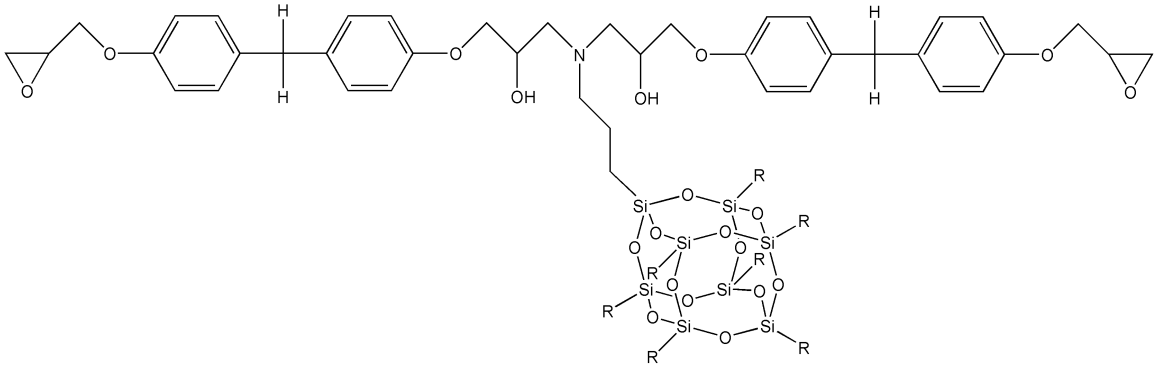

$POSS_{trimer}$

Figure 17. $POSS_{trimer}$ structure.

Toluene (ACS reagent grade, Fisher) was used as received. Water, methyl ethyl ketone (MEK), and acetone were HPLC grade, supplied by Fisher and used as received for fluid uptake studies. Their structures are shown in Figure 18.

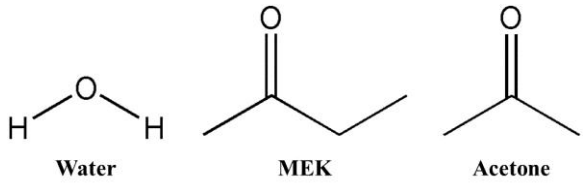

Figure 18. Solvent structures.

Sample Preparation

Epoxy Blends

Blends of difunctional and tri- or tetrafunctional epoxies were formulated from DGEBA and *m*TGAP (trifunctional), *p*TGAP (trifunctional), or TGDDM (tetrafunctional) in weight ratios of 75:25, 50:50, and 25:75. All blends were cured with 3,3'-DDS or 4,4'-DDS using a 1:1 stoichiometric equivalent of oxirane to amine active hydrogen. Binary samples consisting of DGEBA/DDS, TGAP/DDS, and TGDDM/DDS were prepared for benchmarks. In a typical reaction, 75.0 g (0.211 mol) DGEBA and 25.0 g (0.083 mol) of *m*TGAP were charged to a 500 ml Erlenmeyer flask equipped with a vacuum fitting and magnetic stirring device. The epoxide blend was heated to 100 °C and 41.6 g (0.168mol) 3,3'-DDS was added over a 10 minute period. Pressure was slowly decreased to ~10^{-3}torr and temperature was increased to 120 °C. The mixture was stirred until the amine fully dissolved. At that point the clear solution was poured into preheated (100 °C) silicone test coupon molds of various dimensions. Samples were cured in two steps: 5 hours at 125 °C and 2 hours at 200 °C. Two sample formulations series are listed in Table 3. The same nomenclature is employed in this dissertation for all polymer blends: "F" and "A" denote DGEBF and DGEBA; "*m*T," "*p*T,"and "TG" denote *m*TGAP, *p*TGAP, and TGDDM; and "33" and "44" denote 3,3'-DDS and 4,4'-DDS. Weight and molar ratios were similar; hereafter samples will be referred to by their weight ratios for clarity.

Table 3

Selected Epoxy Blend Formulations (discussed in Chapter IV)

Sample Name	Blend (w/w)	Blend (mol/mol)	Curative
DGEBA-33	100% DGEBA	100% DGEBA	3,3'-DDS
75A-25*m*T-33	75% DGEBA/ 25% *m*TGAP	72% DGEBA/ 28% *m*TGAP	3,3'-DDS
50A-50*m*T-33	50% DGEBA/ 50% *m*TGAP	46% DGEBA/ 54% *m*TGAP	3,3'-DDS
25A-75*m*T-33	25% DGEBA/ 75% *m*TGAP	22% DGEBA/ 78% *m*TGAP	3,3'-DDS
*m*TGAP-33	100% *m*TGAP	100% *m*TGAP	3,3'-DDS
DGEBF-44	100% DGEBF	100% DGEBF	4,4'-DDS
75F-25TG-44	75% DGEBF/ 25% TGDDM	80% DGEBF/ 20% TGDDM	4,4'-DDS
50F-50TG-44	50% DGEBF/ 50% TGDDM	57% DGEBF/ 43% TGDDM	4,4'-DDS
25F-75TG-44	25% DGEBF/ 75% TGDDM	31% DGEBF/ 69% TGDDM	4,4'-DDS
TGDDM-44	100% TGDDM	100% TGDDM	4,4'-DDS

Off-Stoichiometry Epoxies

Epoxies were formulated with a 1.25:1 molar excess of epoxide to amine active hydrogen. Benchmark epoxies were also made with 1:1 stoichiometry. The epoxies were formulated using DGEBA and DGEBF and cured with 3,3'-DDS and 4,'4-DDS. The samples were prepared as described above for epoxy blends. IR samples were prepared by placing uncured resin between two glass microscope slide covers, separated by a

Teflon washer. IR samples were stored in the freezer until analysis. The remaining material from each sample was cured according to a two-step cure prescription (5 h at 125 °C, 2 h at 200-225 °C) or a one-step cure prescription (3 h at 180 °C). The off-stoichiometry epoxies are listed in Table 4.

Table 4

Off-stoichiometry Epoxy Formulations (discussed in Chapter V)

Sample Name	Epoxide (mol)	Curative (mol)	Epoxide (g)	Curative (g)
DGEBF-33	0.30	0.15	100.00	36.73
DGEBF-44	0.30	0.15	100.00	36.73
DGEBA-33	0.28	0.14	100.00	34.97
DGEBA-44	0.28	0.14	100.00	34.97
$DGEBF_{XS}$-33	0.37	0.15	125.00	36.73
$DGEBF_{XS}$-44	0.37	0.15	125.00	36.73
$DGEBA_{XS}$-33	0.35	0.14	125.00	34.97
$DGEBA_{XS}$-44	0.35	0.14	125.00	34.97

Epoxies with Bulky Pendant Groups

Epoxies were formulated using amines (NA and AA) with bulky pendant groups. The epoxies were based on DGEBA cured with 3,3'-DDS. A 1:1 stoichiometric ratio of epoxide to amine active hydrogen was maintained for all materials. The bulky amine comprised 0, 5, or 10 weight percent of the total sample mass. The epoxy and amine were mixed and prepared for IR analysis as described above. Uncured resin was used for cure studies. The uncured resin was stored in a freezer and removed immediately before

analysis. PALS samples were made by curing resin in a two-step process (5 h at 125 °C, 2 h at 200 °C). All AA and NA samples are listed in Table 5.

Table 5

Epoxies with Bulky Pendant Groups (discussed in Chapter III)

Sample Name	DGEBA (g)	3,3'-DDS (g)	Bulky Amine (g)
DGEBA	73.82	26.18	0.00
5% AA	73.16	21.84	5.00
10% AA	72.49	17.51	10.00
5% NA	73.20	21.80	5.00
10% NA	72.58	17.42	10.00

POSS Epoxies

Unmodified POSS samples. Epoxies were formulated using unmodified AI-POSS. In a typical reaction, to obtain a final composite with 2.5 weight percent POSS, 0.75 g AI-POSS (0.858 mmol), 21.75 g DGEBA (61.3 mmol), and 7.50 g 3,3'-DDS (30.2 mmol) were charged to a round-bottom flask. Pressure was slowly decreased to ~10^{-3} torr.The contents were mixed at 90 °C for 2 h, at 100 °C for 1 h, and at 110 °C for 30 min. The epoxies were cast and cured according to one-stage or two-stage curing prescriptions. The two-stage consisted of a 5 h cure at 125 °C followed by a 2 h postcure at 200 °C. The one-stage prescription consisted of a 3 h cure at 180 °C. The unmodified POSS samples are listed in Table 6 and Table 7.

Table 6

DGEBA/DDS Samples with Unmodified POSS (discussed in Chapter VI)

Sample Name	POSS Loading (weight percent)	Epoxy Matrix	Curing Prescription
DGEBA/DDS_125	0	DGEBA/3,3'-DDS	5 h at 125 °C, 2 h at 200 °C
DGEBA/DDS_180	0	DGEBA/3,3'-DDS	3 h at 180 °C
2.5POSS_125	2.5	DGEBA/3,3'-DDS	5 h at 125 °C, 2 h at 200 °C
2.5POSS_180	2.5	DGEBA/3,3'-DDS	3 h at 180 °C
10POSS_125	10	DGEBA/3,3'-DDS	5 h at 125 °C, 2 h at 200 °C
10POSS_180	10	DGEBA/3,3'-DDS	3 h at 180 °C

Table 7

DGEBF/DDS Samples with Unmodified POSS (discussed in Chapter VII)

Sample Name	POSS Loading (weight percent)	Epoxy Matrix	Curing Prescription
DGEBF/DDS	0	DGEBF/3,3'-DDS	4 h at 180 °C
0.5POSS	0.5	DGEBF/3,3'-DDS	4 h at 180 °C
1.0POSS	1.0	DGEBF/3,3'-DDS	4 h at 180 °C
1.5POSS	1.5	DGEBF/3,3'-DDS	5 h at 180 °C
2.0POSS	2.0	DGEBF/3,3'-DDS	5 h at 180 °C

Table 7 (continued).

Sample Name	POSS Loading (weight percent)	Epoxy Matrix	Curing Prescription
2.5POSS	2.5	DGEBF/3,3'-DDS	5 h at 180 °C
5.0POSS	5.0	DGEBF/3,3'-DDS	5 h at 180 °C
7.5POSS	7.5	DGEBF/3,3'-DDS	5 h at 180 °C
10POSS	10	DGEBF/3,3'-DDS	5 h at 180 °C
15POSS	15	DGEBF/3,3'-DDS	5 h at 180 °C
20POSS	20	DGEBF/3,3'-DDS	5 h at 180 °C

POSS pre-reaction. The POSS pre-reaction is shown in Figure 19. To a dry 1000 mL round-bottom flask fitted with a condenser were charged 10.00 g of AI-POSS (11.43 mmol), 38.92 g of DGEBA (109.6mmol), and 500 mL of toluene. The flask containing the clear solution was immersed in an oil bath heated to 120 °C and the solution was stirred using a magnetic stir bar for 12 h. The solution was then removed from the oil bath and allowed to cool to room temperature. The toluene was removed via rotary evaporation. The product, a viscous white resin mixture of unreacted DGEBA and DGEBA/AI-POSS oligomers, was dried *in vacuuo* for 24 h at 50 °C.[29] Si was performed on the reagent and pre-reaction product and NMR spectra confirmed that the POSS cages were intact after the pre-reaction.

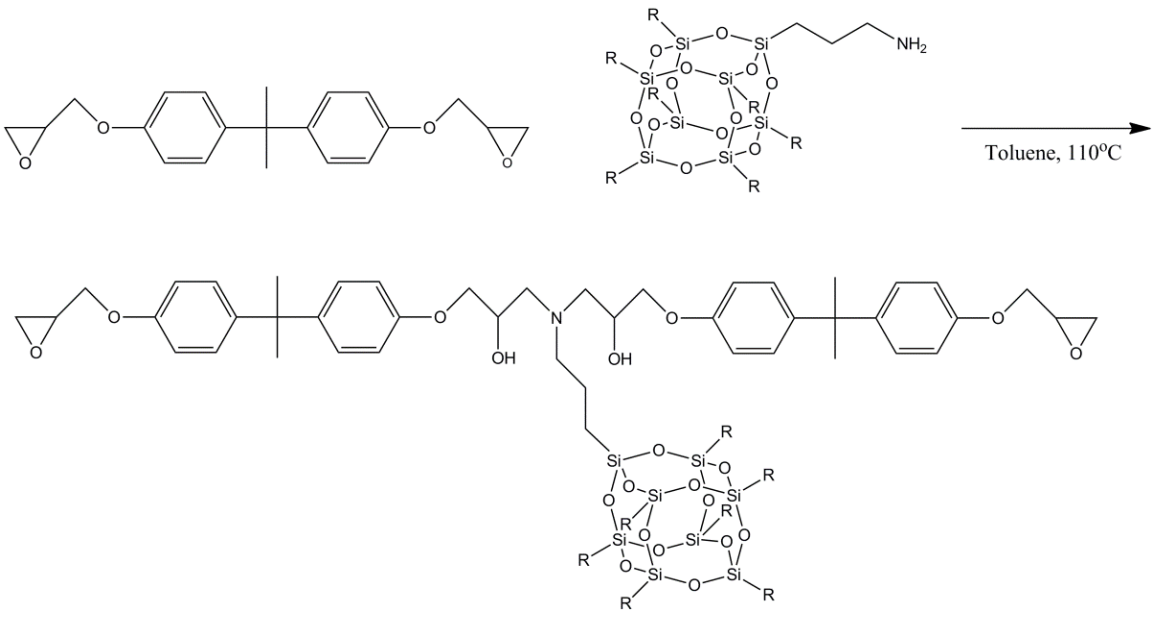

Figure 19. POSS pre-reaction scheme.

Epoxies were formulated with the POSS pre-reaction product mixture in quantities necessary to achieve the target POSS concentrations. The cured samples are listed in Table 1. The known initial concentrations of DGEBA and AI-POSS in the product mixture were used for stoichiometric calculations. All samples were formulated with a 1-1.05:1 ratio of oxirane to active hydrogen. To obtain a sample with 2.5 weight percent POSS, 3.79 g POSS pre-reaction product, 18.71 g DGEBA, and 7.50 g 3,3'-DDS were charged to a round-bottom flask. The flask was fitted with a magnetic stir bar and immersed in an oil bath pre-heated to 60 °C. The contents were slowly heated to 90 °C while degassing under vacuum. The contents were stirred under vacuum at 90 °C for 1 h, at 100 °C for 1 h, and at 110 °C for 30 min. At that time, the mixture was cast into pre-heated silicone molds. This process was repeated for the 10% pre-reacted POSS sample (10POSS-PR) using 15.18 g POSS product mixture, 8.14 g DGEBA, and 6.68 g 3,3'-DDS. The samples with pre-reacted POSS are listed in Table 8.

Table 8

DGEBA/DDS Samples with Pre-reacted POSS (discussed in Chapter VI)

Sample Name	POSS Loading (weight percent)	Epoxy Matrix	Curing Prescription
2.5POSS-PR_125	2.5	DGEBA/3,3'-DDS	5 h at 125 °C, 2 h at 200 °C
2.5POSS-PR_180	2.5	DGEBA/3,3'-DDS	3 h at 180 °C
10POSS-PR_125	10	DGEBA/3,3'-DDS	5 h at 125 °C, 2 h at 200 °C
10POSS-PR_180	10	DGEBA/3,3'-DDS	3 h at 180 °C

POSS trimer. A series of epoxies based on DGEBF/3,'3-DDS was formulated using a POSS trimer molecule (shown in Figure 17). The samples were mixed, cast, and cured using the procedure described for other POSS-modified epoxies. The samples are listed in Table 9.

Table 9

DGEBF/DDS Samples with $POSS_{trimer}$ (discussed in Chapter VII)

Sample Name	POSS Loading (weight percent)	Epoxy Matrix	Curing Prescription
$0.5POSS_{trimer}$	0.5	DGEBF/3,3'-DDS	4 h at 180 °C
$1.0POSS_{trimer}$	1.0	DGEBF/3,3'-DDS	4 h at 180 °C
$1.5POSS_{trimer}$	1.5	DGEBF/3,3'-DDS	4 h at 180 °C

Table 9 (continued).

Sample Name	POSS Loading (weight percent)	Epoxy Matrix	Curing Prescription
2.0POSS$_{trimer}$	2.0	DGEBF/3,3'-DDS	4 h at 180 °C
2.5POSS$_{trimer}$	2.5	DGEBF/3,3'-DDS	5 h at 180 °C
5.0POSS$_{trimer}$	5.0	DGEBF/3,3'-DDS	5 h at 180 °C
7.5POSS$_{trimer}$	7.5	DGEBF/3,3'-DDS	5 h at 180 °C
10POSS$_{trimer}$	10	DGEBF/3,3'-DDS	5 h at 180 °C

Characterization

Near-Infrared Spectroscopy (IR)

Near-IR spectra in transmission mode were recorded using a Thermo Scientific Nicolet 6700 FT-IR in the range of 4000-8000 cm^{-1}. A white light source was used in conjunction with a KBr beam splitter and a DTGS KBr detector. Samples were prepared by placing uncured resin between glass slides separated by a 0.8mm Teflon spacer. The reaction progressed according to varying curing prescriptions in a Simplex Scientific Heating Cell. Thirty-two scans at 4 cm^{-1} resolution were acquired every 15 minutes during cure.

IR spectra were analyzed using the method developed by Min et al.[36] and used extensively in epoxy-amine research.[25,35,37,40] In this method, peaks corresponding to amine and epoxide moieties are integrated. The total absorbance of the peak (integral) is related to concentration using the following form of the Beer-Lambert law:

$$A = \varepsilon c l$$

where A is the total absorbance, ε is the molar absorptivity of the functional group in mol kg^{-1} cm^{-1}, c is the concentration of the functional group in kg mol^{-1}, and l is the path length (sample thickness) in cm. The peaks of interest in these reactions and their integral areas are listed in Table 10.

Table 10

Near-IR Peak Integral Areas for Epoxy-Amine Cure Process

Peak	Integral area (cm^{-1})
Epoxide	4495-4555
Aromatic region	4600-4640
1° amine	5110-5035
1° amine + 2° amine	6550-6760

Prior to analysis, spectra were normalized using the aromatic region at 4600-4640 cm^{-1}. All calculations were made assuming zero conversion (i.e., assuming that no functional groups had reacted) at the start of the test. Secondary amine absorptivity was calculated from the absorbance at 6550-6760 at 30 min, with the assumptions that all 1° amine consumed in the first 30 min converted to 2° amines and that no 2° amine converted to 3° amine during that time.

Broadband Dielectric Resonance Spectroscopy (DRS)

The Netzsch DEA 230/1 Epsilon DS system was used to accurately measure the shift in molecular dynamics during thermoset resin cure. All sensors were calibrated in air for specific values of gain and phase provided by Netzsch before use.

DRS was conducted using a new dielectric analyzer, the Netzsch DEA 230/1 Epsilon, developed by Netzsch Instruments. The new analyzer uses remote interdigitated electrode sensors (IDEX sensors) instead of the conventional parallel plate electrodes. The interdigitated sensors can be used in a variety of processing and temperature conditions. For these experiments, the sensor was coated in a small amount of uncured resin and placed in an oven with precise thermal control for the duration of the experiment. The uncured material was subjected to a standard cure profile. The changes in dielectric variables including storage permittivity (ε') and loss permittivity (ε'') were recorded as a function of time at frequencies of 1-10 Hz. All sensors were calibrated in air, for specific values of gain and phase provided by Netzsch, before usage.

Dynamic Scanning Calorimetry (DSC)

DSC was performed on cured and uncured epoxy samples using a TA Instruments Q200 DMA. Samples were prepared by sealing 5-10 mg of material in an aluminum pan. Cured samples were cycled from 40 °C to 250 °C to 40 °C three times at a heating rate of 10 °C/min. Glass transition temperature (T_g) was calculated as the midpoint of the change in slope in the heating curve. If T_g did not increase by more than 10 °C between the first and last scans, the material was said to be fully cured.

DSC testing of uncured epoxy material was conducted using a nonisothermal protocol. The temperature was ramped from 40 °C to 350 °C at rates of 5, 10, 15, and 20 °C/min. The total heat of the cure reaction (ΔH) was calculated from the area under the exotherm curve in the DSC scan. Isoconversional analysis using the Flynn-Wall-Ozawa equation was applied to the DSC data to determine activation energy as a function of conversion.

Dynamic Mechanical Analysis (DMA)

Dynamic mechanical properties, including storage modulus (E') and thermomechanical T_g, were measured with a Thermal Analysis Q800 DMA in tensile mode with a strain amplitude of 0.05% and a frequency of 1 Hz. Temperature was ramped from 50 °C to 300 °C (POSS materials) or 350 °C (epoxy blends) at a rate of 3 °C/min.

Mechanical Testing

Compression tests were conducted on cylindrical samples 0.90-1.00 inches long, with the diameter equal to half the length (0.45-.50 inches). Testing was performed using an MTS 810 hydraulic test frame with a cylindrical compression sub-press supplied by Wyoming Test Fixtures, in accordance with the method proscribed by ASTM 695-02a. The displacement was 0.050 in/min and tests were terminated at 20% strain.

Positron Annihilation Lifetime Spectroscopy (PALS)

Samples for PALS analysis were cast as circular discs with average diameters in the range of 9.5-9.9 mm and thicknesses of ~1-2 mm. Two identical pieces of epoxy sandwiched a 5 μCi ^{22}Na positron source that was sealed between two sheets of 13 μm thick kapton (kapton stops ~ 5% of the positrons but produces no positronium signal). After wrapping in aluminum foil this two-sided sample-source arrangement was placed in a small vacuum canister (pumped to ~ 10^{-2} torr by a mechanical rotary pump). This evacuated source chamber was located between the fast plastic gamma detectors of a typical PALS spectrometer with time resolution of 280 ps. A lifetime spectrum with 4-5 million events was acquired in about 20 hours. Standard discrete lifetime fitting showed that only one positronium lifetime in the range 1.6 ns to 1.8 ns was required for adequate

fitting and the relative intensity of this positronium component was ~20% for all the samples. The fitted positronium lifetime for each sample was then converted to an average spherical free volume using the well known Tao-Eldrup model.[99,100]

Pressure-Volume-Temperature (PVT) Dilatometry

PVT measurements were conducted on an automated GNOMIX PVT high pressure dilatometer, with mercury as the confining fluid. Samples were machined into cylinders measuring 20.0 mm in length and 10.0 mm in diameter. Experiments were run in isothermal mode, for temperatures ranging from 30-310 °C with a temperature increment of 20 °C. Pressures were varied from 10-150 MPa. Specific volumes at the applied pressures were measured with an accuracy of ± 0.0002 cm^3/g. Specific volumes for atmospheric pressure were then extrapolated automatically by the GNOMIX software using the Tait equation.[101] Specific free volumes were calculated at 30 °C from the measured macroscopic volume determined from the PVT dilatometer, using the Simha-Somcynsky lattice hole theory.[102,103,104] Data was not available for samples with T_g's higher than 210 °C due to degradation. PVT analysis requires dilatational data at least 40 °C above T_g, and epoxies are known to degrade at ~250 °C.[105,106]

Density

Densities at ambient conditions for each of the samples were determined using a XS104 Mettler Toledo microbalance with a density determination feature based on Archimedes' principle. The measurements were conducted at 21 °C in air and deionized water with an accuracy of ± 0.002 cm^3/g.

Fluid Uptake

Fluid uptake studies were conducted using water, MEK, and acetone. Rectangular epoxy samples having mass of approximately 300 mg and thickness of 1.5 mm were conditioned in a vacuum oven for 12 hours at 100 °C prior to measuring initial weights. Dry polymer samples were placed in 20 mL scintillation vials containing ~15-18 mL of fluid. The vials were sealed and stored at 25 °C in a Fisher Scientific Model 146E incubator. To measure fluid uptake, samples were periodically removed from solution, patted dry, and weighed to the nearest 0.1 mg. Percent change in mass for each sample was calculated as follows:

$$\%\ Change\ in\ Mass = \frac{m_w - m_i}{m_i} \times 100$$

where m_w is the wet mass and m_i is the initial mass. Four samples were averaged to give each data point. Diffusivity was calculated from plots of normalized absorption versus $t^{1/2}$, using the following equation:

$$\frac{M_t}{M_{inf}} = \frac{4}{L}\sqrt{\frac{Dt}{\pi}}$$

where M_t is the water absorption at time t, M_{inf} is the equilibrium water absorption, and L is half the sample thickness (to account for diffusion from both sides).

Size Exclusion Chromatography (SEC)

Molecular weights (M_n and M_w) of DGEBA/AI-POSS oligomers were determined by SEC using a TOSOH Bioscience EcoSEC HLC-8320 gel permeation chromatography system. THF was used as an eluent and polystyrene was used as the standard. The eluents were monitored with a refractive index detector and a UV detector at 254 nm.

Scanning Electron Microscopy (SEM)

The morphologies of the epoxy-POSS compositeswere studied via SEM. Cured samples were fractured under cryogenic conditions using liquid nitrogen and the fracture surfaces were sputter-coated with gold. The sputtered samples were examined using an FEI Quanta 200 SEM in high vacuum mode with an accelerating voltage of 20 kV. Particle and agglomeration sizes were measured for some micrographs using an image analysis software package (ImageJ, National Institutes of Health). Energy dispersive X-ray analysis (EDX) was performed on the bulk epoxy and on microstructural features to determine elemental composition.

Transmission Electron Microscopy (TEM)

The morphology of epoxy matrices modified with 2.5 weight percent POSS in a DGEBA/DDS matrix was investigated using a Zeiss 900 transmission electron microscope (Carl Zeiss, Inc., Thornwood, NY) at an accelerating voltage of 50 kV. Samples were cut into ultrathin (≈100 nm), trapezoidal-shaped sections with a Porter-Blum MT-2B ultramicrotome (Ivan Sorvall, Inc.), using a diamond knife (Micro Star Technologies, Inc.) at room temperature. Sections were collected on a Formvar-coated, 300 mesh copper TEM grid (Electron Microscopy Sciences) and imaged without staining. The particle size distribution for each micrograph was calculated using the ImageJ software package.

^{29}Si Nuclear Magnetic Resonance (NMR) Spectroscopy

Silicon spectra were obtained for the POSS pre-reaction product using a BrukerAvance III NMR spectrometer operating at a frequency of 119.23 MHz. Acquisition parameters included a pre-scan delay of 74.34 s and an acquisition time of

0.66 s, yielding a 75 s delay between transients. The 90º pulse width was 14 μs, with 72 scans accumulated for the reagent and 512 scans for the product. Composite pulse decoupling was used to remove proton coupling, with the 1H decoupler gated off between scans to prevent negative NOE enhancements. Peak referencing was done externally using the glass peak due to the NMR tubes (-115.0 ppm).

CHAPTER III

CURE KINETICS AND ARCHITECTURAL DEVELOPMENT IN EPOXIES MODIFIED WITH BULKY AMINES

Abstract

The effect of bulky pendant groups on epoxy network growth was evaluated by characterizing the cure process with complementary techniques. Epoxies based on DGEBA and 33DDS were modified with 5-10 weight percent napthylamine (NA) and adamantylamine (AA). The cure process was analyzed via near-IR spectroscopy, broadband dielectric spectroscopy (DRS), and dynamic scanning calorimetry (DSC) with isoconversional analysis. IR results indicated increased "microgel-type" growth for the samples with 10% NA and AA, compared to more "linear-type" growth for the DGEBA benchmark material. The loss factor curves obtained via DRS suggested two separate steps in the network-forming process all of the materials except the 10% NA sample, which exhibited one prolonged step. The two steps were presumed to be the 1° amine-epoxy and 2° amine-epoxy reactions, which are simultaneous in microgel-type growth. Plots of E_a vs. conversion, generated from DSC results, indicated a pronounced autocatalytic effect in the 10% NA sample that was not present for other materials. The enhanced autocatalytic activity in that sample was attributed to the increased basicity of 3° amines based on NA. The autocatalyzed etherification reaction occurred throughout the cure, obscuring the two separate reaction steps apparent in the other samples.

Results and Discussion

DGEBA-33DDS epoxies were modified with two bulky amines, naphthylamine (NA) and adamantylamine (AA). The cure kinetics of the resins were characterized via

near-infrared (IR) spectroscopy, broadband dielectric relaxation spectroscopy (DRS), and nonisothermal dynamic scanning calorimetry (DSC). These are complementary techniques, measuring concentration of functional groups, polarity and molecular mobility, and extent of reaction as a function of cure time. The following cure profile was used: 5 h cure at 125 °C followed by 2 h postcure at 200 °C (180 °C postcure for DRS). The cure kinetics of the resin were altered by NA and AA in ways observable using all three techniques. Hole size (V_h) data, obtained with position annihilation lifetime spectroscopy (PALS), provided insight into changes in architecture of the cured networks as a result of their different cure kinetics.

IR Results

Concentration of epoxide, primary amine, and secondary amine groups were recorded as a function of reaction time during the cure process. Linear-type or microgel-type network growth can be inferred from the concentration profiles of these functional groups. In the extreme case of linear-type growth, all primary amine moieties react to form secondary amines *before* secondary amines react to form tertiary amines. This behavior is manifested in the IR results as a distinctive "hump" in the secondary amine concentration curve, as this 2° amine is first generated and then consumed. In the extreme case of microgel-type growth, primary and secondary amine reactions occur simultaneously. This behavior is manifested in the IR results as a broad, flat plateau in the secondary amine concentration curve, as secondary amine groups are concurrently generated and consumed. Linear-type and microgel-type growth can produce networks with different architectures and therefore different properties.

The IR cure profile for DGEBA (shown in Figure 20) exhibits mostly linear-type growth, as evidenced by the characteristic secondary amine hump. Early in the reaction, 1° amine concentration dropped to zero and 2° amine concentration rose to its maximum value (at t = 120 min). As the reaction proceeded, the 2° amine concentration decreased, eventually reaching zero in the postcure. A concentration of zero for amine and epoxide groups after 7 h signified complete conversion of monomers to crosslinked epoxy.

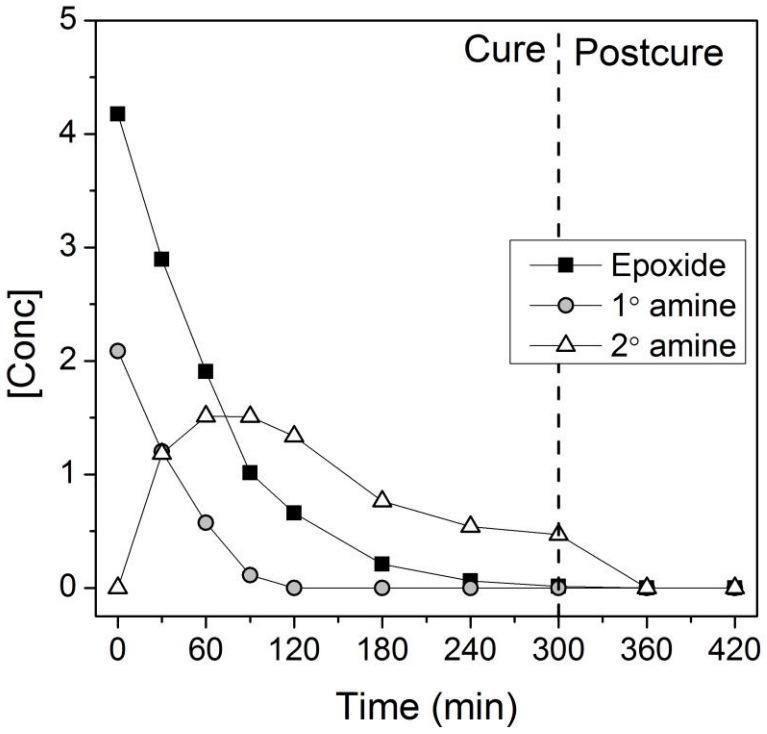

Figure 20. Epoxide, 1° amine, and 2° amine concentration vs. time for DGEBA-DDS.

The secondary amine hump was less pronounced in the epoxies containing 5 and 10 weight percent AA. In the 5% AA sample (Figure 21a), a small peak was discernible in the 2° amine concentration at t = 75 min. In the 10% AA sample (Figure 21b), the peak in the 2° amine concentration had broadened, and the maximum concentration was lower. Full conversion of functional groups was achieved in both epoxies.

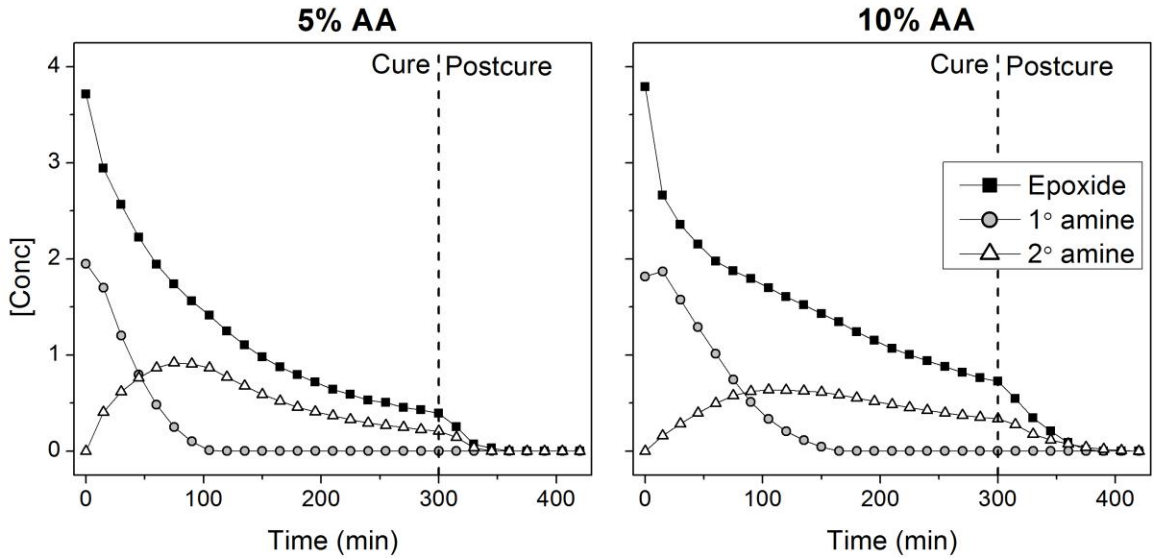

Figure 21. Epoxide, 1° amine, and 2° amine concentration vs. time for epoxy with (a) 5% AA and (b) 10% AA.

The secondary amine curves of the AA-modified epoxies are compared directly in Figure 22. The peak shape for the 5% AA sample was similar to the peak shape for unmodified DGEBA, indicating similar growth kinetics. Between the two AA samples, the 2° amine curve broadened and decreased in intensity as AA concentration increased from 5% to 10%. Overall, the changes in curve shape indicated that network growth switched from a linear-type scheme to a microgel-type scheme when AA content was increased to 10%.

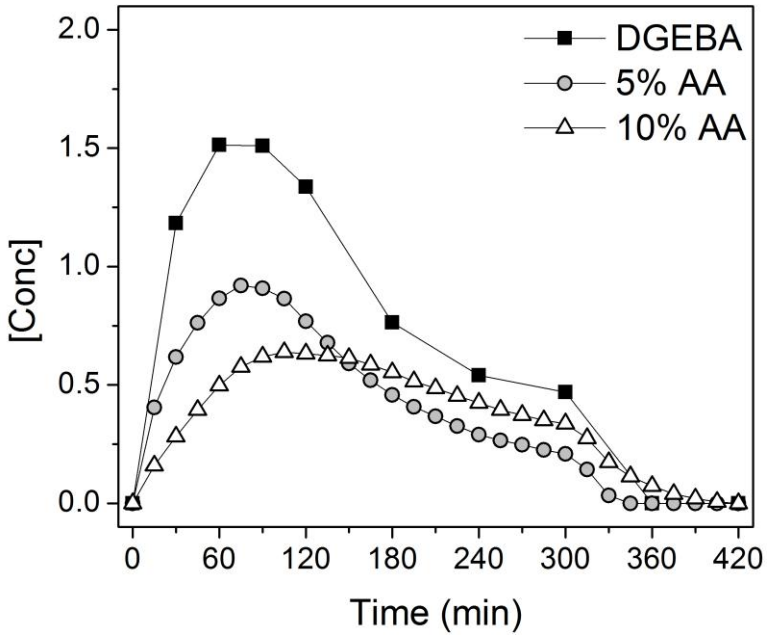

Figure 22. 2° amine concentration vs. time for epoxies with 0, 5, and 10% AA.

The IR cure profiles of the samples modified with NA are shown in Figure 23. The sample with 5% NA had a slight peak at t = 60 min, but 2° amine persisted until the end of the cure cycle (Figure 23a). The epoxide peak reached zero at the end of the postcure, indicating that some etherification occurred in this epoxy. The sample with 10% NA had a broad 2° amine plateau indicative of microgel-type growth, with complete conversion of all functional groups at the end of the postcure (Figure 23b). The broadening of the 2° amine peak with NA concentration is illustrated in Figure 24. Secondary amine concentration did not reach zero in the NA-containing samples until at least 420 min, compared to 360 min in the DGEBA specimen.

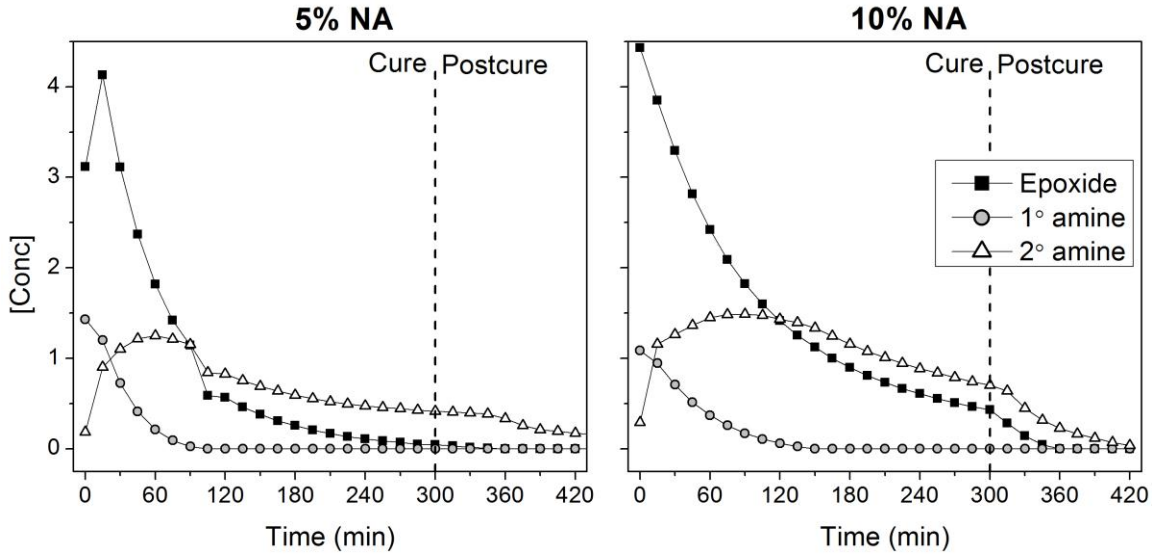

Figure 23. Epoxide, 1° amine, and 2° amine concentration vs. time for epoxy with (a) 5% NA and (b) 10% NA.

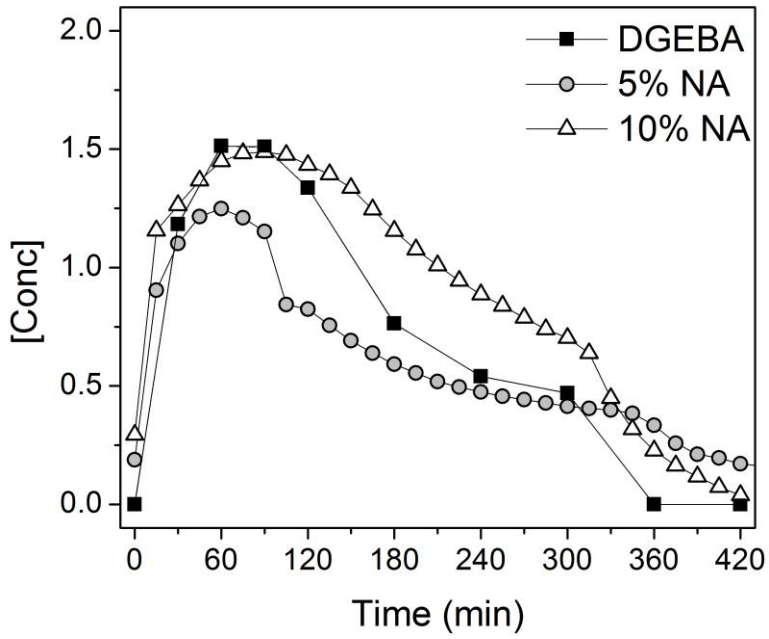

Figure 24. 2° amine concentration vs. time for epoxies with 0, 5, and 10% AA.

The IR results illustrated subtle changes in network growth kinetics for the AA- and NA-modified epoxies. For the AA-modified epoxies, network growth in the 5% AA sample was similar to the DGEBA sample, with linear-type growth. When AA concentration increased to 10%, the network growth shifted to a more microgel-type

regime. For the NA-modified epoxies, network growth in both samples was more microgel-like than the DGEBA benchmark. Differences in cure behavior between NA and AA materials were also observed via DRS and DSC.

DRS Results

Dielectric spectroscopy is an appealing candidate for studying network development. Permittivity is a measure of the electric susceptibility of a material, i.e., its ability to transmit an electric field.[107] Permittivity in polymers is greatly affected by the polarizability and the molecular mobility of the system. In DRS analysis, an oscillating electric field is applied to the sample and the complex permittivity (ε^*) is measured. The process is analogous to dynamic mechanical analysis, in which an oscillating mechanical strain is applied to the sample and the complex modulus is measured. The complex permittivity measured by DRS can be resolved into relative permittivity (ε') and loss factor (ε'') components.[108]

The relative permittivity and loss factor are very sensitive to changes in a dielectric material that affect the speed and strength to which it responds to an electrical field.[109] A highly polar material whose polar moieties have great mobility will respond more rapidly and more strongly to an applied electric field than a nonpolar material with restricted chain motions. In an epoxy system, polarizability and molecular mobility both decrease as the system transitions from monomers to gel to solid state. Hence changes in ε' and ε'' can be correlated to important developments in network architecture in the course of the cure process.[110] As epoxy and amine monomers react, their polarity and polarizability decrease as primary amines and epoxides become tertiary amines and hydroxypropylether moieties. The shift from individual monomers into a crosslinked

network hinders molecular motion. Hence decreases in ε' indicate progression of network growth. Peaks in the ε'' curve correspond to dipolar relaxation. In epoxy-amine cure studies, these relaxations have been attributed to irreversible chemical reactions.[111]

Further insight into network structure can be provided by varying the frequency of analysis. Different frequencies probe different timescales of motion; therefore peaks at different frequencies correspond to different sets of molecular motion.[108] DRS has been used to characterize the cure of epoxy-amine systems under a variety of conditions.[41,42,43,44]

The relative permittivities of AA-modified samples are shown in Figure 25. Permittivity decreased sharply after ~40 min. This decrease was attributed to the onset of gelation, at which point dipole motion became severely hindered. The postcure temperature was chosen because it was higher than the T_g of the epoxies. Returning the material to a rubbery state enables the completion of crosslinking reactions, which generally slow or cease after vitrification in the cure phase. Permittivity rose slightly at the beginning of the postcure due to the increased temperature of the system, but continued to decrease as crosslinking reactions proceeded.

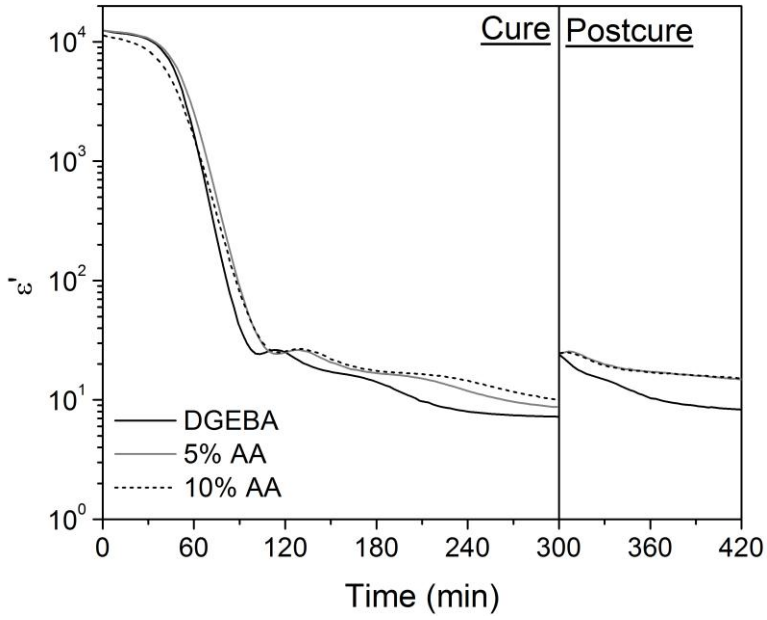

Figure 25. *ε'* vs. time for epoxies with 0, 5, and 10% AA.

The loss permittivities for AA-modified samples are shown in Figure 26. The first peak in the *ε"* curve for the AA samples occurred at ~40 min. This peak was attributed to a gelation phenomenon. Gelation, defined traditionally as a sharp decrease in macroscopic viscosity, is not always visible in DRS spectra; more often, the "gelation" observed in DRS relates to a sharp decrease in ionic viscosity.[112] After gelation, *ε"* decreased for all samples as chain motions became increasingly hindered. In the DGEBA sample, *ε"* began to rise again at ~170 min, resulting in a second small peak at t = 186, and then continued to decrease for the remainder of the cure.

A second peak in the loss permittivity curve generally signifies a second step in the reaction, due to relaxations associated with the new reaction step. The second peak in this case was considered in light of IR results, which suggested that DGEBA undergoes linear-type network growth. In that growth scheme, linear chains form from 1° amine-epoxy reactions, and those chains are eventually crosslinked together via 2° amine-epoxy reactions. Therefore the second step in the DGEBA cure process (as signified by a second

peak in the ε" curve) may be attributable to crosslinking of linear chains. A second peak was also observed for the samples with 5% and 10% AA, indicating a second step in those reactions as well. The quasi-linear two-step mechanism inferred from DRS for those materials is consistent with IR results.

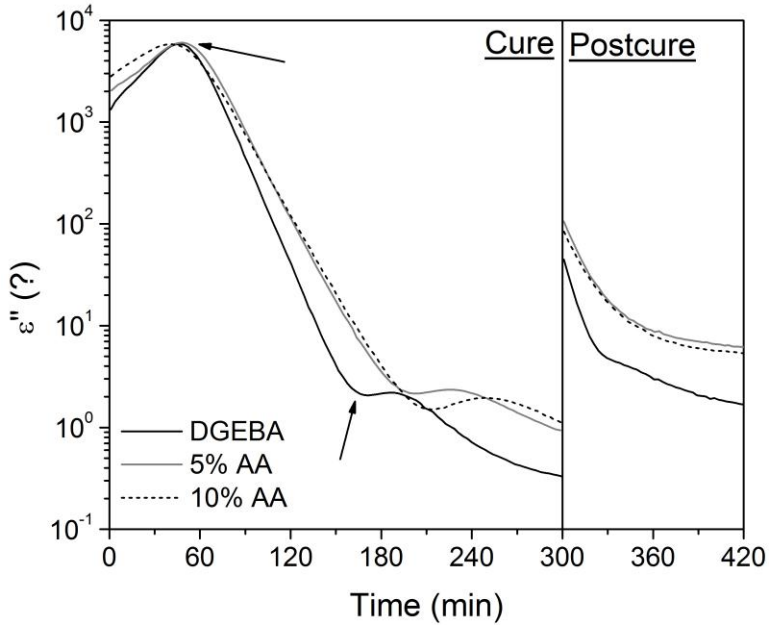

Figure 26. ε" vs. time for epoxies with 0, 5, and 10% AA.

At the onset of the postcure, initial ε" values were higher for all the epoxies due to the elevated temperature (Figure 26). The loss factor immediately decreased for all samples during the beginning of the postcure as crosslinking proceeded.

In both the cure and postcure regions, the ε"curves for 5% AA and 10% AA were very similar to each other and somewhat different from the ε" curve for DGEBA. This result suggests that the cure process changes slightly when 5% AA is added to the DGEBA epoxy, but the process does not change further with increased AA. The second peak in the spectra for AA samples occurred at a later time than the corresponding peak in the DGEBA spectrum. The delay in onset of the second peak may be due to the

gradual shift towards more microgel-type growth in the AA epoxies. With more microgel-type growth, the separation between the first step of the reaction (linear chain growth) and the second step (crosslinking) may have become less well-defined.

The relative permittivities of NA-modified samples are shown Figure 27. The same general trends in ε' vs. time during the cure and postcure of AA were observed for NA. The sharp decrease in ε' at the beginning of the reaction was attributed to gelation, while gradual decreases in ε' throughout the cure and postcure were attributed to network growth.

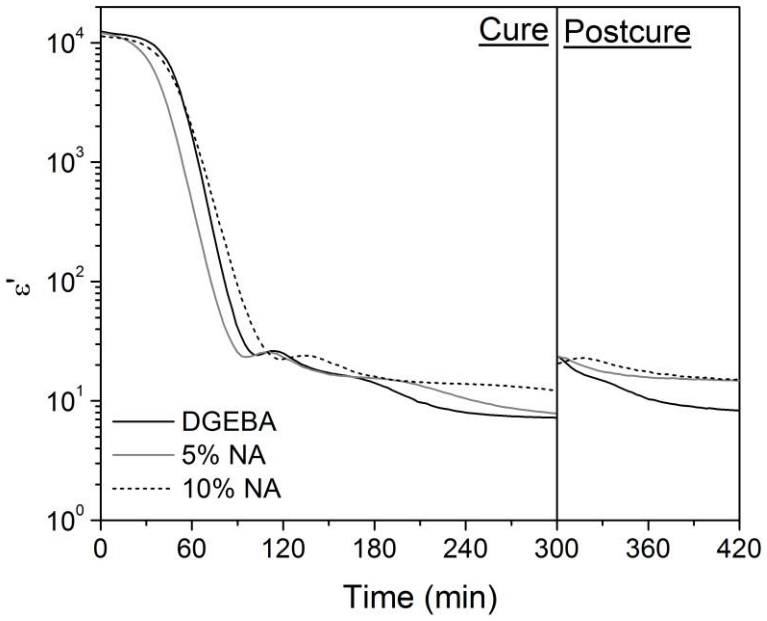

Figure 27. ε' vs. time for epoxies with 0, 5, and 10% NA.

The ε'' curves for the cure profiles of the NA epoxies, shown in Figure *28*, were somewhat different than the ε'' curves for the AA samples. The sample with 5% NA had a similar profile to the DGEBA material, with two peaks attributed to gelation (earlier peak) and crosslinking of linear chain segments (later peak). The sample with 10% NA did not have a distinct second peak. Instead, the first peak was considerably broader. Loss permittivity began to increase again towards the end of the

cure cycle, suggesting a second peak may have developed at t > 300 min if the cure step had continued.

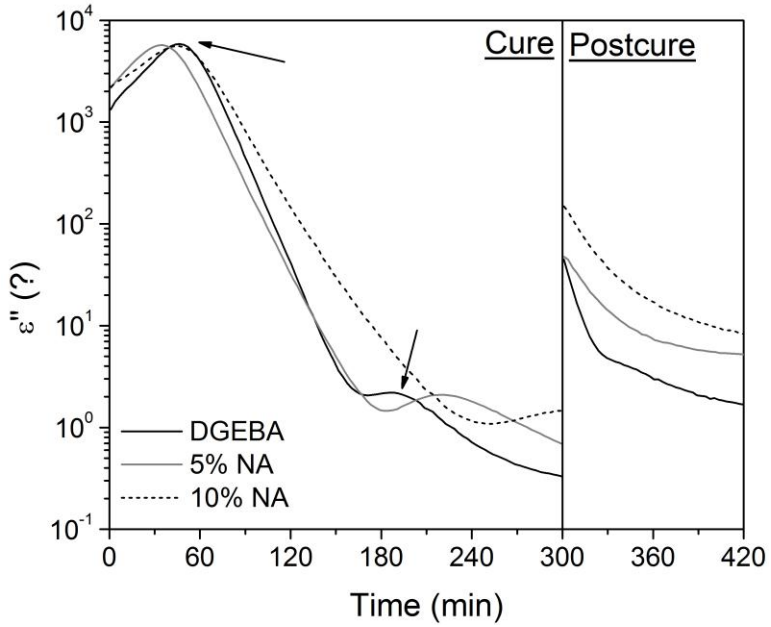

Figure 28. *ε"* vs. time for epoxies with 0, 5, and 10% NA

The single broad peak for 10% NA, compared to two distinct peaks in DGEBA and 5% NA, was attributed to microgel-type growth. It is possible that primary and secondary amines reacted simultaneously, producing highly-crosslinked microgels from the beginning of polymerization. This process could not be resolved into two separate steps in 300 min. The onset of a second peak in *ε"* at ~240 min may have been due to reactions between microgels as they began to impinge on each other. Overall, the loss permittivity curves for DGEBA, 5% NA, and 10% NA were all slightly different. This difference suggests a continuous change in network growth kinetics (and therefore final architecture) with NA addition.

Additional insight into network cure kinetics can be obtained from DRS frequency sweeps. When spectra at different frequencies and a constant temperature are

evaluated, the relationship between frequency (f) and time of maximum ε'' value (t_{max}) is as follows:

$$f = f_0 \exp(-k t_{max})$$

where f_0 and k are constants determined empirically from plots of ln(f) vs. t_{max}.[111,113] The k obtained from this analysis is a rate constant associated with the process that produces the ε'' peak. In this case, k was presumed to relate to the onset of gelation as a result of network growth.

The frequency sweep for unmodified DGEBA is shown in Figure 29. The ε''peak shifted to lower times as frequency increased. This shift was expected, based on fundamental understanding of $\varepsilon''$and molecular motions. The ε''peak corresponds characteristic relaxation time for a given frequency. Shorter timescales of motion are probed by analysis at higher frequencies. Shorter timescales of motion generally correspond to smaller or less hindered molecules. Therefore the ε'' peak measured at 10 Hz occurred early in the reaction, when molecular mobility in the system was higher with a short characteristic relaxation time, and the ε'' peak measured at 1 Hz occurred later in the reaction, when molecular mobility in the system was lower with a long characteristic relaxation time.

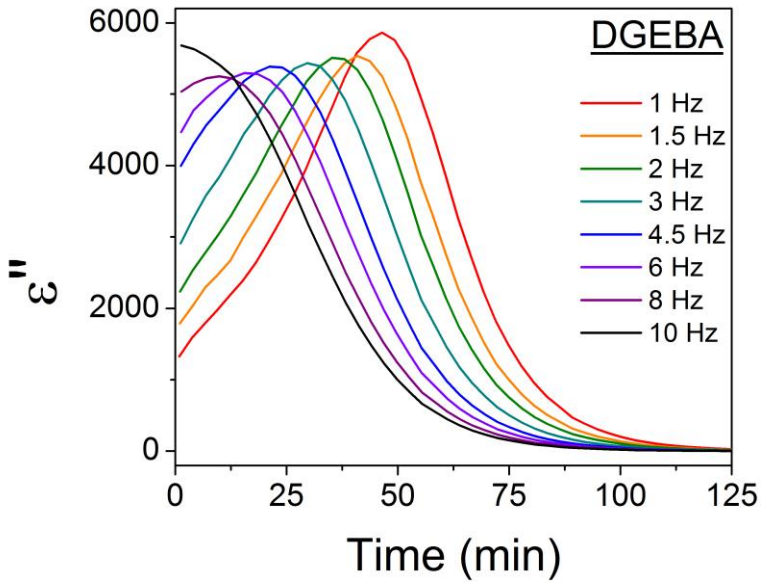

Figure 29. *ε"* vs. time for DGEBA-DDS at 125 °C and frequencies of 1-10 Hz.

The frequency sweeps for the AA-modified epoxies are shown in Figure 30. These *ε"* peaks showed the same qualitative frequency dependence as the DGEBA sample, with peaks in loss permittivity occurring at shorter times for higher frequencies. The same trend was observed for the NA-modified epoxies, shown in Figure 31.

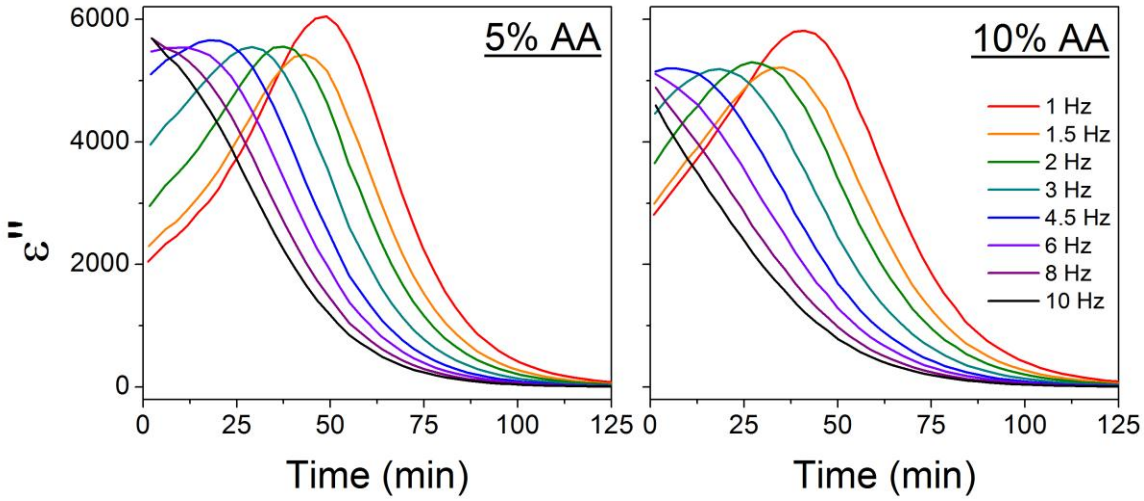

Figure 30. *ε"* vs. time for epoxies with (a) 5% AA and (b) 10% AA, at 125 °C and frequencies of 1-10 Hz.

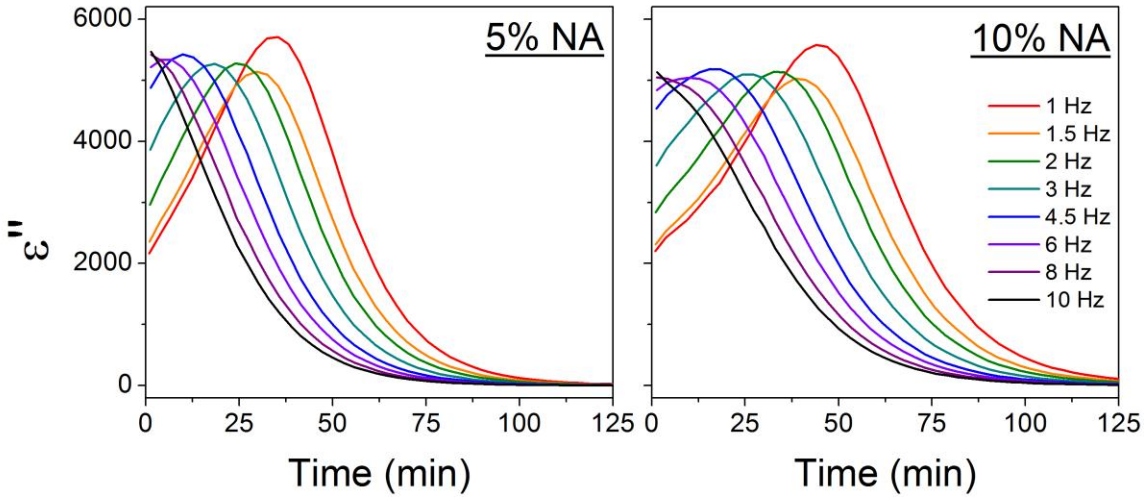

Figure 31. *ε"* vs. time in epoxies with (a) 5% NA and (b) 10% NA, at 125 °C and frequencies of 1-10 Hz.

The rate constant for gelation was determined from plots of *f* vs. t_{max} for the *ε"* peaks. The plots for AA (Figure 32) and NA (Figure 33) exhibited a strong linear correlation between *f* and t_{max}, as expected. The rate constants (*k*) and pre-exponential factors (f_0) for the epoxies are listed in Table 11.

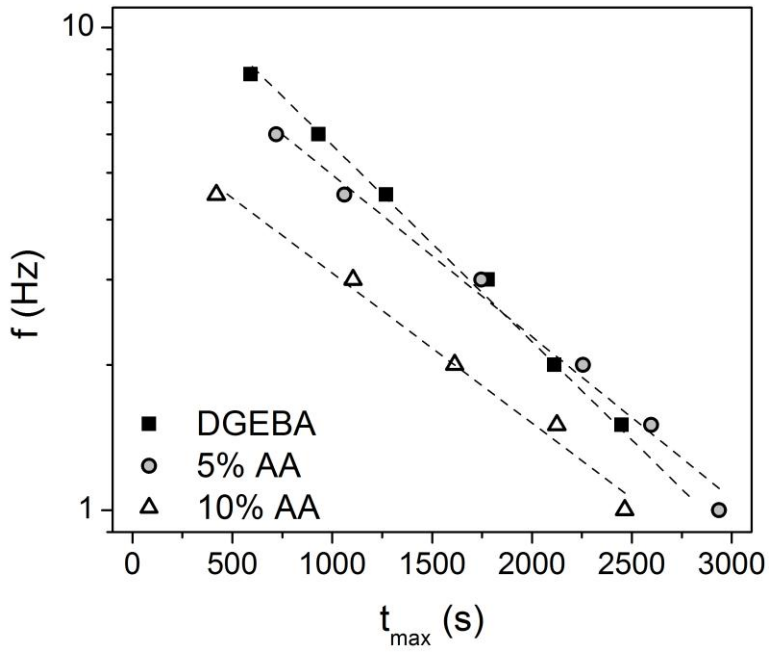

Figure 32. *f* vs. t_{max} for frequency sweep of epoxies with 0-10% AA at 125 °C.

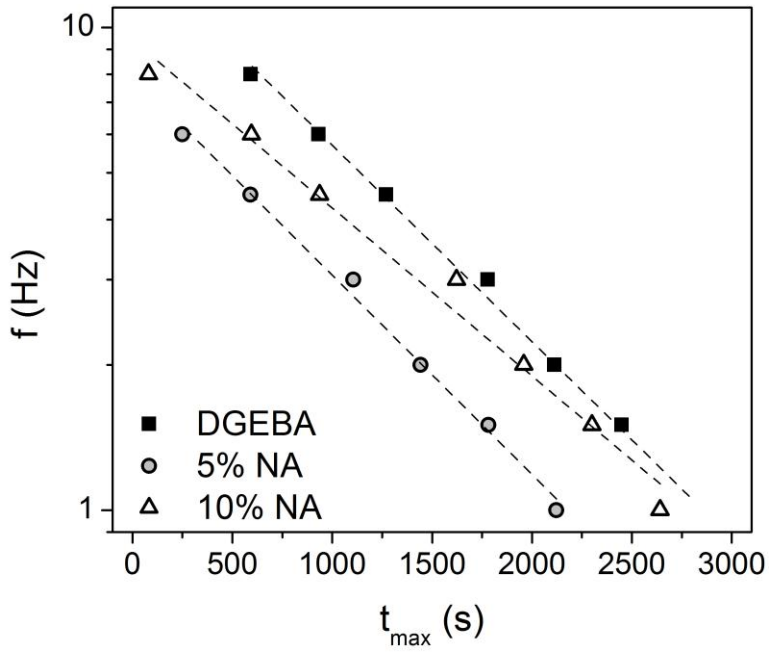

Figure 33. *f* vs. t_{max} for frequency sweep of epoxies with 0-10% NA at 125 °C.

Table 11

Rate Constants and Pre-exponential Factors for Gelation Peak in ε" Curves

Sample	k (s^{-1})	f_0 (Hz)	Sample	k (s^{-1})	f_0 (Hz)
DGEBA	9.37×10^{-4}	14.5	DGEBA	9.37×10^{-4}	14.5
5% AA	7.72×10^{-4}	10.7	5% NA	9.50×10^{-4}	7.9
10% AA	7.16×10^{-4}	6.3	10% NA	8.01×10^{-4}	9.4

The characteristic rate of gelation decreased with AA content, from 9.37×10^{-4} s^{-1} for DGEBA to 7.16×10^{-4} s^{-1} for 10% AA. The decrease in gelation rate may be due to the average functionality of the system, which decreased as tetrafunctional DDS was replaced with difunctional AA. According to classical understanding of functionality and

gel point, a decrease in average functionality is expected to delay the onset of gelation.[14,15]

A clear trend was absent for the rate data for NA materials, which increased for 5% NA and decreased for 10% NA. The initial increase in gelation rate may have been due to pi-pi stacking between NA and aromatic groups in the network backbone. The pi-pi interactions may have functioned as physical crosslinks, resulting in an increase in apparent rate of gelation. However, at sufficient NA content, the effect of decreased average functionality may have overcome the effect of increased physical crosslinking, resulting in an ultimate decrease in gelation rate.

DSC Results

Isoconversional analysis was applied to nonisothermal DSC data to generate plots of activation energy vs. conversion. This treatment provides for an investigation of changes in reaction mechanism without requiring a kinetic model. The isoconversional method was developed by Vyazovkin and Sbirrazzuoli[39,114] and is now widely used throughout the polymer community.[45,46,47] This approach is an elaboration on the well-known Flynn-Wall-Ozawa (FWO) and Kissinger-Akahira-Sunose (KAS) methods for determining E_a from DSC data.

In the FWO method, uncured material is subjected to temperature ramps at different heating rates, and E_a is determined from the following equation:

$$\log(\beta) = \frac{-1.052E_a}{RT} + A'$$

where β is the heating rate in K s^{-1}, T is the temperature in K of the center of the exotherm peak, and R is the universal gas constant. In the isoconversional method, conversion is calculated as a function of temperature. For each degree of conversion (α)

evaluated, the *T* in the FWO equation is the temperature at which that conversion is reached.

This process is illustrated below for DGEBA. The baseline-corrected exothermic peaks for four heating rates (Figure 34a) were integrated to give a total heat of reaction, ΔH, for each scan. The integral value for each temperature was divided by ΔH to determine conversion as a function of temperature (Figure 34b). Conversions of 10-90% were evaluated for this experiment. For each conversion level, the temperature at which that conversion was reached (*T*) was calculated for each heating rate (β). Plots of ln(β) vs. 1/*T* were approximately linear for each conversion, as shown in Figure 35. Activation energy was calculated from the best-fit lines of these plots, according to the FWO equation above.

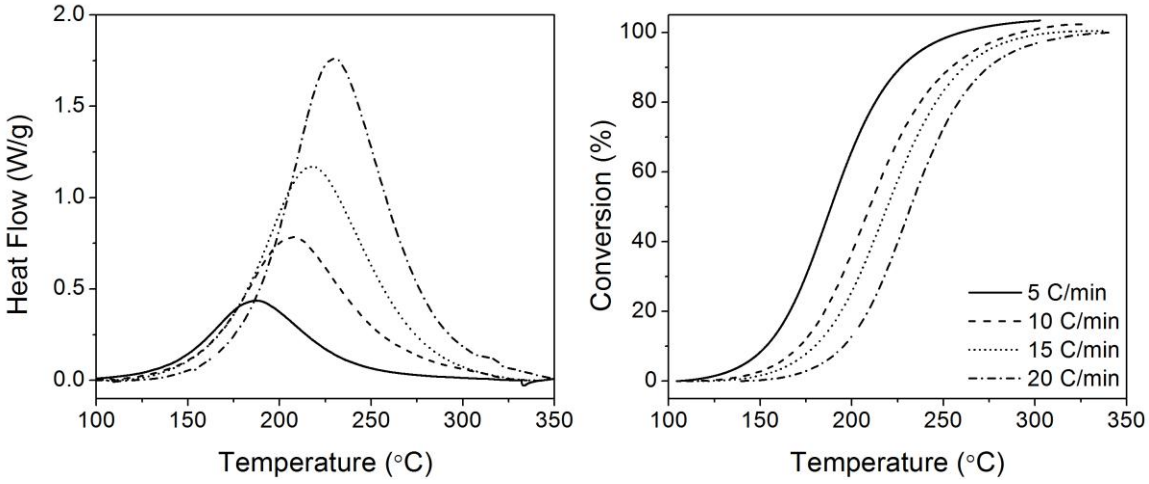

Figure 34. (a) Heat flow vs. temperature and (b) conversion vs. temperature for DGEBA-DDS.

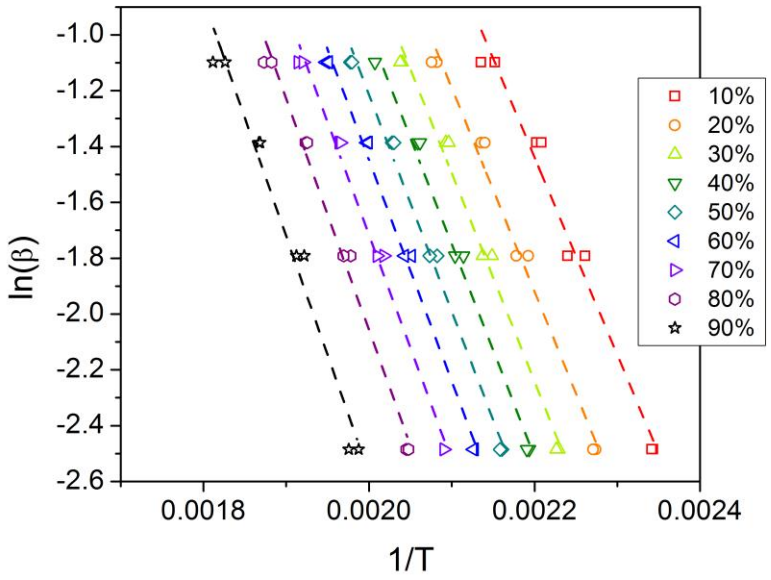

Figure 35. ln(β) vs. 1/T for DGEBA at conversions of 10-90%.

The final result of this analysis was a plot of activation energy versus conversion, shown in Figure 36. E_a gradually increased over the course of the reaction. This increase has been attributed to increasing hindrance of chain motions as monomers formed a gel and then a crosslinked network. The slope of the E_a-α curve remained nearly constant. In isoconversional analysis, a change in slope of the E_a vs. α plot signifies a change in reaction mechanism. For the DGEBA material, it appears that reaction mechanism (as measured by DSC) did not change over the course of crosslinking.

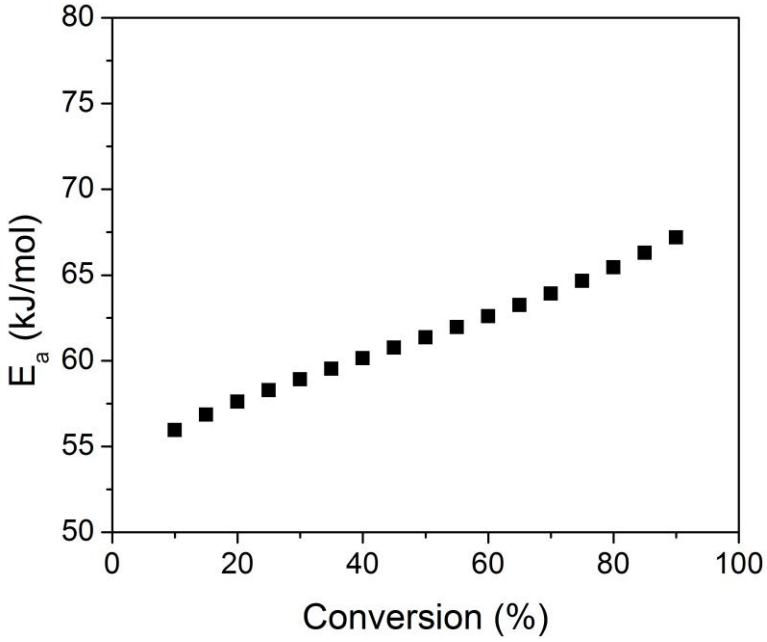

Figure 36. E_a vs. conversion for DGEBA based on isoconversional analysis with FWO equation.

These steps were repeated to perform an isoconversional analysis on AA- and NA-modified epoxies. The exotherms and conversions vs. temperature for 5% AA and 10% AA are shown in Figure 37 and Figure 38, respectively. The plots of $\ln(\beta)$ vs. $1/T$ for both systems are shown in Figure 39. The final result of the analytical process, the E_a vs. α plot, is shown in Figure 40.

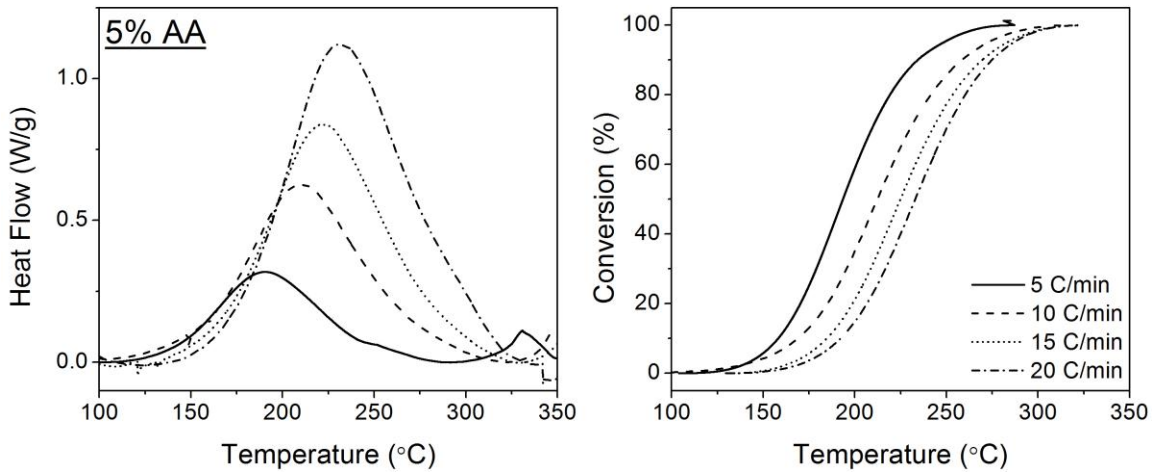

Figure 37. (a) Heat flow vs. temperature and (b) conversion vs. temperature for epoxy with 5% AA

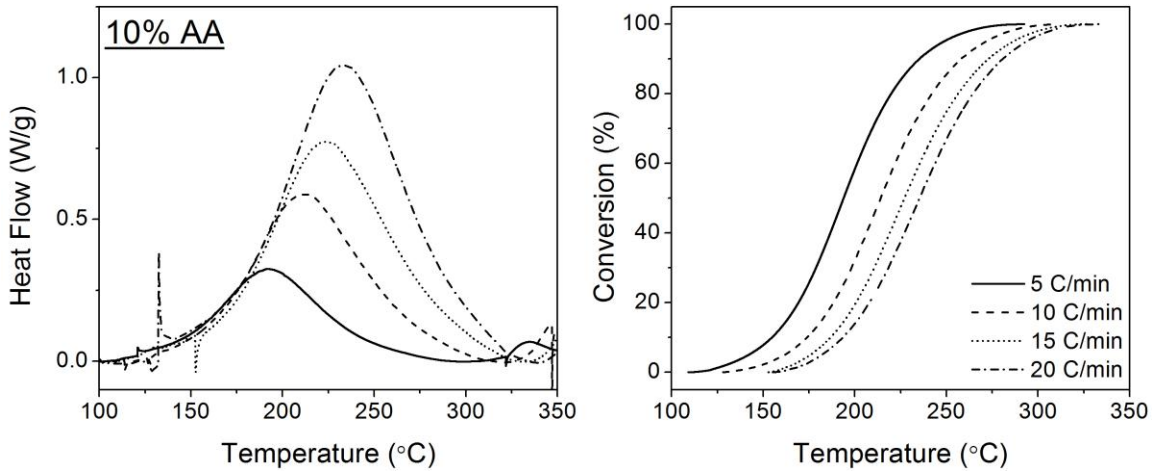

Figure 38. (a) Heat flow vs. temperature and (b) conversion vs. temperature for epoxy with 10% AA.

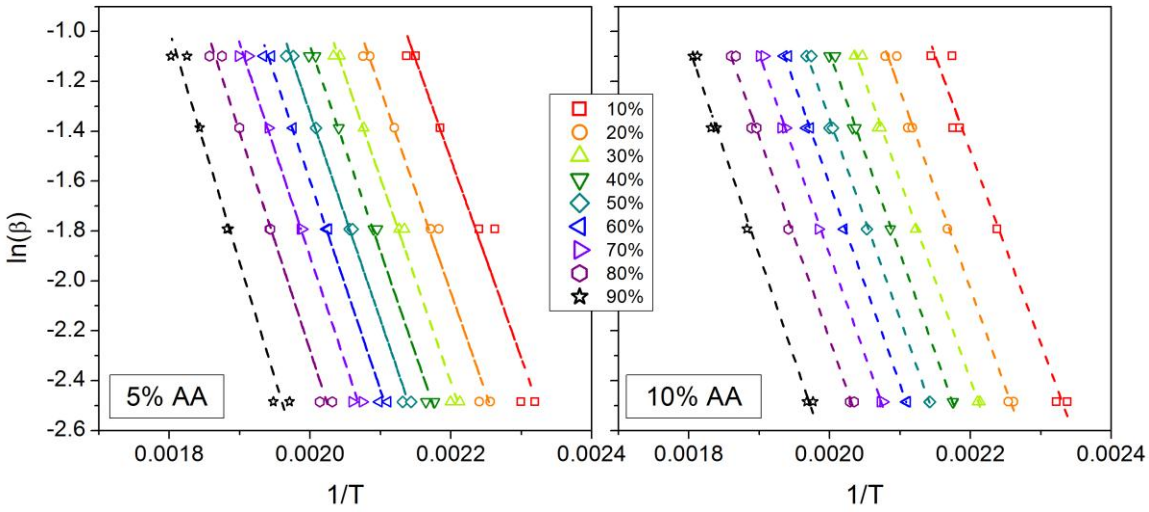

Figure 39. ln(β) vs. 1/T for epoxy with (a) 5% AA and (b) 10% AA at conversions of 10-90%.

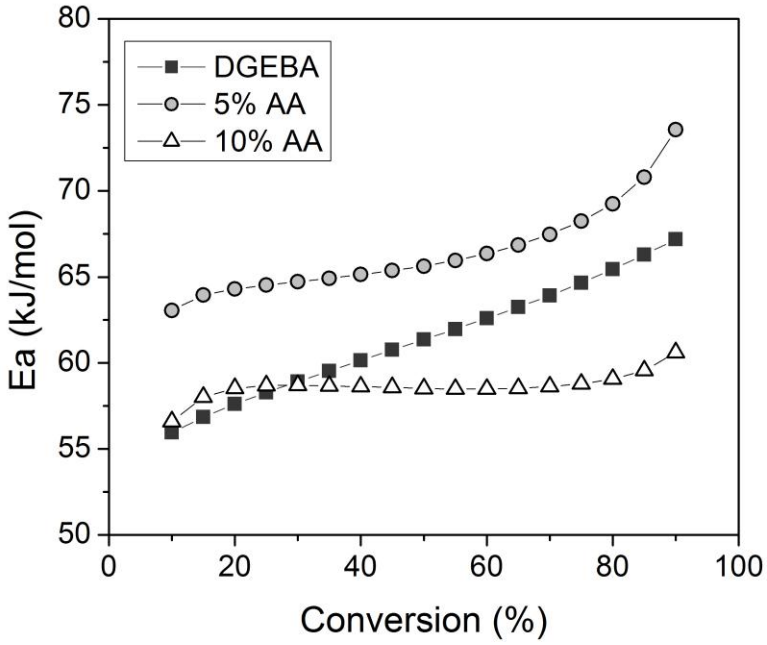

Figure 40. E_a vs. conversion for epoxy with 0-10% AA based on isoconversional analysis with FWO equation.

The E_a vs. α plot shows a clear difference between DGEBA and the AA-modified materials in the dependence of E_a on temperature. The shapes of the curves for 5% AA and 10% AA were similar to each other and different from DGEBA. The same trend was

observed for ε'' plots obtained from DRS. In both cases, this trend indicated that epoxy network development was modified by the addition of 5% AA, but was not modified further by increasing the amount of AA.

The shapes of the curves in Figure 40 suggest that chain motions in the AA epoxies became significantly more hindered at ~80% conversion, as evidenced by the increase in the slope of the E_a-α curve near that point.[115] The lower crosslink densities of AA-modified epoxies may be responsible for that increase. It is possible that chain motion was less hindered at low conversions in epoxies containing AA due to the lower average functionality of those monomers. The materials with lower average functionality had less restricted chain motions than the benchmark system at the same degree of chemical-group conversion. However, after conversion reached a certain threshold, the crosslink density was sufficient to substantially hinder chain motions. At that point, activation energy increased as network growth proceeded via reactions between the hindered chains.

The exotherms and conversions vs. temperature for 5% NA and 10% NA are shown in Figure 41 and Figure 42, respectively. The plots of $\ln(\beta)$ vs. $1/T$ for both systems are shown in Figure 43. The final result of the analytical process, the E_a vs. α plot, is shown in Figure 44.

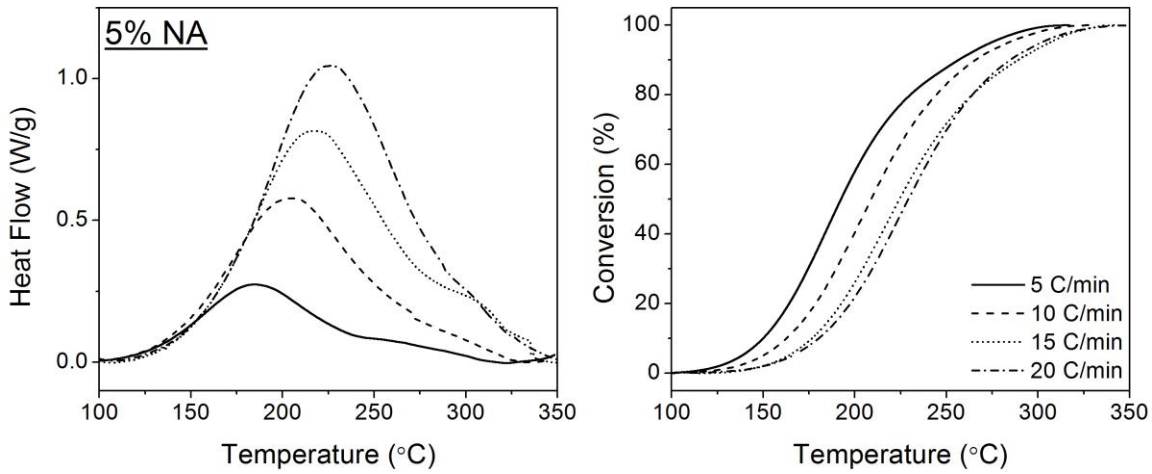

Figure 41. (a) Heat flow vs. temperature and (b) conversion vs. temperature for epoxy with 5% NA.

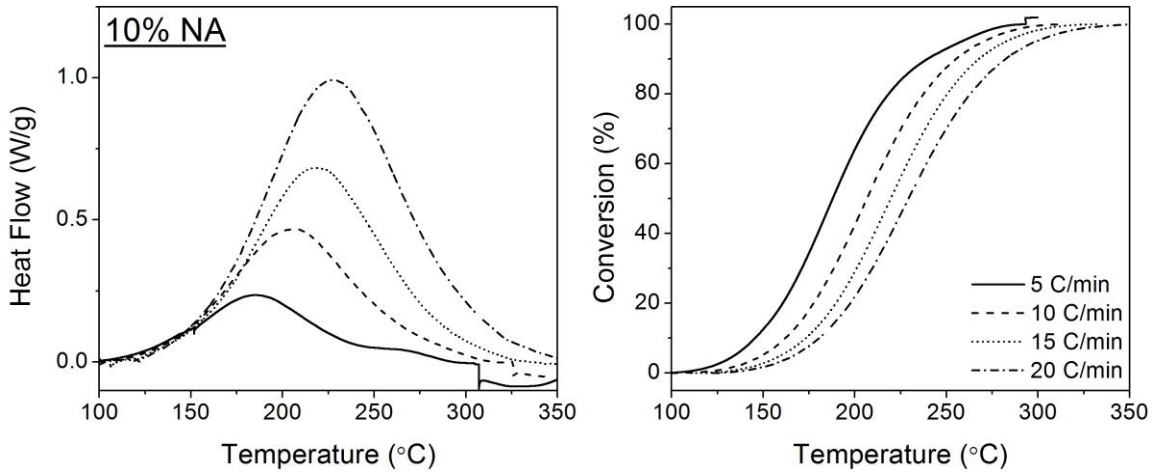

Figure 42. (a) Heat flow vs. temperature and (b) conversion vs. temperature for epoxy with 10% NA.

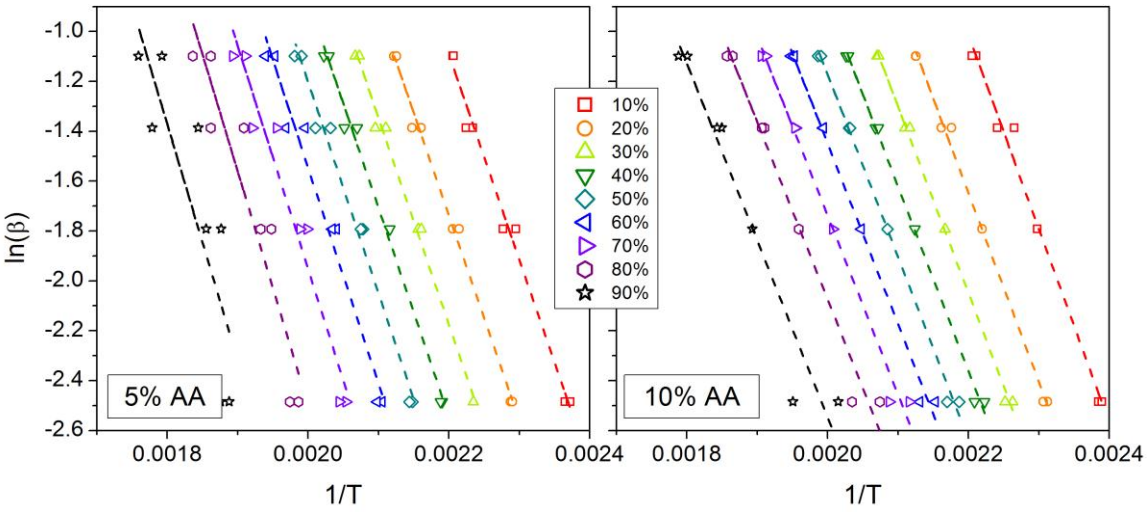

Figure 43. ln(β) vs. 1/T for epoxy with (a) 5% NA and (b) 10% NA at conversions of 10-90%.

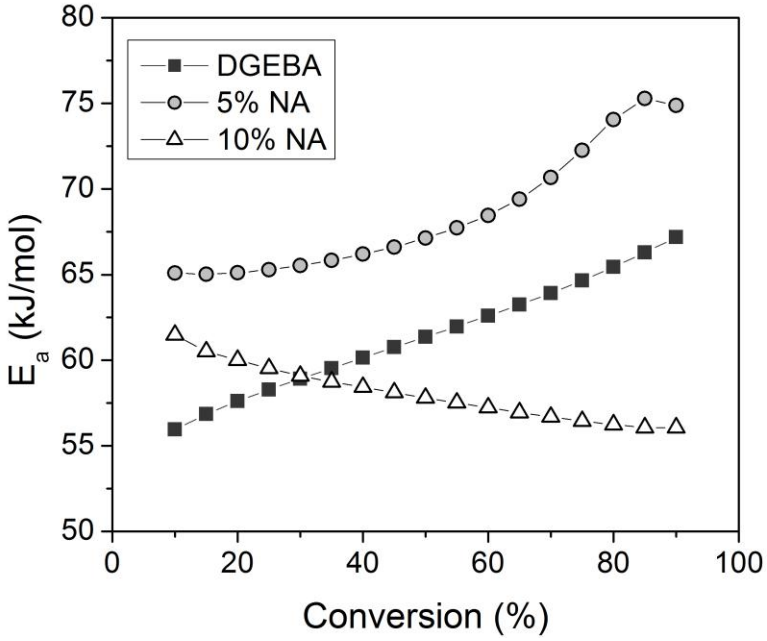

Figure 44. E_a vs. conversion for epoxy with 0-10% NA based on isoconversional analysis with FWO equation.

The E_a-α curves for DGEBA, 5% NA, and 10% NA varied from sample to sample. The E_a-α curve for the sample with 5% NA resembled that of the AA-containing samples. The increase in slope at higher conversions was attributed to crosslinking between chains whose motions had become hindered. The E_a-α curve for the sample with

10% NA exhibited a gradual decrease from its initial value. The slope of the plot was constant, indicating that the reaction proceeded according to a single mechanism. However, the slope was negative, indicating that the single mechanism operative for 10% NA was not the same single mechanism operative for DGEBA.

The decrease in E_a with conversion has been attributed to autocatalysis.[114,115,116] Autocatalysis occurs in epoxy-amine curing as tertiary amines and hydroxyls are generated in the course of the reaction. Hydroxyls catalyze epoxy-amine and epoxy-hydroxyl (etherification) reactions,[114] whereas tertiary amines only catalyze etherification.[117,118] The different bulky substituents on the amine may have been responsible for the different autocatalysis behaviors seen in the E_a vs. α curves.

The AA-modified epoxies, with an adamantyl group attached to some of the amine groups, did not appear to promote or limit autocatalysis. The NA-modified epoxies, with an aromatic napthyl group attached to some of the amine moieties, produced a prolonged autocatalytic effect as conversion proceeded. The chemical structure of the naphthyl group, when attached to a tertiary amine, may have enhanced the amine's catalytic efficiency by increasing its basicity. Therefore the epoxy with the highest NA content showed the most marked autocatalytic behavior in its E_a vs. α profile. The increased role of etherification in the growth of the 10% NA network, as evidenced by tertiary amine autocatalysis, may have been partly responsible for the one-step cure observed via DRS. Etherification reactions occurred throughout the cure process, resulting in a microgel-type growth pattern.

PALS Results

Average hole size (V_h) in DGEBA, 10% AA, and 10% NA samples was measured via PALS. The results are listed in Table 12. PALS indicated a slight decrease in V_h with the addition of 10% AA and a larger decrease in V_h with the addition of 10% NA. These architectural differences were considered in light of variations in crosslink density and network growth kinetics.

Table 12

V_h Data for Selected Epoxies

Sample	V_h (Å^3)
DGEBA	75
10% AA	74
10% NA	71

Discussion

Cure behavior for epoxies modified with 5 and 10% bulky amine (adamantylamine and naphtyhlamine) were monitored using IR, DRS, and DSC. Functional group conversions, calculated from IR spectra, were used to characterize epoxy network growth as "microgel-type" or "linear-type." The IR results showed that the DGEBA-DDS benchmark grew in a linear-type fashion. Linear growth is favored when the primary amine is much more reactive than the secondary amine, i.e., 1° E_a< 2° E_a. Incorporating NA or AA caused the network to grow in a more microgel-type fashion. Microgel growth is favored when primary and secondary amines have equal reactivity. The most extreme example of the microgel growth pattern was the 10% NA epoxy.

The different growth regimes identified by IR were also evidenced by broadband DRS spectra. Graphs of loss permittivity as a function of time had two peaks for most of the samples, indicating two separate steps in the cure process. The only *ε"* curve that did not exhibit two peaks was the one corresponding to 10% NA. After considering both the IR and DRS results, it was hypothesized that the two steps in the reaction identified by DRS corresponded to the linear-type chain growth (first step) and eventual crosslinking of linear segments (second step) identified by IR.

A possible explanation for the microgel-type growth in the 10% NA sample was provided by isoconversional DSC analysis. The E_a vs. α curves generated for these samples showed positive slopes for most of the epoxies, indicating an increase in activation energy as chain motions became more hindered. However, the E_a vs. α curve for the 10% NA material had a negative slope, which may indicate autocatalytic activity in the epoxy. Tertiary amines can catalyze etherification reactions. The napthyl-substituted 3° amines may be more effective catalysts than adamantyl-substituted 3° amines due to increased basicity. The enhanced catalytic efficiency of the NA-based 3° amine caused more etherification throughout the cure for the 10% NA sample. The constant contribution of etherification to network growth resulted in a microgel-type growth pattern for that epoxy.

Comparison of DRS and DSC data also indicated some subtle similarities and differences in network growth kinetics. The curves of *ε"* vs. time for 5% and 10% AA were similar to each other and somewhat different from the *ε"* curve for DGEBA. The *ε"*curves for all the NA samples were slightly different. This trend was repeated in plots of E_a vs. α generated by isoconversional DSC analysis. The shape of the E_a curve was

similar for 5% and 10% AA, and both were distinct from the DGEBA curve. However, the E_a vs. conversion curves for 5% NA and 10% NA had different shapes, and both were distinct from the DGEBA curve. Thus those results both indicate that addition of 5% AA or 5% NA was sufficient to shift network growth kinetics. Increased addition of NA further impacted network growth, while increased addition of AA did not.

The cured network architectures varied between samples. V_h was almost unchanged between DGEBA (75 $Å^3$) and for 10% AA (74 $Å^3$). This finding was not surprising, given the general similarities in network growth kinetics for the two materials. V_h decreased for 10% NA (71 $Å^3$). There are two possible explanations for the drop in hole size for that sample. Microgel-type growth, which occurred more in the 10% NA sample than any other material, may have produced a network architecture with smaller holes. Alternatively, the aromatic naphthyl groups added to that network may have engaged in pi-pi stacking with each other and with the epoxy backbone, reinforcing the network and reducing hole size.

Conclusions

The cure process of DGEBA-DDS modified with bulky amines was examined via IR, DSC, and DRS. The complementary techniques uncovered differences in network growth scheme from sample to sample. Most of the epoxies were shown to undergo linear-type growth, as demonstrated by the 2° amine concentration in IR spectra and the presence of two *ε"* peaks in the DRS spectra. The major exception to that trend was 10% NA, which tended towards microgel-type growth. Isoconversional DSC analysis suggested enhanced autocatalytic activity in the 10% NA epoxy. A stronger autocatalytic effect could explain the shift towards microgel-type growth in that material.

Sample-to-sample changes in curve shape within the set of AA-modified epoxies were observed via DRS and DSC. The same differences from sample to sample were recorded for the NA-modified epoxies. These techniques measure two different properties during the cure process: molecular mobility as a function of time, and activation energy as a function of conversion. The similarity in trends between the two techniques indicates that changes in network growth kinetics have an impact on molecular motions as well as reactivity of the growing network.

CHAPTER IV

FLUID UPTAKE BEHAVIOR OF MULTIFUNCTIONAL EPOXY BLENDS

Abstract

Profound changes in network architecture from blending multifunctional epoxides (*m*TGAP, *p*TGAP, or TGDDM) and difunctional epoxides (DGEBA or DGEBF) and a curative amine (3,3'-DDS or 4,4'-DDS) were apparent from DMA analysis and fluid ingress behavior. Two blends were subjected to extensive free volume analysis via PALS and PVT. Increasing multifunctional content, which increased the crosslink density(with the expected increase in T_g), produced a *decrease* in the average free volume hole size (V_h) accompanied by a counterintuitive *increase* in fractional free volume (FFV). This unusual inverse relationship between FFV and V_h allowed clear resolution of their respective roles in equilibrium moisture uptake vs. the rate of uptake (diffusivity). Equilibrium water uptake increased with increasing multifunctional content, concomitant with the increase in FFV. Water diffusivity, on the other hand, decreased with increasing multifunctional content, concomitant with the decrease in V_h. The decreasing V_h in the epoxy blends also had interesting consequences for organic solvent sensitivity. MEK ingress was almost completely inhibited for most of the blends, implyinghole size selectivity was responsible for the MEK uptake inhibition. MEK uptake was precluded in epoxies whose V_h was below a critical threshold value of ~68 $Å^3$. A small amount of *m*TGAP, *p*TGAP, or TGDDM was sufficient to reduce the V_h of DGEBA/DDS epoxy below the threshold and prevent MEK uptake.

Results and Discussion

The epoxy blends displayed unexpected relationships between multifunctional content, network architecture, and fluid sensitivity. Trends in DMA, PALS, and PVT data suggest that multifunctional epoxides simultaneously increased the fractional free volume and decreased the free volume hole size of the glassy networks. These inverse changes in free volume characteristics had a profound impact on moisture sensitivity and allow the clear resolution of the separate dependencies of equilibrium moisture uptake and uptake rate on FFV and V_h, respectively. Sensitivity to MEK was also significantly affected by the changes in V_h, in accordance with the hole size selectivity theory previously published.[10,16]

DMA Results

Storage moduli and tan delta curves for the epoxy blends are plotted in Figures 45-48. The tan delta peak, corresponding to T_g, was sharp and well-defined for the binary DGEBA and DGEBF benchmarks. The T_g peaks for the binary *m*TGAP, *p*TGAP, and TGDDM benchmarks, on the other hand, were broad and bimodal. This peak shape indicates heterogeneity in the cured multifunctional epoxy[27,28], most likely due to the early onset of vitrification in this high-crosslink-density material. In the blends, the T_g peaks for the blend materials fell between the two benchmark extremes, increasing with multifunctional content. The positive dependence of T_g on multifunctional content is consistent with an increase in crosslink density with higher fractions of the multifunctional epoxide. T_g values for the two systems selected for comprehensive analysis (DGEBA-*m*TGAP-33 and DGEBA-TGDDM-33) are summarized in Table 13.

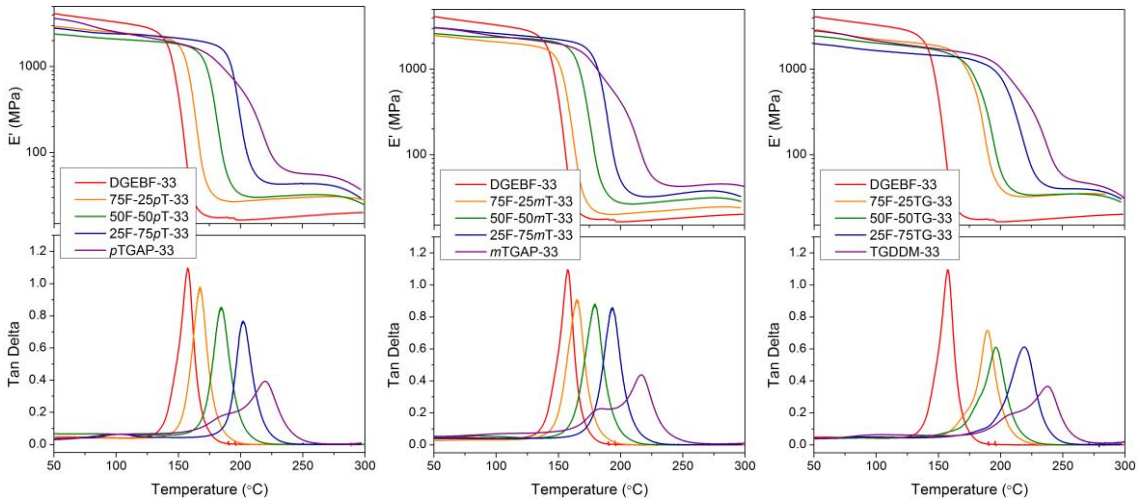

Figure 45. E' vs. temperature (top) and tan delta vs. temperature (bottom) for epoxy blends based on DGEBF-33DDS.

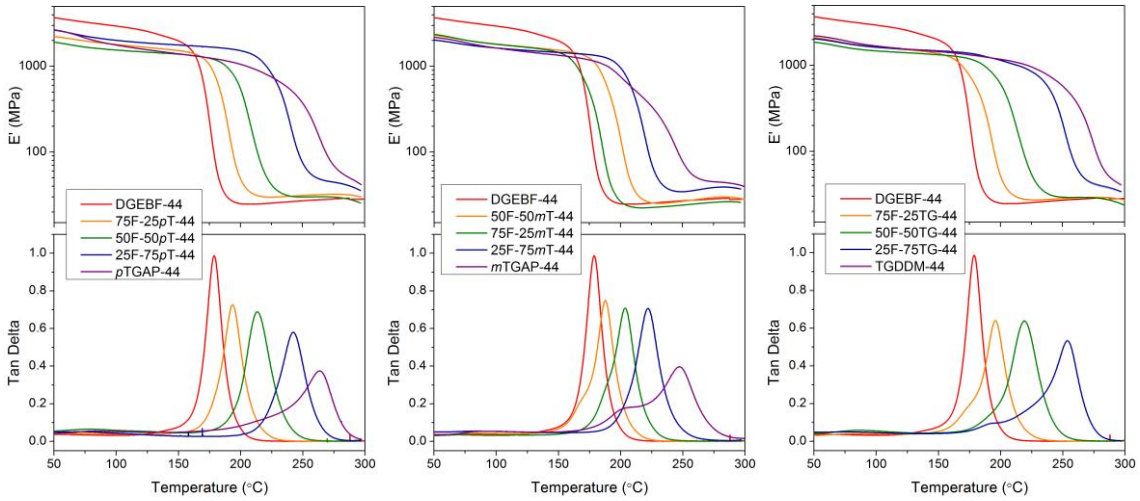

Figure 46. E' vs. temperature (top) and tan delta vs. temperature (bottom) for epoxy blends based on DGEBF-44DDS.

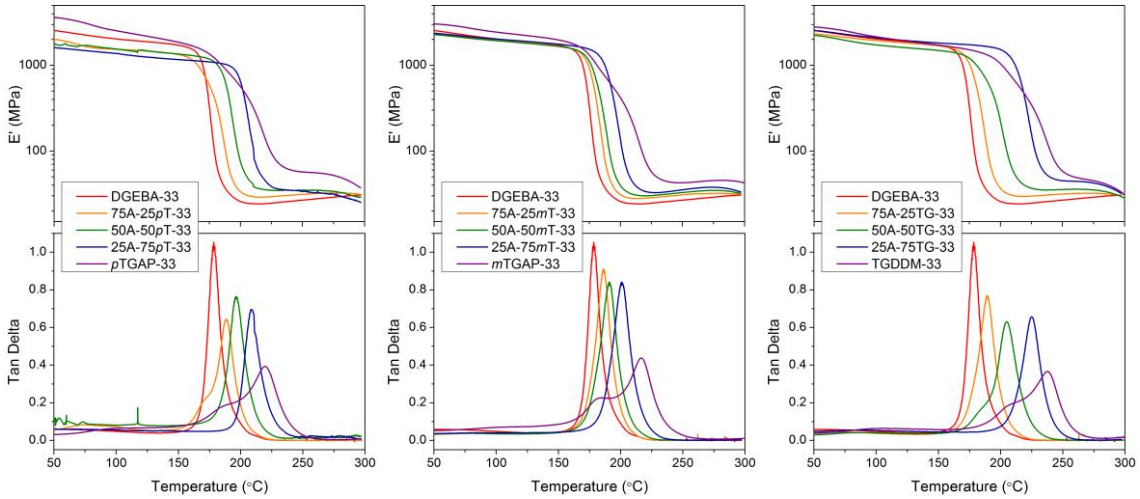

Figure 47. E' vs. temperature (top) and tan delta vs. temperature (bottom) for epoxy blends based on DGEBA-33DDS.

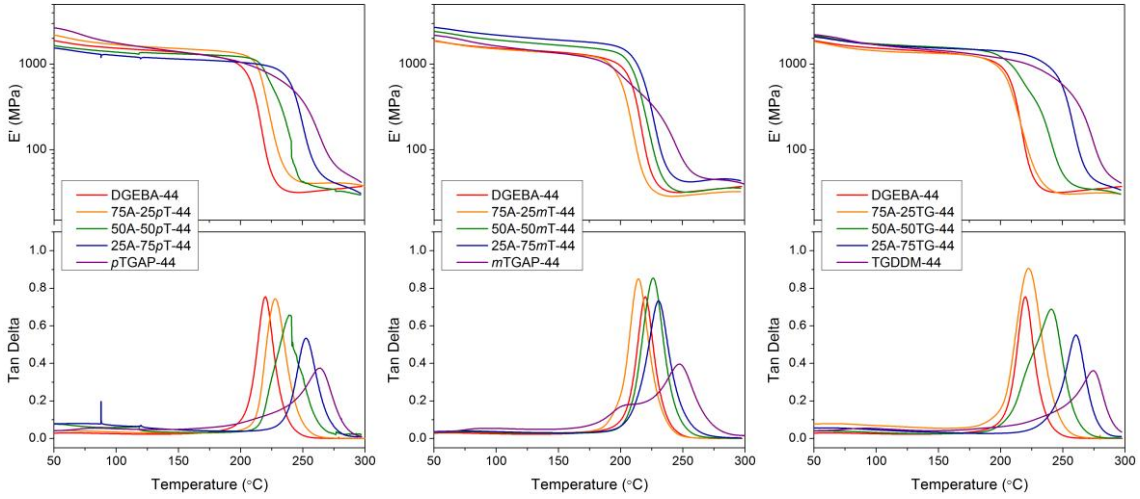

Figure 48. E' vs. temperature (top) and tan delta vs. temperature (bottom) for epoxy blends based on DGEBA-44DDS.

The crosslink densities of the epoxies were calculated using the rubbery plateau values of the storage moduli (*E'*) at T_g + 30 °C or 40 °C, according to the classical theory of rubber elasticity.[15] The results are plotted in Figure 49. In general, crosslink density increased with increasing multifunctional content. The increase in crosslink density was

most pronounced for the blends based on DGEBF-44 and DGEBA-44, due to the higher crosslink densities of the starting materials.

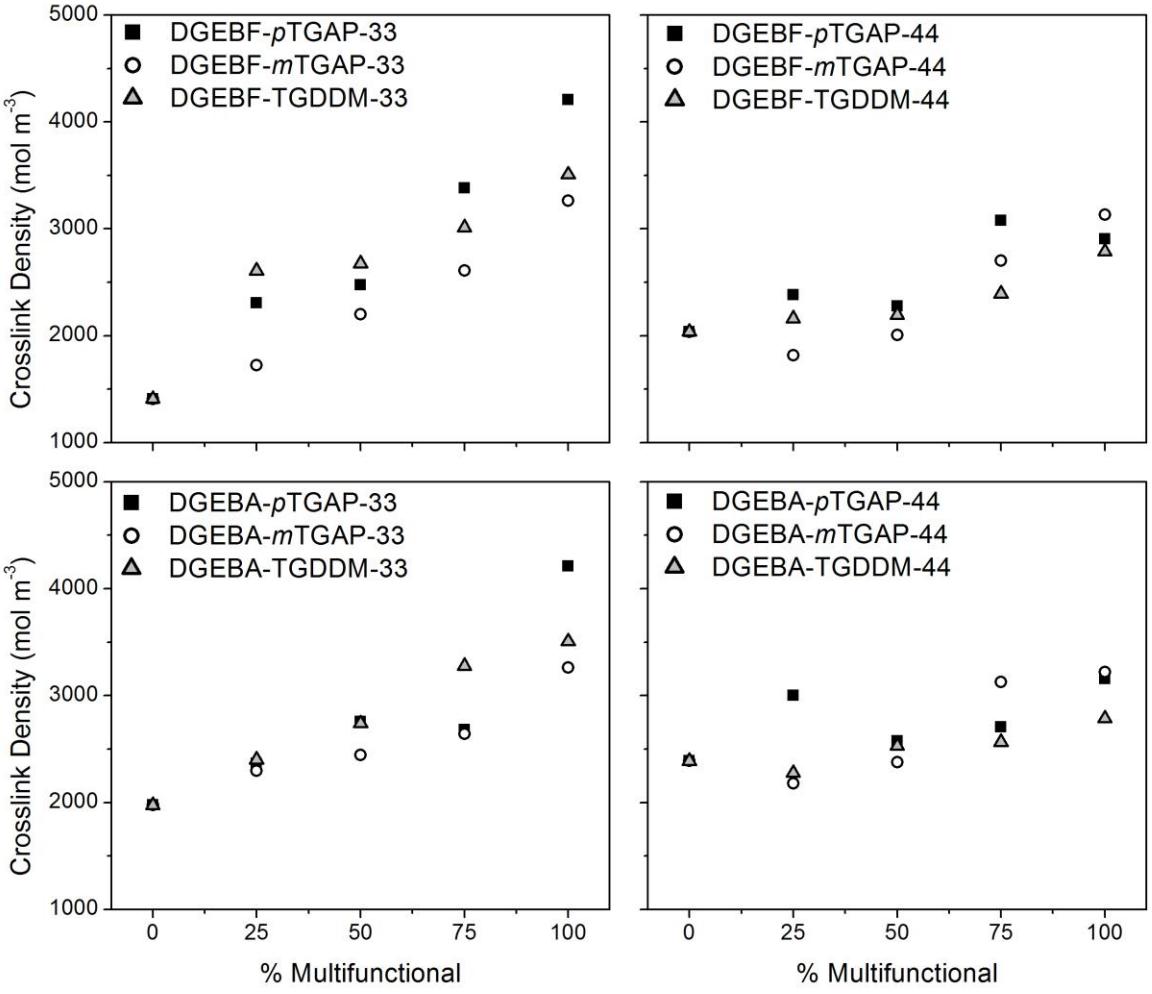

Figure 49. Crosslink density vs. multifunctional content for epoxy blends.

The changes in T_g and crosslink density from difunctional to multifunctional materials were evidence of evolving network architecture. As average functionality increased, the networks became more densely crosslinked. However, the increasing functionality also precipitated a decrease in the vitrification time. The most densely crosslinked epoxies vitrified earliest, locking in the architecture they had adopted at the

time of vitrification. The changes in network architecture with blend ratio had interesting and significant consequences for free volume characteristics of the epoxies.

Free Volume Analysis

Free volume hole sizes for two blend systems (DGEBA-*m*TGAP-33 and DGEBA-TGDDM-33) were measured with positron annihilation lifetime spectroscopy (PALS). The hole sizes calculated for the epoxy blends are plotted in Figure 50 as a function of composition and crosslink density. For both sets of blends, V_h decreased linearly with multifunctional content. For the *m*TGAP blends, hole size decreased from 75 $Å^3$ for DGEBA/DDS to 48 $Å^3$ for *m*TGAP/DDS. The hole size of the binary TGDDM/DDS epoxy was slightly larger (54 $Å^3$). The decrease in V_h was attributed to the increase in crosslink density that resulted from replacing difunctional DGEBA with multifunctional *m*TGAP or TGDDM. The average hole sizes were larger for the TGDDM blends than for *m*TGAP, despite their higher crosslink densities. We attribute this result to the backbone of the TGDDM molecule being longer and more flexible than *m*TGAP, resulting in slightly larger V_h values for the TGDDM blends.

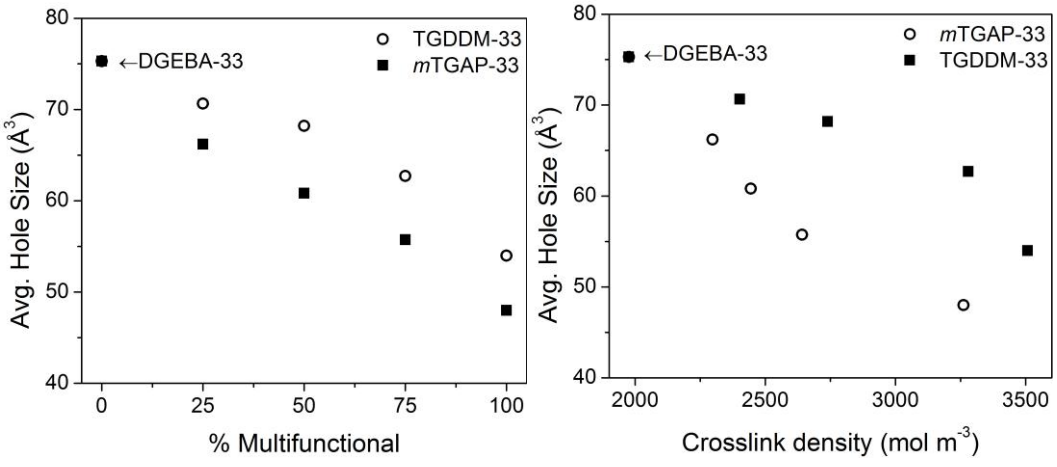

Figure 50. (a) Average hole size vs. multifunctional content and (b) average hole size vs. crosslink density for DGEBA-*m*TGAP-33 and DGEBA-TGDDM-33 blends.

Fractional free volume, as measured by PVT dilatometry, increased with additional multifunctional content for the DGEBA-*m*TGAP-33 and DGEBA-TGDDM-33 blends. The FFV measured for the epoxy blends is plotted in Figure 51. FFV data was not available for the binary *m*TGAP and TGDDM blends, due to thermal degradation. FFV increased from 4.6% for DGEBA/DDS to 9.1% for 75% *m*TGAP and 13.0% for 75% TGDDM.

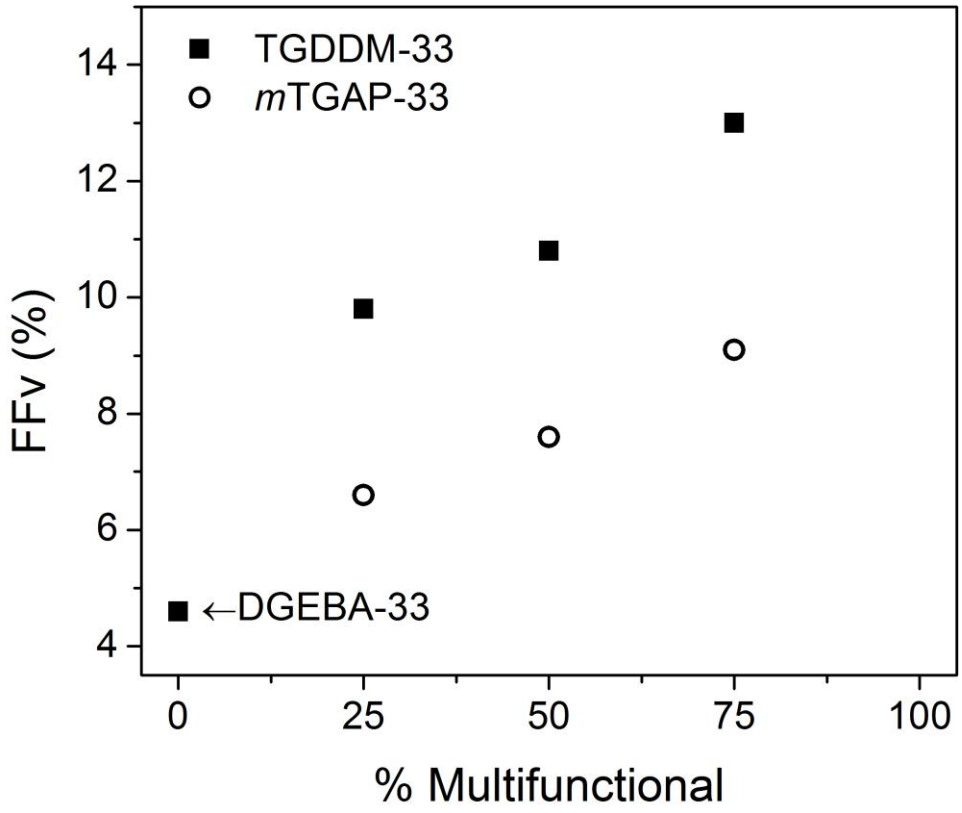

Figure 51. Fractional free volume (FFV) vs. multifunctional content for *m*TGAP and TGDDM blends.

The simultaneous increase in FFV and decrease in V_h was counter-intuitive. Typically, V_h and FFV are linked, and they increase and decrease in tandem.[72,119] We hypothesize that the multifunctional monomers influence fractional free volume by modifying the vitrification time of the epoxies. Systems with greater average

functionality vitrify at shorter times and lower conversions. In a vitrified system, free volume is essentially frozen in the configuration it had adopted at the onset of vitrification, establishing the ultimate architecture of the glassy epoxy network. Binary *m*TGAP/DDS had higher FFV than DGEBA/DDS because the system vitrified very early, trapping many more free volume holes in the glassy state. In the epoxy blends, vitrification occurred earlier for systems with more multifunctional content, giving rise to the positive correlation between FFV and multifunctional content seen in Figure 51. Higher fractional free volumes were measured for the TGDDM blends than for the equivalent *m*TGAP blends because the crosslink densities of the TGDDM materials were higher (Figure 49), resulting in even earlier vitrification.

FFV and V_h were only measured for two blends systems. However, the observed relationships between FFV or V_h and multifunctional content were presumed valid for all the epoxy blends considered in this experiment. While the exact hole sizes or FFV percentages may change for different blends, the effect of multifunctional monomers on network architecture is fundamentally the same. This assumption was confirmed by fluid uptake ingress studies, which showed that the changes in free volume architecture in these epoxies had profound implications for their moisture and solvent uptake behavior.

Water Uptake

A free volume approach is used to explain water uptake kinetics in these epoxies. In the past, researchers have attempted to relate moisture ingress in epoxies primarily to polarity and hydrogen bonding in the material.[56,58] While it is clear that hydrogen bonding plays an important role in water uptake in epoxies, these considerations alone do not explain why similar epoxies have markedly different moisture uptake kinetics. The

epoxy blends studied herein, which have similar chemistries and hence similar polarities, are illustrative of this phenomenon.

Trends in equilibrium water uptake and uptake rate of the epoxy blends were correlated to the observed changes in FFV and V_h measured for selected blends. Water uptake, shown in Figure 52, Figure 53, Figure 54, and Figure 55, followed Fickian diffusion kinetics. The equilibrium uptake values for the two blends subjected to free volume analysis (DGEBA-*m*TGAP-33 and DGEBA-TGDDM-33) are summarized in Table 13. Equilibrium water uptake increased with multifunctional content. From these results, it can be stated that equilibrium uptake increases with FFV. This conclusion is reasonable in light of the water diffusion mechanism in epoxy, in which water fills available free volume sites until the material is saturated.

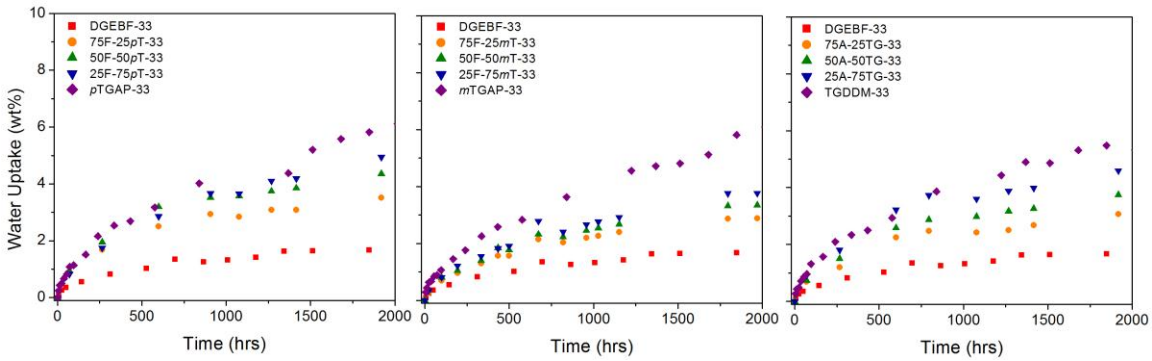

Figure 52. Water uptake vs. time for epoxy blends based on DGEBF-33DDS.

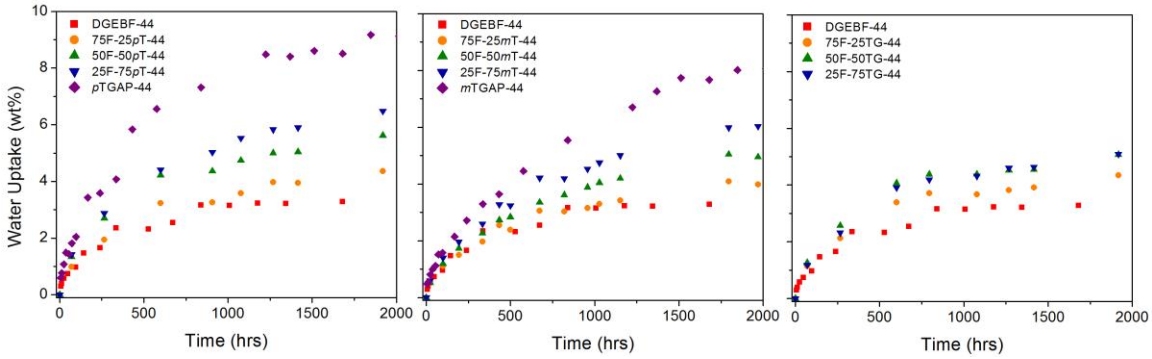

Figure 53. Water uptake vs. time for epoxy blends based on DGEBF-44DDS.

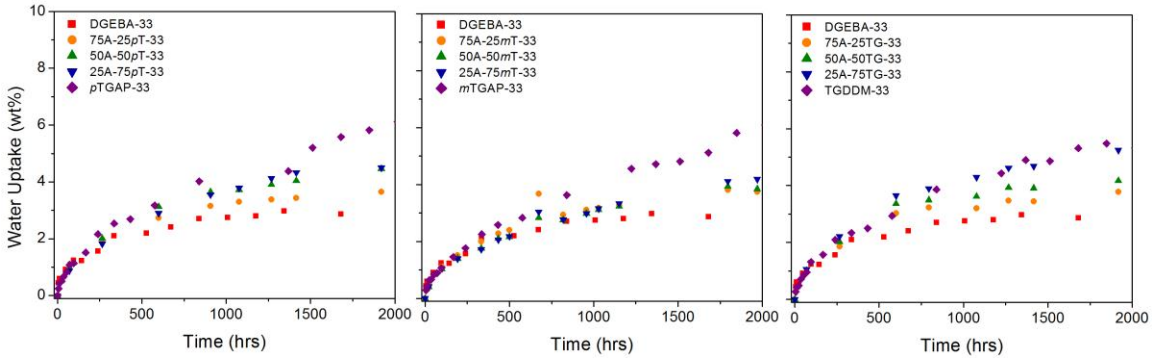

Figure 54. Water uptake vs. time for epoxy blends based on DGEBA-33DDS.

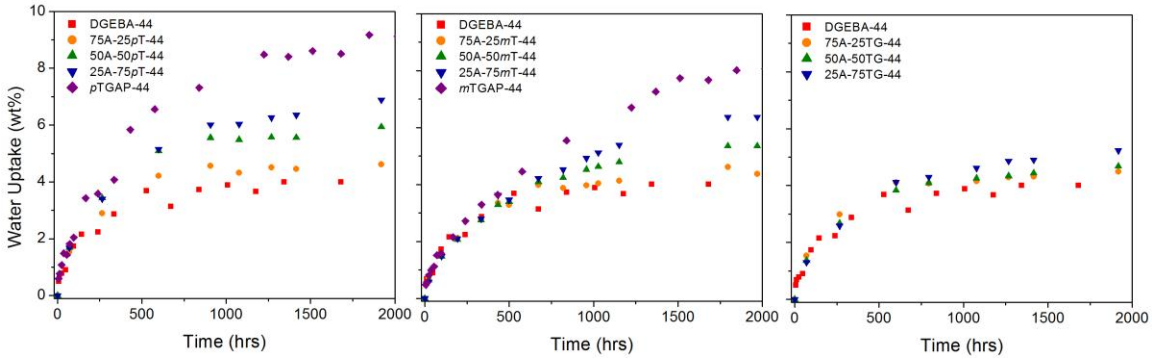

Figure 55. Water uptake vs. time for epoxy blends based on DGEBA-44DDS.

The Fickian diffusion coefficient (diffusivity, *D*), which represents a normalized diffusion rate, was calculated from the water uptake curves. At short times diffusivity can be approximated as follows:[120]

$$\frac{M_t}{M_{inf}} = \frac{4}{L}\sqrt{\frac{Dt}{\pi}}$$

where M_t is the water absorption at time t, M_{inf} is the equilibrium water absorption, and L is half the sample thickness (to account for diffusion from both sides). Diffusivities were calculated from the slopes of the linear regression best-fit lines of plots of M_t/M_{inf} vs. $t^{1/2}$ (Figure 56, Figure 57, Figure 58, and Figure 59). Diffusivity values for two blends are listed in Table 13. Diffusivity decreased with multifunctional content, concurrently with the decrease in hole size. The change in diffusivity was least pronounced for the blends incorporating TGDDM. The difference in V_h from binary difunctional to binary multifunctional epoxy was lowest for this resin. Therefore the smaller change in hole size was manifested as a smaller change in diffusivity, compared to the TGAP resins.

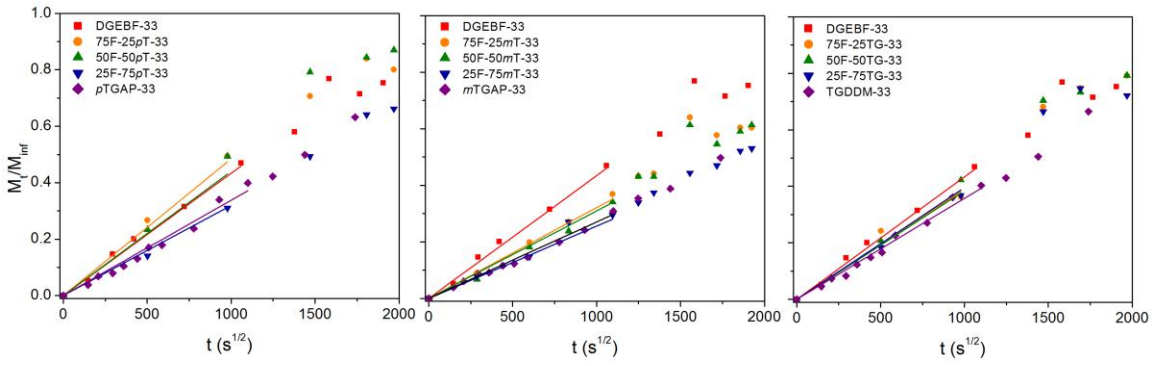

Figure 56. M_t/M_{inf} vs. $t^{1/2}$ for epoxy blends based on DGEBF-33DDS.

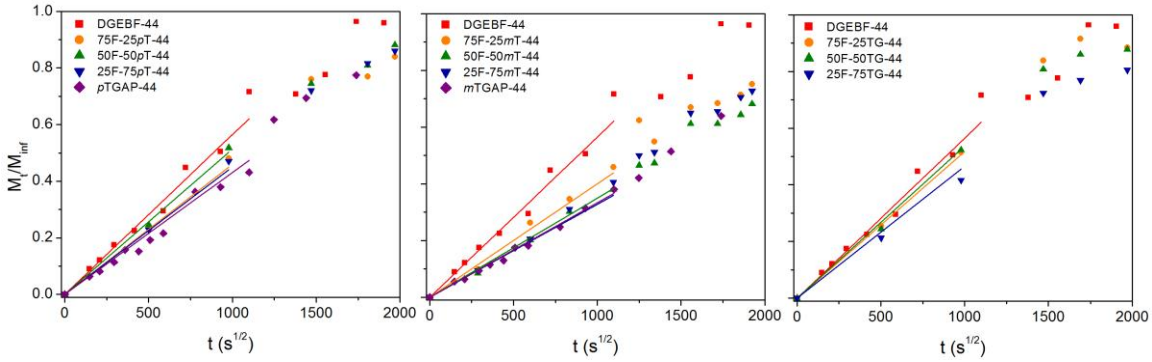

Figure 57. M_t/M_{inf} vs. $t^{1/2}$for epoxy blends based on DGEBF-44DDS.

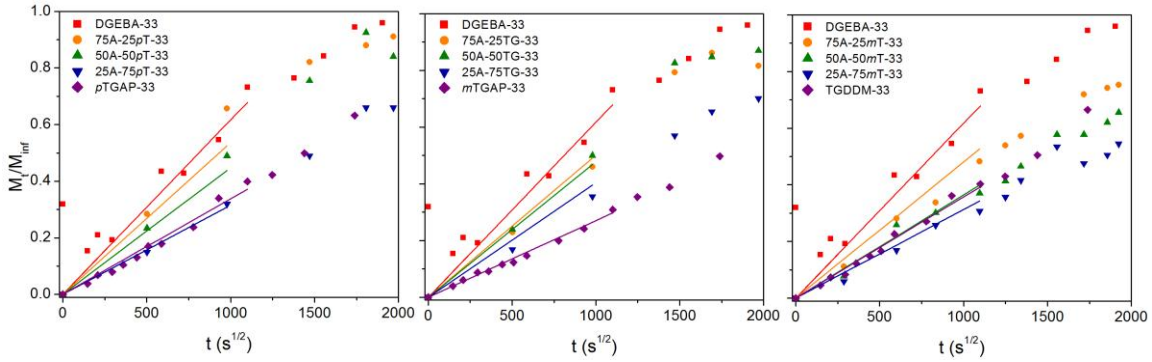

Figure 58. M_t/M_{inf} vs. $t^{1/2}$ for epoxy blends based on DGEBA-33DDS.

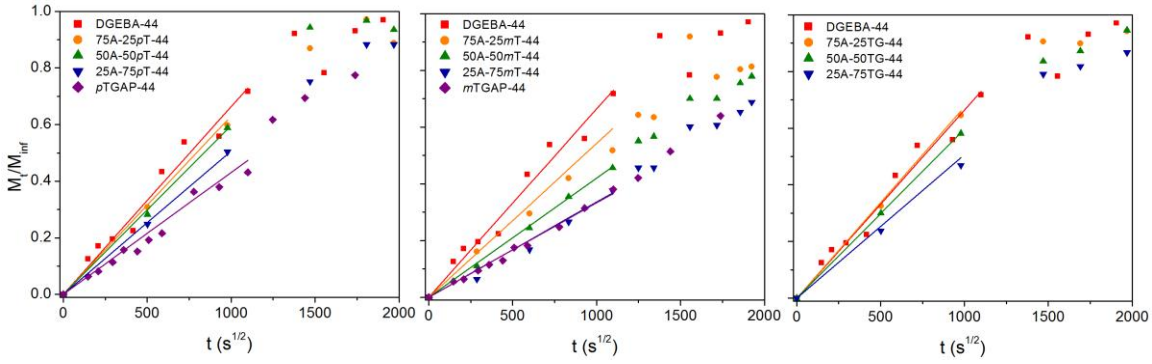

Figure 59. M_t/M_{inf} vs. $t^{1/2}$for epoxy blends based on DGEBA-44DDS.

Table 13

Water Uptake Results and Free Volume Data for Epoxy Blends

Sample	T_g (°C)	V_h (Å^3)	FFV (vol%)	Equilib. Water Uptake (weight percent)	D (x 10^{-9} cm^2 s^{-1})
DGEBA-33	178	75	4.6	2.9	0.48
75A-25*m*T-33	186	66	6.6	4.11	0.25
50A-50*m*T-33	191	61	7.6	4.62	0.16
25A-75*m*T-33	201	56	9.1	5.44	0.11
*m*TGAP-33	217	48	N/A	7.3	0.09
75A-25TG-33	189	71	9.8	3.77	0.34
50A-50TG-33	204	68	10.8	4.30	0.31
25A-75TG-33	225	63	N/A	5.49	0.23
TGDDM-33	233	54	N/A	5.8	0.16

It has been suggested previously that equilibrium water uptake in epoxies depends on fractional free volume, while diffusivity depends on hole size. VanLandingham et al. postulated a free volume explanation for changes in water absorption for epoxies with different stoichiometries, but did not distinguish between effects of FFV and V_h.[32] Soles and co-workers studied the effects of fractional free volume on moisture uptake and concluded that FFV played a significant role.[53,60] These hypotheses have been difficult to prove convincingly because FFV and V_h increase and decrease simultaneously in many materials, and their separate effects on moisture uptake cannot be deconvoluted. The epoxy blends considered in this study provided a unique opportunity to characterize water

ingress because the FFV and V_h trends of the materials diverged. Therefore it is possible to state that equilibrium water uptake in epoxies varies with FFV, regardless of hole size, and diffusivity varies with hole size, regardless of FFV.

The correlation between V_h and diffusivity for these materials was exponential and independent of epoxide structure. This relationship is shown in Figure 60, which includes V_h data collected for this experiment as well as for previous work by this research group. The following empirical relationship was determined for diffusivity and V_h:

$$D = 5.05 \times 10^{-12} \exp\left(\frac{V_h}{16.9}\right)$$

where the numerical constants 3.99 x 10^{-12} cm^2 s^{-1} and 15.9 $Å^3$ were determined from the linear regression best-fit line of the data in Figure 60.

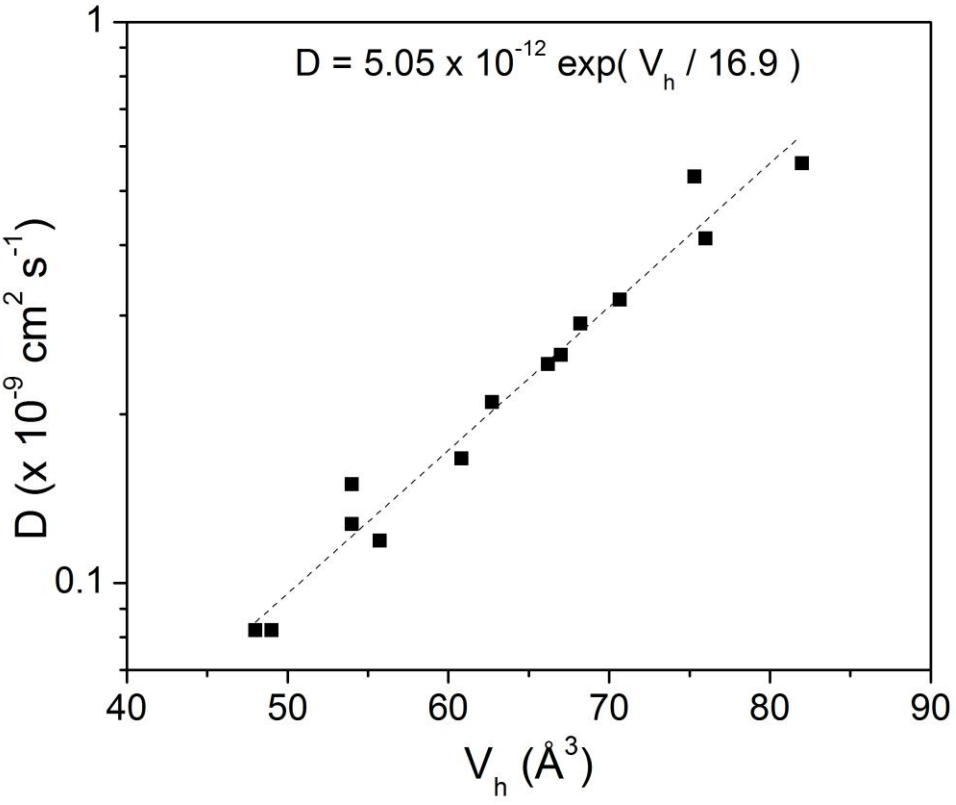

Figure 60. D vs. V_h for epoxy blends.

The observed trends in equilibrium water uptake and diffusivity may also be related to hydroxyl content in the epoxy blends. When an oxirane ring reacts with an amine to produce a crosslink, a hydroxyl is generated. Therefore systems with higher crosslink density have more hydroxyl groups. Hydroxyl groups are polar moieties that can hydrogen-bond with ingressing water molecules.[32,58,60] As crosslink density increased, the rising number of hydroxyl groups may have increased the amount of total water absorption. The tendency of water molecules to become "bound" to hydroxyls may have contributed to the slower diffusion rates in epoxies with higher crosslink density. The bound water molecules may have been more resistant to movement through the network, resulting in lower diffusivities.

Organic Solvent Uptake

Glassy epoxies absorb most organic solvents according to Case II diffusion kinetics. Attempts to predict this behavior have relied on a model first introduced by Thomas and Windle, which used characteristic viscosity constants to model absorption.[67] The original model and elaborations on it have successfully described the uptake profiles in linear systems.[68,69] However, when these models are applied to crosslinked systems the viscosity constant has limited relevance and predictive capabilities become limited. In our earlier work, the relationship between V_h and Case II diffusion kinetics was qualitatively elucidated. In the present research, that analysis is extended to MEK uptake in epoxy blends.

Many of the epoxy blend material properties discussed thus far, including T_g, FFV, V_h, and equilibrium water uptake, exhibited a linear or near-linear dependence on multifunctional content. MEK uptake, plotted in Figure 61, Figure 62, Figure 63, and Figure 64, displayed a very different trend. The binary difunctional epoxies were known to absorb MEK at varying rates, while the binary multifunctional epoxies were known to be completely impervious to MEK. The MEK uptake profiles of the epoxy blends were very similar to the profiles for the multifunctional epoxies and very different from the profile for the difunctional epoxies. The MEK ingress patterns can be considered in terms of the base epoxy systems as well as the multifunctional additive.

The binary DGEBF-33DDS epoxy was previously identified as more resistant to MEK than the other difunctional epoxy systems under consideration. The epoxy blends based on this system exhibited no MEK uptake after >8000 h (Figure 61).

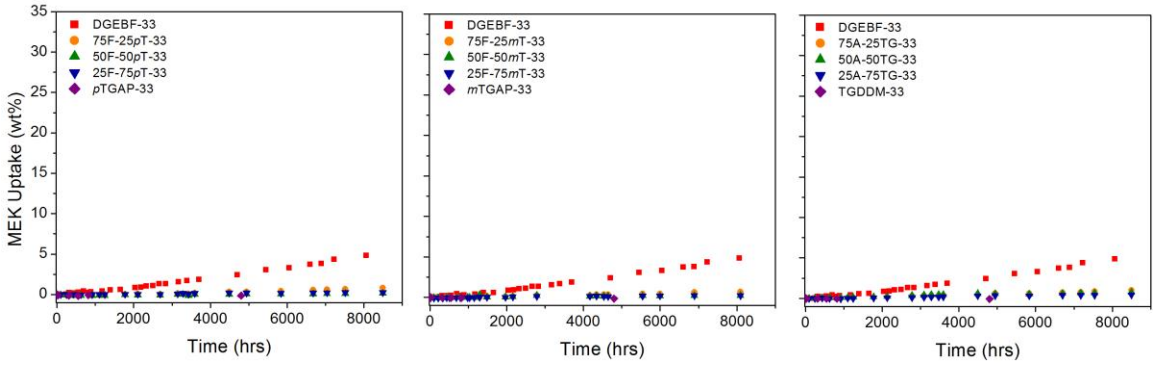

Figure 61. MEK uptake vs. time for blends based on DGEBF-33DDS.

The binary DGEBF-44DDS and DGEBA-33DDS epoxies are somewhat more susceptible to MEK ingress. In the blends based on these systems (Figure 62 and Figure 63), very slow uptake was observed for the epoxies with 25% multifunctional content, with no uptake recorded for the rest of the blends in the series.

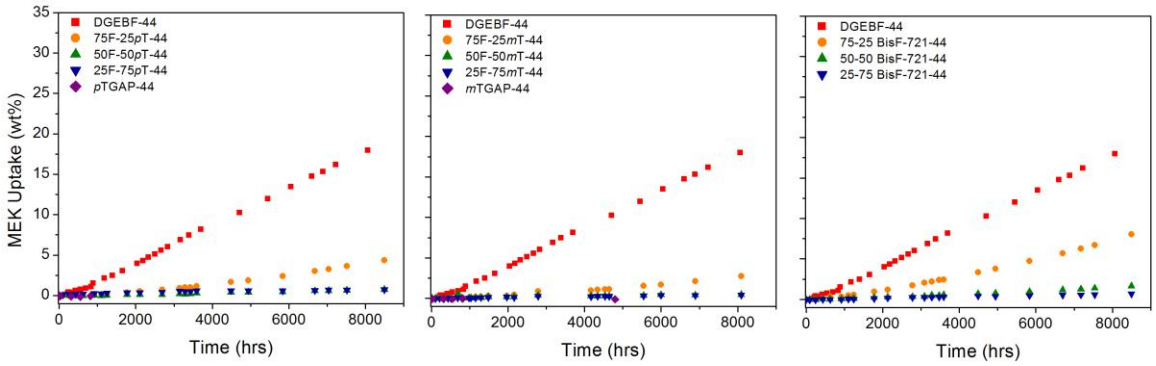

Figure 62. MEK uptake vs. time for blends based on DGEBF-44DDS.

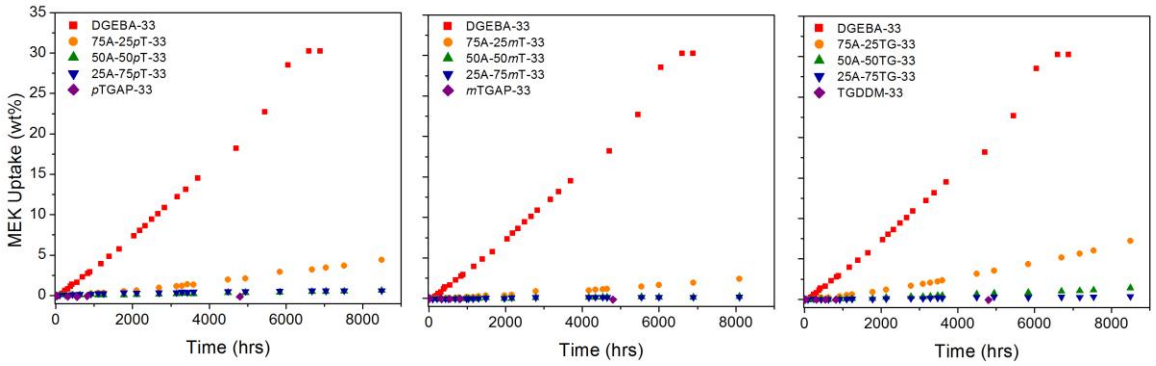

Figure 63. MEK uptake vs. time for blends based on DGEBA-33DDS.

The binary DGEBA-44DDS epoxy was known to have the greatest MEK susceptibility of the binary epoxies in the present study. In the blends based on this epoxy, moderate uptake was observed for the samples containing 25% multifunctional content (Figure 64). In the TGDDM blend, uptake also proceeded (albeit slowly) for the sample with 50% multifunctional content. However, uptake was insignificant in all blends containing 75% multifunctional content.

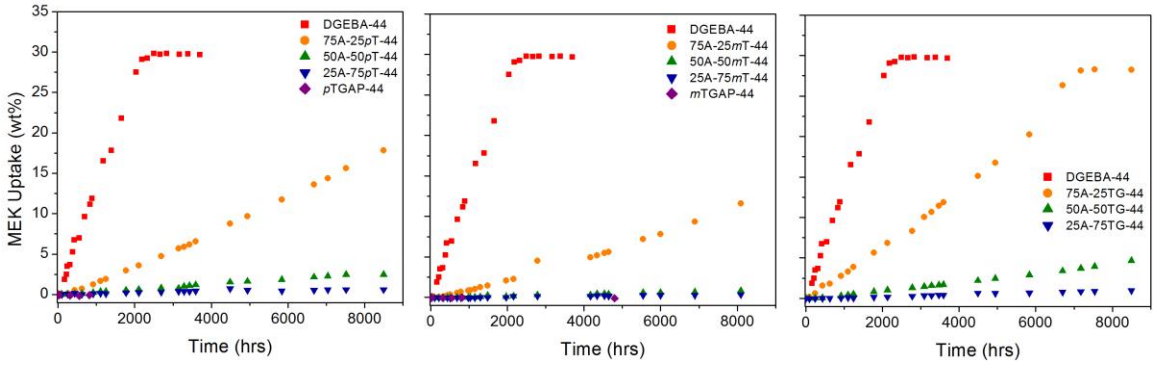

Figure 64. MEK uptake vs. time for blends based on DGEBA-44DDS.

The inclusion of TGAP or TGDDM reduced MEK uptake in all cases, but the extent of their effectiveness varied somewhat. TGDDM was least effective at inhibiting MEK ingress, with 75% TGDDM required to prevent uptake in the DGEBA-44DDS system. In that same system, only 25% *m*TGAP was necessary to prevent MEK ingress. *m*TGAP was also slightly more effective than *p*TGAP at preventing ingress. Both the overall MEK uptake behavior of the polymer blends as well as the difference between TGAP and TGDDM blends can be explained in terms of hole size selectivity.

The binary difunctional are similar to MEK ingress because their hole sizes are approximately the same size as the MEK molecules. The multifunctional benchmarks, on the other hand, are almost completely impervious to MEK. The small hole sizes of the multifunctional epoxies are responsible for the resistance to MEK ingress. MEK uptake is

very slow if the V_h of the epoxy is smaller than the van der Waals volume of the solvent molecule. The PALS measurements for theDGEBA-*m*TGAP-33 and DGEBA-TGDDM-33 blends showed that V_h decreased with increasing multifunctional content. MEK uptake was almost completely inhibited when the hole size of the epoxy blend became smaller than a critical threshold size. For the *m*TGAP blends, 25% *m*TGAP was sufficient to reduce the hole size of the DGEBA/DDS epoxy below the critical threshold value for MEK uptake. For the TGDDM blends, the blend with 25% TGDDM exhibited appreciable MEK uptake, and 50% TGDDM was required to completely inhibit MEK ingress.

MEK uptake rate for multifunctional blends compared as follows: TGDDM >*p*TGAP>*m*TGAP. The different efficacies of *m*TGAP, *p*TGAP, and TGDDM in preventing MEK uptake are reasonable in light of the PALS measurements for those materials. Hole sizes were slightly larger in the DGEBA-TGDDM-33 blends than in the DGEBA-*m*TGAP-33 blends. Therefore more multifunctional content was required in the TGDDM blends to reduce V_h below the critical threshold for MEK ingress. This effect was apparent in all of the blends under consideration: MEK uptake was faster in the TGDDM blends than in the systems containing *m*TGAP or *p*TGAP. No PALS data was available for a system containing *p*TGAP, but it can be inferred from previous research on structural isomers that the hole sizes in *p*TGAP blends were slightly larger than those in *m*TGAP blends. In the difunctional benchmark epoxies, the meta-substituted DDS isomer formed networks with smaller V_h's than the para-substituted isomer, due to a linear-type network growth mechanism and improved chain packing.[16] That effect was active in the meta- and para-substituted TGAP isomers. Therefore the systems blended

with *m*TGAP had smaller hole sizes (inferred) and improved fluid resistance (proven) than the *p*TGAP blends.

From these results and data collected previously by Jackson et al., ~68 Å^3 is proposed as the critical threshold V_h for MEK ingress. The epoxy with 25% *m*TGAP, which had no MEK uptake, had a V_h of 66 Å^3. The epoxy with 25% TGDDM, which had appreciable MEK uptake, had a V_h of 71 Å^3, while the epoxy with 50% TGDDM had a V_h of 68 Å^3 and no MEK uptake.

Hole size selectivity was confirmed by acetone uptake behavior. The DGEBA-*m*TGAP-33 and DGEBA-TGDDM-33 blends were subjected to soaking in acetone. Acetone is chemically similar to MEK, but the molecule is somewhat smaller. Acetone has a hydrodynamic volume of 66Å^3, compared to 82 Å^3 for MEK. Acetone ingresses into epoxy according to a Case II diffusion mechanism. Therefore acetone is an appealing solvent to use in tandem with MEK to probe hole-size effects in epoxies.

Acetone ingress, shown in Figure 65, occurred at a much faster rate than MEK ingress in the selected blends. Acetone ingress was faster in the TGDDM blends than in the *m*TGAP blends. These observations are both reasonable, considering the smaller size of the acetone molecule and the smaller V_h in the *m*TGAP blends. The benchmark DGEBA-33 material reached equilibrium in acetone after ~700 h, whereas the same material required ~6000 h to reach saturation in MEK. The 75A-25*m*T-33 blend had absorbed 11% acetone after 2000 h, but just 0.35% MEK after soaking the same amount of time. The larger hole sizes of the TGDDM blends increased the rate of acetone uptake in those materials compared to the *m*TGAP blends. The 75A-25TG blend absorbed 23% acetone after 2000 h. These results suggest a smaller threshold size to inhibit acetone

diffusion in glassy epoxies. However, this research group has not collected sufficient data on acetone uptake in other epoxies to suggest what that threshold value might be. These graphs indicate that a higher level of multifunctional content (i.e., a higher crosslink density) is required to completely inhibit acetone ingress in the epoxy blends.

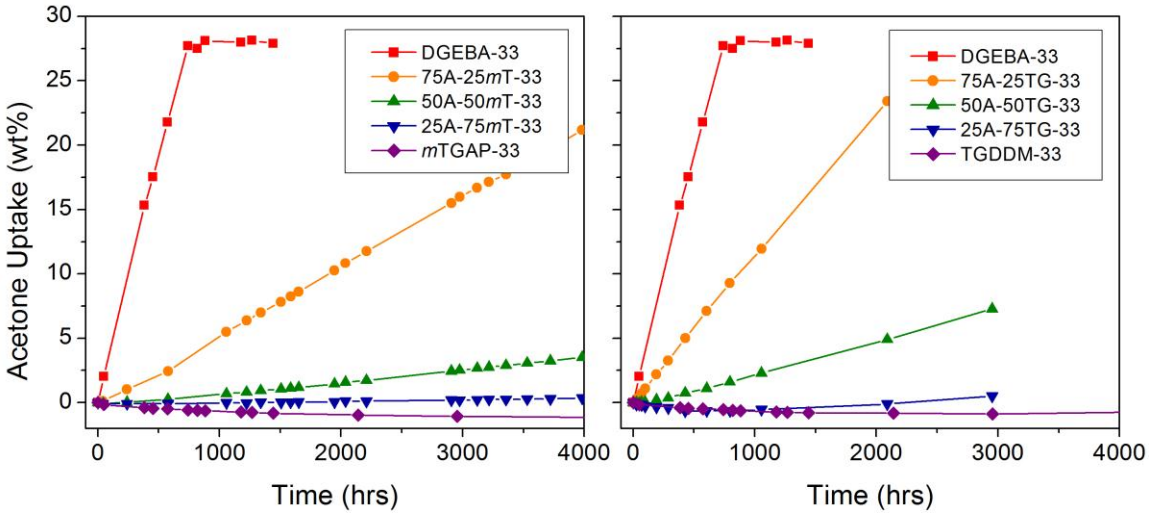

Figure 65. Acetone uptake vs. time for DGEBA-*m*TGAP-33 and DGEBA-TGDDM-33 blends.

Conclusions

Blends of DGEBA with trifunctional (*m*TGAP) and tetrafunctional (TGDDM) epoxies in ratios of 75/25, 50/50, and 25/75 (w/w) were cured with 3,3'-DDS. DMA evaluation demonstrated the anticipated trends, with blend T_g and crosslink density increasing with multifunctional content. PVT and PALS analysis showed how multifunctional resins significantly affected network architecture. Fractional free volume increased with increasing multifunctional content. This increase was attributed to the decrease in vitrification time for the systems with higher average functionality. Faster vitrification trapped more free volume holes in the glassy state, giving rise to the observed correlation between multifunctional content and FFV. The TGDDM blend had

higher crosslink densities and more fractional free volume values than their *m*TGAP analogues because TGDDM is higher in functionality and vitrifies faster.

Hole size decreased with multifunctional content. This decrease was attributed to increasing crosslink density for the multifunctional materials. TGDDM blends had larger V_h values than *m*TGAP blends because the TGDDM backbone segments were longer and more flexible than the *m*TGAP backbone moities. The divergent trends in V_h and FFV for both the epoxy blends had profound implications for their moisture sensitivity.

Equilibrium water uptake increased with increasing multifunctional content, concomitant with the increase in FFV. Water diffusivity, on the other hand, decreased with increasing multifunctional content, concomitant with the decrease in hole size. An empirical exponential relationship was calculated for the dependence of water diffusivity on V_h in these epoxies. Increasing hydroxyl concentration with crosslink density may have also contributed to the trends in water uptake due to hydrogen bonding between hydroxyl groups and water molecules.

The decreasing hole size in the epoxy blends also had interesting consequences for organic solvent sensitivity. MEK ingress was substantial in the DGEBA/DDS epoxy, yet it was completely inhibited for most of the blends. Hole size selectivity, previously observed by this research group for other epoxy/solvent systems, was responsible for the MEK uptake inhibition. MEK uptake was precluded in epoxies whose V_h was below a critical threshold value of ~68 $Å^3$. A small amount of *m*TGAP (25%) was sufficient to reduce the hole size of DGEBA/DDS epoxy below the threshold and prevent MEK uptake. A larger amount of TGDDM (50%) was required to produce the same effect, due to the larger hole sizes in the TGDDM-modified epoxies. Acetone uptake supported the

hole size selectivity theory. Acetone is a smaller molecule than MEK, and its ingress into these epoxies was considerably faster. More multifunctional content was required to inhibit acetone ingress due to the lower critical threshold V_h for acetone resistance.

These epoxy blends provided a unique opportunity to independently study the effects of hole size and fractional free volume on fluid ingress in epoxies with similar chemical structures. By understanding the fundamental relationships between solvent molecular size, polymer V_h, and crosslink density, we can begin to control solvent sensitivity in epoxies by manipulating the glassy polymer network architecture.

CHAPTER V

EFFECT OF STOICHIOMETRY AND CURE PRESCRIPTION ON FLUID INGRESS IN EPOXY NETWORKS

Abstract

Stoichiometry and cure temperature were evaluated for four epoxy systems, based on the diglycidyl ethers of bisphenol-A (DGEBA) and bisphenol-F (DGEBF), and cured with 3,3'- or 4,4'-diaminodiphenylsulfone (33DDS and 44DDS). The materials were formulated as stoichiometric benchmarks and with an excess of epoxide and cured in two steps (125 °C/200 °C) or one step (180 °C). Infrared (IR) cure studies confirmed that etherification occurred in most excess-epoxy materials. Dynamic mechanical analysis and free volume testing indicated decreased crosslink density and increased chain packing in the excess-epoxy materials, as well as a narrowing gap in properties between 33- and 44-cured networks when excess epoxy was used. The narrowing gap was not as pronounced in materials cured at 180 °C. The excess-epoxy materials were more resistant to water ingress, exhibiting reduced equilibrium water uptake for most systems. The excess-epoxy materials were also more resistant to MEK ingress, which occurred at a slower rate in most excess-epoxy materials than in stoichiometric analogues. The improvement in fluid resistance was attributed to enhanced chain packing in the materials with lower crosslink densities.

Results and Discussion

The network architecture and fluid resistance of benchmark and excess-epoxy networks were evaluated as a function of chemical composition and cure prescription. Difunctional epoxide monomers (DGEBA and DGEBF) were mixed with aromatic

amines (33DDS and 44DDS) and cured with two-step (125 °C/200 °C) and one-step (180 °C) curing prescriptions. The thermoset networks were formulated as stoichiometric benchmarks or with an excess of epoxy.

Excess-epoxy networks were predicted to have different network architectures than their stoichiometric analogues, due to their divergence from the "ideal" step-growth thermoset. This divergence could be evidenced by a decrease in crosslink density and an increase in molecular weight between crosslinks (M_c). The increased presence of dangling chain ends may also affect structure-property relationships in the networks. Excess-epoxy treatments can further alter network architecture by increasing the probability of etherification. Etherification is non-negligible when excess epoxy is present at high temperatures.[13] Etherification increases crosslink density, but the ether-based crosslink is chemically different from the amine-based crosslink that develops from epoxy-amine reactions. In addition to the effect on network backbone, the number of hydroxyl groups differs for the two crosslink structures. Every epoxy-amine reaction generates a new hydroxyl group, whereas the overall number of hydroxyls does not change when an etherification reaction occurs. Hydroxyl groups have been associated with increased water ingress due to their ability to hydrogen-bond with the water molecule.[32,61]

Architectures of the cured networks were probed via dynamic mechanical analysis (DMA) and mechanical testing. Free volume hole sizes (V_h) were determined using positron annihilation lifetime spectroscopy (PALS). The network was studied through its development using near-infrared (IR) spectroscopy. The fluid sensitivity of the epoxies

was evaluated with MEK and water, and the fluid ingress properties of the materials were correlated to their network architectures.

IR Cure Profiles

The extent of etherification was ascertained using near-IR spectroscopy using the peak at 4525 cm^{-1}, which associated with the epoxide group. Residual epoxide would be expected for a system in which only epoxy-amine reactions occurred, due to the stoichiometric excess of epoxy. Conversely, a final epoxy concentration below the level predicted by stoichiometry would indicate that etherification reactions occurred. The evolution of the epoxy peak throughout the cure cycle is shown in Figure 66 (two-step cure) and Figure 67 (one-step cure). For most systems, the epoxide peak was reduced to nearly zero by the end of curing. The disappearance of the epoxide peak qualitatively demonstrated etherification for all excess-epoxy materials.

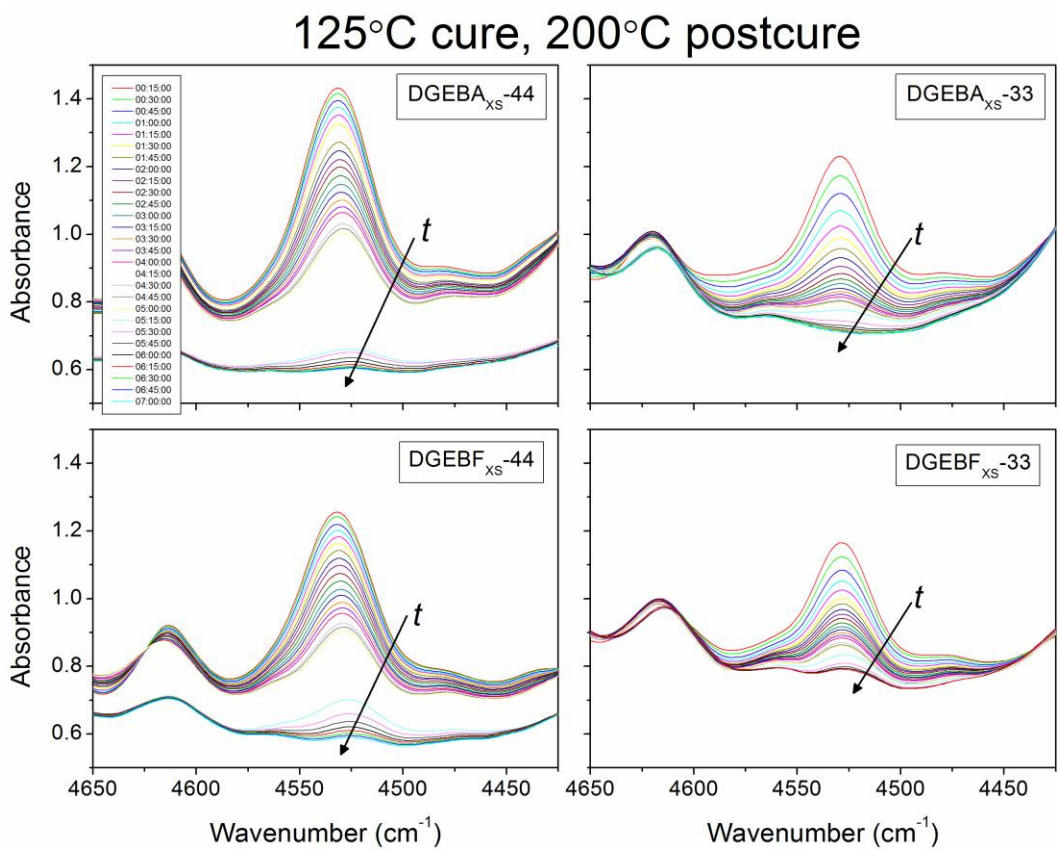

Figure 66. Near-IR peak at 4525 cm^{-1} for epoxies subjected to two-step cure (125 °C/200 °C): (a) DGEBA$_{XS}$-44 (b) DGEBA$_{XS}$-33 (c) DGEBF$_{XS}$-44 (d) DGEBF$_{XS}$-33.

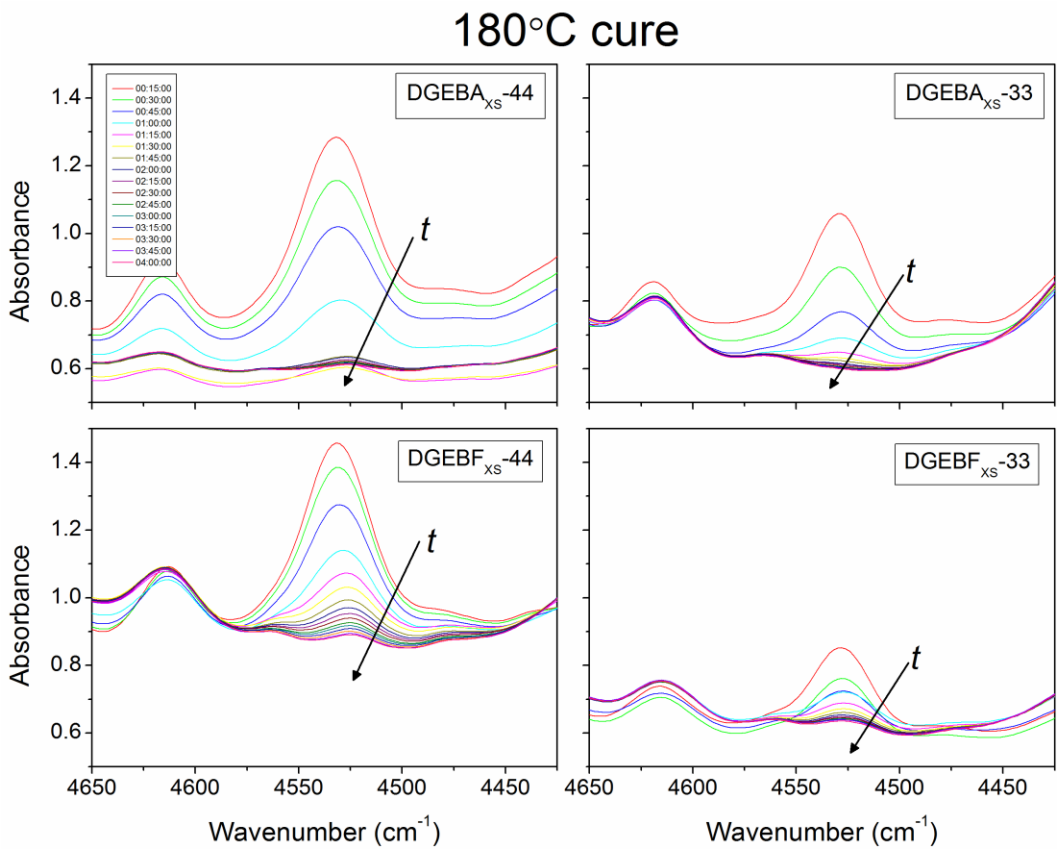

Figure 67. Near-IR peak at 4525 cm^{-1} for epoxies subjected to one-step cure (180 °C): (a) DGEBA$_{XS}$-44 (b) DGEBA$_{XS}$-33 (c) DGEBF$_{XS}$-44 (d) DGEBF$_{XS}$-33.

For quantitative evaluation of epoxide concentration ([epox]), the Beer-Lambert Law was employed. Initial [epox] was calculated from epoxide concentration in the neat resin and adjusted for the proportion of resin the epoxy-amine mixture. Projected final [epox] was calculated based on reaction stoichiometry, assuming no etherification reactions. Final [epox] was calculated from the 4525 cm^{-1} peak in the final scan of the cure process. The results of these calculations are listed in Table 14 (two-step cure) and Table 15 (one-step cure).

Table 14

Near-IR Epoxide Concentrations in Epoxies Subjected to Two-Step Cure (125 °C/200 °C)

System	Initial [Epox] (mol kg^{-1})	Proj. Final [Epox] (mol kg^{-1})	Final [Epox] (mol kg^{-1})
$DGEBA_{XS}$-44	4.40	0.88	1.03
$DGEBA_{XS}$-33	4.40	0.88	0.00
$DGEBF_{XS}$-44	4.57	0.91	0.39
$DGEBF_{XS}$-33	4.57	0.91	0.00

Table 15

Near-IR Epoxide Concentrations in Epoxies Subjected to One-Step Cure (180°)

System	Initial [Epox] (mol kg^{-1})	Proj. Final [Epox] (mol kg^{-1})	Final [Epox] (mol kg^{-1})
$DGEBA_{XS}$-44	4.40	0.88	0.93
$DGEBA_{XS}$-33	4.40	0.88	0.00
$DGEBF_{XS}$-44	4.57	0.91	0.41
$DGEBF_{XS}$-33	4.57	0.91	0.77

All of the excess-epoxy materials except $DGEBA_{XS}$-44 exhibited a lower final [epox] than predicted by the stoichiometric relationship, indicating that etherification reactions occurred. Etherification was more prominent in the epoxies cured at 125 °C/200 °C. The increased etherification with that cure prescription may be attributed to the postcure step at 200 °C, because etherification is more favorable at higher temperatures.

The network architecture of the etherified epoxies was presumed to be slightly different from the architecture of benchmark materials, as discussed above. The impact of etherification was considered in the interpretation of PALS, DMA, and fluid uptake results.

PALS Results

Hole sizes of the benchmark and excess-epoxy materials subjected to a two-step cure are listed in Table 16. The benchmark epoxies exhibited a distribution of hole sizes from 67 to 82 $Å^3$. In the excess-epoxy materials, hole sizes in $DGEBA_{XS}$-33 and $DGEBF_{XS}$-33 decreased slightly and hole sizes in $DGEBA_{XS}$-44 and $DGEBF_{XS}$-44 decreased significantly. Overall, the effect of the excess epoxy on hole size was to reduce all V_h's and to reduce V_h difference between 33DDS- and 44DDS-cured epoxies.

Table 16

Hole Sizes from PALS for Epoxies Cured at 125 °C and Postcured at 200 °C

Epoxy System	V_h ($Å^3$)	Epoxy System	V_h ($Å^3$)
DGEBF-33	67	$DGEBF_{XS}$-33	64
DGEBF-44	76	$DGEBF_{XS}$-44	64
DGEBA-33	77	$DGEBA_{XS}$-33	76
DGEBA-44	82	$DGEBA_{XS}$-44	73

The decrease in V_h for all materials may have been due to increased M_c and enhanced chain packing, which could result in smaller hole sizes. The reduced difference in V_h between 33- and 44-cured epoxies suggested increased architectural similarity for the excess-epoxy networks. The difference in V_h between DGEBA-33 and DGEBA-44

(or DGEBF-33 and DGEBF-44) has been attributed to the differences in chain packing efficiency induced by the two isomeric DDS crosslinkers.[16,20] When excess epoxy was used, the DDS segments became a comparatively smaller fraction of the overall network. The epoxide contributed comparatively more of the total network segments in the excess-epoxy materials. Thus the network architectures of those materials were more similar when the same epoxy resin was used, despite the different amine curatives. Further similarity in the networks may have been induced by etherification, which was more favored under excess epoxy conditions. The ether crosslink was structurally the same whether 33DDS or 44DDS was used. Therefore networks with more etherification were more similar regardless of amine isomer. The similarity in network architectures for excess-epoxy materials was confirmed by DMA and fluid uptake results.

DMA Results

Glass transition temperatures (T_g) and crosslink densities (ν) were determined from dynamic mechanical analysis. DMA curves for the epoxies cured at 125C°/200 °C are shown in Figure 68. Two changes in T_g trends were noted. First, a T_g decrease of 15-40 °C was recorded for the excess-epoxy materials, compared to benchmarks. Second, the T_g difference between epoxies cured with 33DDS and 44DDS narrowed when excess epoxy was used. The T_g difference between DGEBA-33 and DGEBA-44 decreased from 40 °C for the stoichiometric materials to 7 °C in the excess-epoxy materials ($DGEBA_{XS}$-33 and $DGEBA_{XS}$-44). Likewise, the T_g difference between DGEBF-33 and DGEBF-44 decreased from 22 °C for the benchmark networks to 2 °C for the excess-epoxy systems ($DGEBF_{XS}$-33 and $DGEBF_{XS}$-44).

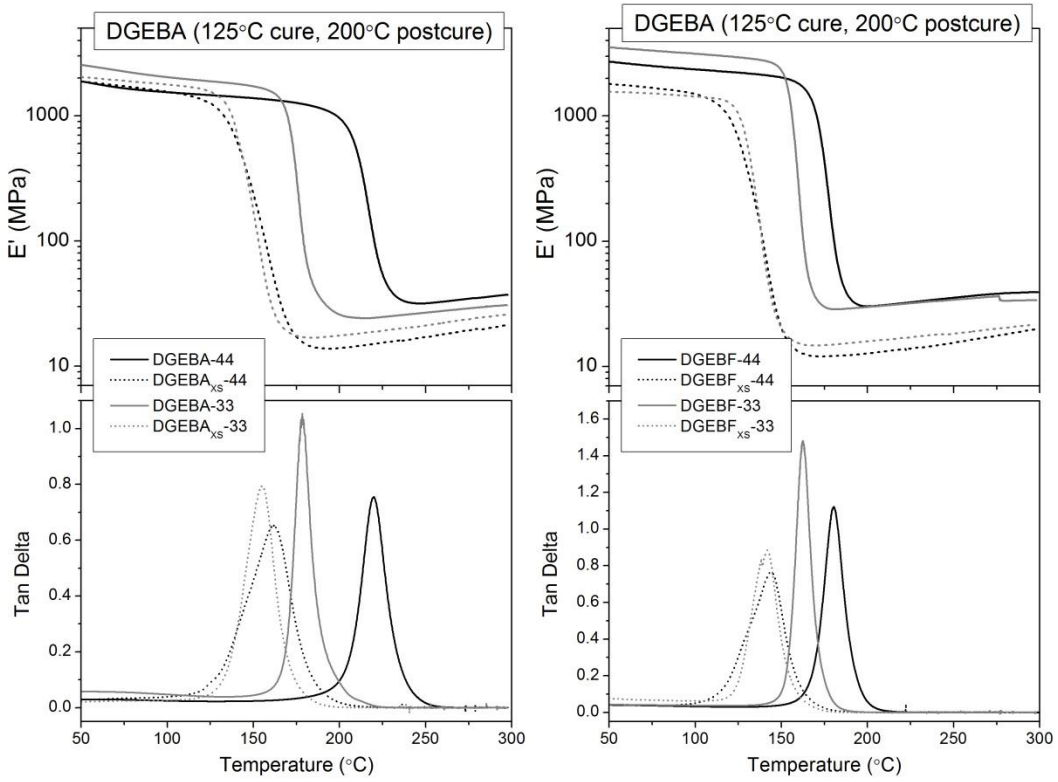

Figure 68. E' and tan delta vs. temperature for (a) DBEGA epoxies and (b) DGEBF epoxies subjected to two-step cure (125 °C/200 °C).

The overall drop in T_g can be attributed to the decrease in crosslink density and increase in M_c expected to accompany excess-epoxy formulation. Chain motions were less hindered in the materials with lower crosslink density, enabling the onset of long-range coordinated molecular motion at lower temperatures.

The narrowing gap between T_g's of 33DDS- and 44DDS-cured epoxies mirrors that seen in PALS results. The increased congruency of the excess-epoxy networks was attributed to the relatively higher fraction of epoxy resin and increased role of etherification in those systems.

The decrease in T_g between stoichiometric variations was also observed for the epoxides cured at 180 °C (Figure 69). T_g decreased in the excess-epoxy formulations compared to the benchmark materials, due to decreased crosslink density. However, the

T_g difference between 33- and 44-cured epoxies did not decrease in the excess-epoxy materials because the T_g difference was already small in the benchmark epoxies cured at 180 °C. According to research by Jackson, when DGEBF or DGEBA were cured at 125 °C/200 °C, different network architectures were developed with 33DDS and 44DDS curatives due to differences in network growth kinetics. However, when the same epoxies were cured at 180 °C, network growth kinetics were similar.[10] Therefore architectures of the cured networks were similar regardless of curatives, and this similarity was maintained in the excess-epoxy formulations.

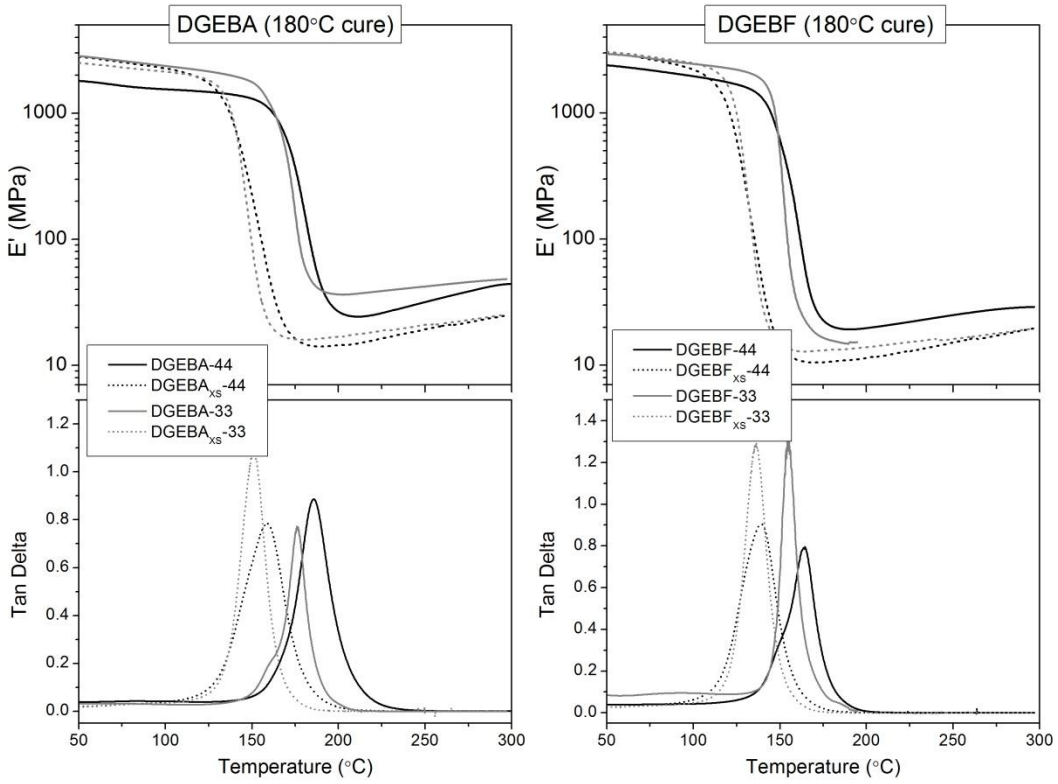

Figure 69. E' and tan delta vs. temperature for (a) DBEGA epoxies and (b) DGEBF epoxies subjected to one-step cure (180 °C).

The tan delta curves for all DGEBA-based epoxies are shown in Figure 70. The tan delta curves for excess-epoxy DGEBA formulations were similar, regardless of cure temperature or curative . The average T_g of these materials was 158 °C ± 5 °C, compared

to 190 °C ± 20 °C for the benchmark DGEBA epoxies. The same trend was present for the DGEBF-based epoxies, shown in Figure 71. The average T_g of the excess-epoxy DGEBF materials was 139 °C ± 3 °C, compared to 164 °C ± 11 °C for the benchmark DGEBF networks. The convergence of tan delta curves suggests that the excess-epoxy networks represent a "limiting case" in architecture and free volume. Chain packing cannot be enhanced indefinitely, and the excess-epoxy networks reached the maximum packing efficiency achievable this family of networks. Excess-epoxy networks cured with different DDS isomers and at different temperatures exhibited the same T_g because their network architectures had adopted the minimum accessible free volume configuration.

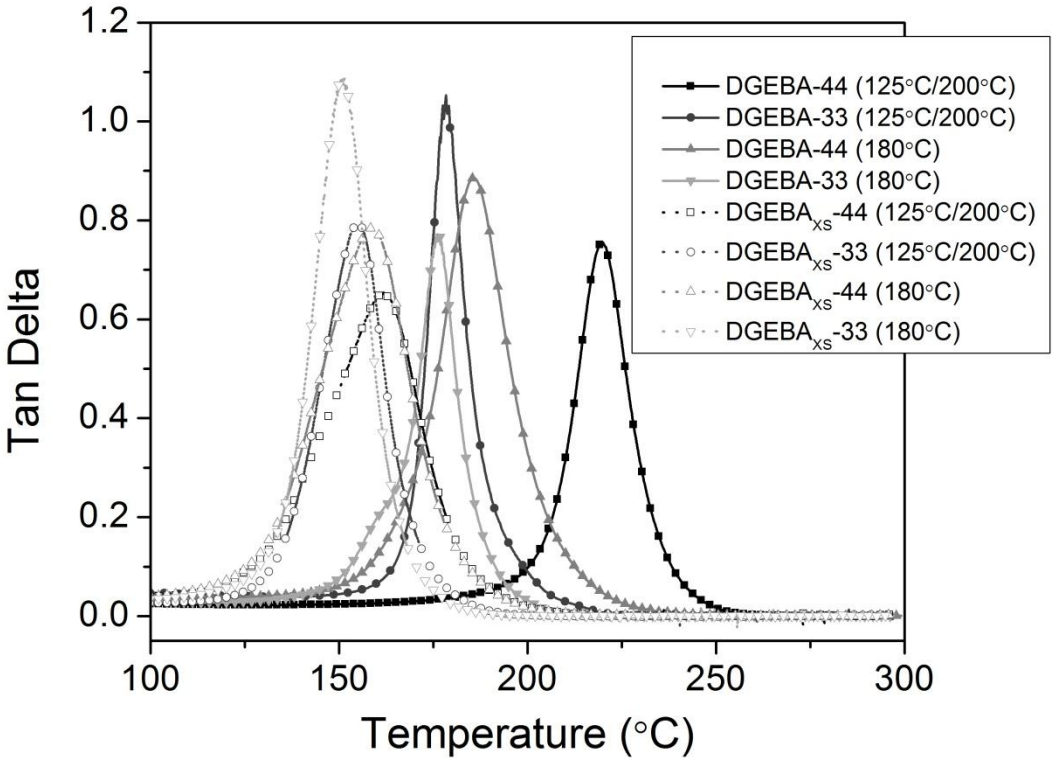

Figure 70. Tan delta vs. temperature for all DGEBA-based epoxies.

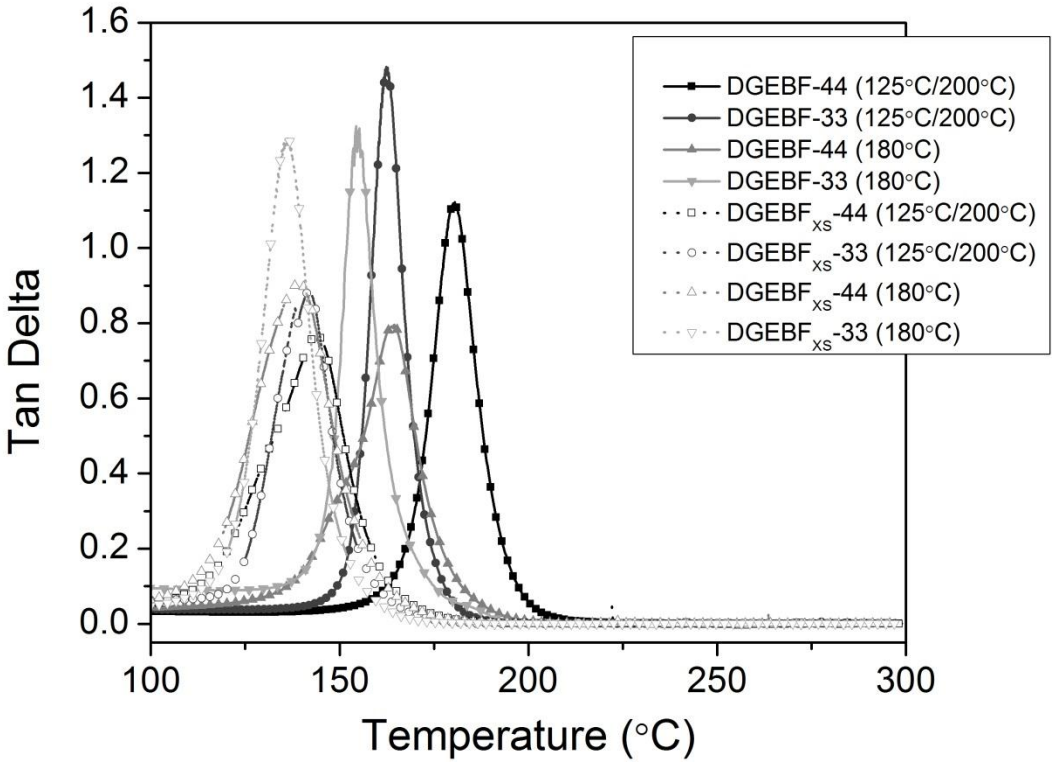

Figure 71. Tan delta vs. temperature for all DGEBF-based epoxies.

The crosslink densities of the epoxies were calculated using the rubbery plateau values of the storage moduli. For all formulations and cure conditions, crosslink density decreased when excess epoxy was used (Figure 72). This result was consistent with expectations. In a step-growth network, crosslink density is predicted to decrease when the mixture deviates from 1:1 stoichiometry because the reactive group in excess cannot complete crosslinking reactions. Differences in crosslink density between different epoxy formulations also narrowed in the excess-epoxy formulations. The crosslink densities of the benchmark epoxies varied widely, but the crosslink densities of the excess-epoxy networks were similar across curatives and cure conditions.

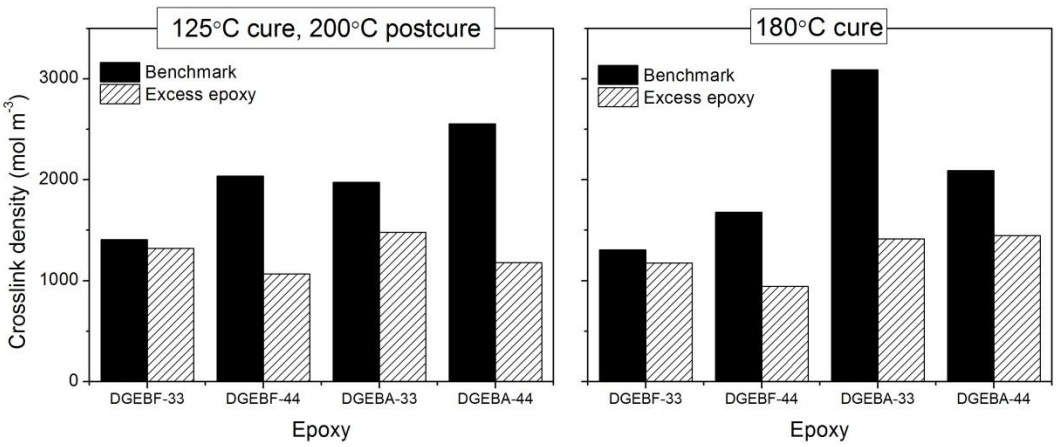

Figure 72. Crosslink densities for (a) epoxies cured at 125 °C/200 °C and (b) epoxies cured at 180 °C.

The crosslink density values for DGEBF-33 epoxies lend support to the "limiting case" argument developed from tan delta curves. Very little change in crosslink density between the excess-epoxy and 1:1 formulations was observed for DGEBF-33 for either cure prescriptions. The theory of DGEBF-33 as a limiting case was further substantiated by water and MEK uptake experiments.

Water Uptake Results

Water uptake in the epoxies proceeded according to Fickian diffusion kinetics. For the DGEBA-based materials cured at 125 °C/200 °C, lower equilibrium uptake was observed for the excess-epoxy samples (Figure 73a). Equilibrium uptake has previously been correlated to fractional free volume (FFV).[53,121] Therefore the decrease in equilibrium uptake for the excess-epoxy materials suggests a decrease in FFV. FFV likely decreased in those formulations due to enhanced packing of longer, more flexible chain segments. The difference in equilibrium uptake between 33- and 44-cured DGEBA also diminished in the excess-epoxy formulation. The gap decreased from 1.13% for the benchmark epoxies (DGEBA-33 and DGEBA-44) to 0.25% for the excess-epoxy

materials ($DGEBA_{XS}$-33 and $DGEBA_{XS}$-44). This data was in good agreement with PALS, T_g, and crosslink density information, which suggested that free volume decreased in the excess-epoxy networks and that the network architectures of 33- and 44-cured DGEBA were more similar in the excess-epoxy formulations.

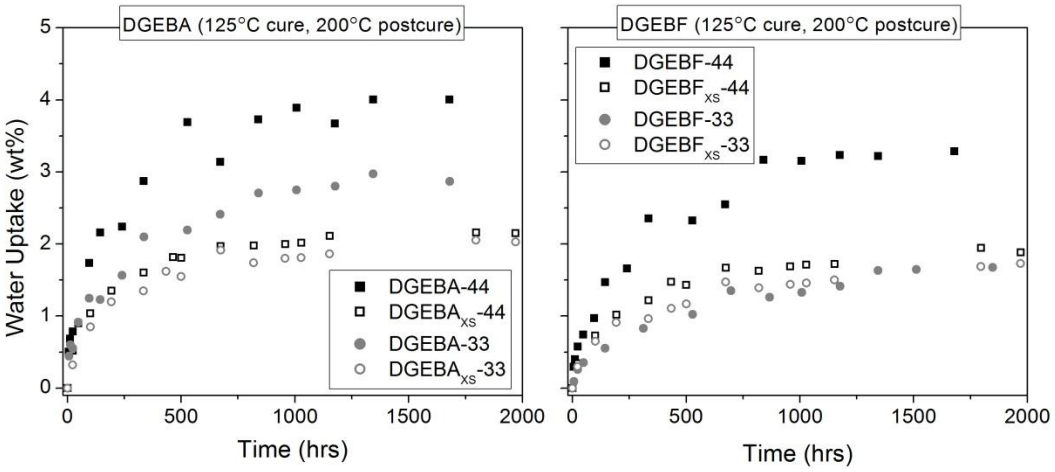

Figure 73. Water uptake vs. time for (a) DGEBA and (b) DGEBF epoxies subjected to two-step cure (125C°/200 °C).

Slightly different trends were observed for the DGEBF-based epoxies cured at 125 °C/200 °C (Figure 73b). Equilibrium water uptake decreased for the $DGEBF_{XS}$-44 epoxy as compared to the benchmark material (DGEBF-44). However, uptake in the $DGEBF_{XS}$-33 epoxy was unchanged compared to DGEBF-33. This data supports the claim that the DGEBF-33DDS benchmark represents the lowest FFV achievable by the epoxies under consideration. $DGEBF_{XS}$-33 did not have substantially lower uptake than DGEBF-33 because the stoichiometric epoxy had already reached maximum packing efficiency and minimum hole size achievable in this family of epoxies. The equilibrium uptake values for all excess-epoxy materials were similar because they encountered the same limit in packing efficiency.

Trends in water uptake for the materials cured at 180 °C were consistent with trends observed for these materials via DMA (Figure 74). The equilibrium uptake was slightly reduced in the excess-epoxy materials as compared to the stoichiometric benchmarks. The equilibrium uptake difference between DGEBA-33 and DGEBA-44 (or DGEBF-33 and DGEBF-44) was narrow in the benchmark materials. The difference, already small, did not decrease substantially with excess-epoxy treatment. Overall, equilibrium uptake for both DGEBA- and DGEBF-based epoxies cured at 180 °C were lower than uptake for the same epoxies cured at 125 °C/200 °C. The lower FFV and V_h of the benchmark epoxies cured at 180 °C has already been reported and attributed to enhanced chain packing in the linear-type network growth regime.[10]

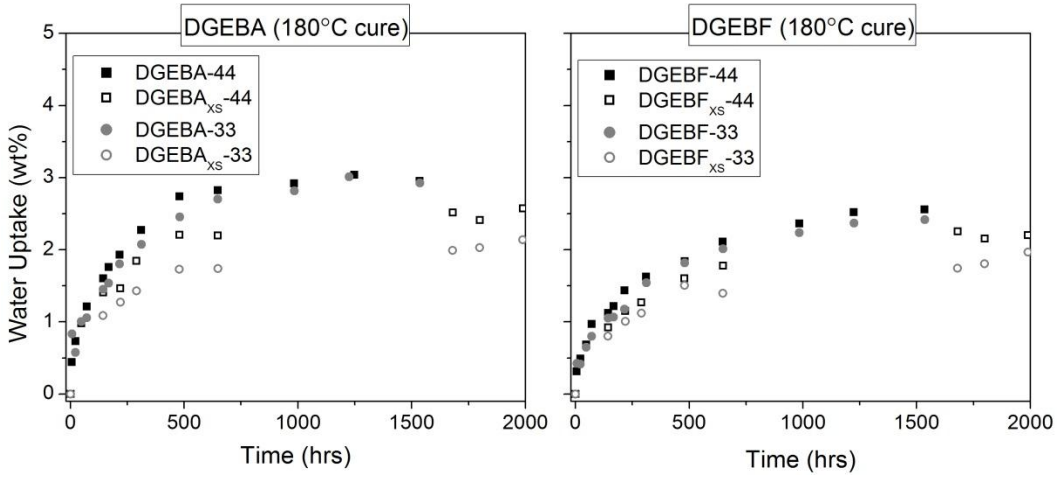

Figure 74. Water uptake vs. time for (a) DGEBA and (b) DGEBF epoxies subjected to one-step cure (180 °C).

Changes in water diffusivity were not as extreme as changes in equilibrium uptake. Diffusivities were calculated from the slope of the best-fit line of M_t/M_{inf} vs. $t^{1/2}$ (Figure 75 and Figure 76) and the values are compared in Figure 77. For most of the materials cured at 125 °C/200 °C, diffusivities were slightly higher for the excess-epoxy materials. This increase could be due to the lower crosslink densities in those materials,

which might hasten water diffusion. For the materials cured at 180 °C, diffusivities were slightly lower in the excess-epoxy materials. The 180 °C epoxies exhibited less etherification than the 125 °C/200 °C epoxies, and therefore they were assumed to have a greater number of unreacted epoxides present in the network as dangling chain ends. The dangling ends may have improved packing efficiency by function as antiplasticizers, thereby decreasing *D* in spite of the lower crosslink density.

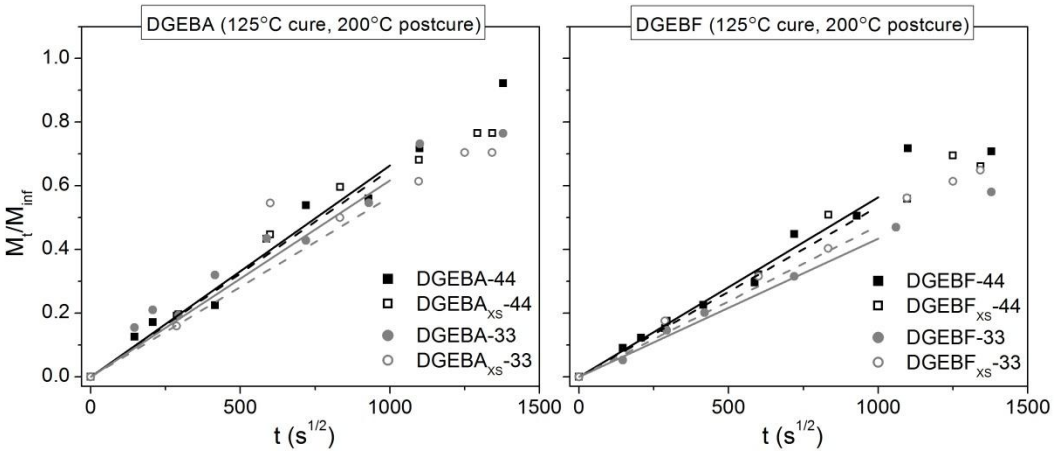

Figure 75. M_t/M_{inf} vs. time $t^{1/2}$ for (a) DGEBA and (b) DGEBF epoxies subjected to two-step cure (125C°/200 °C).

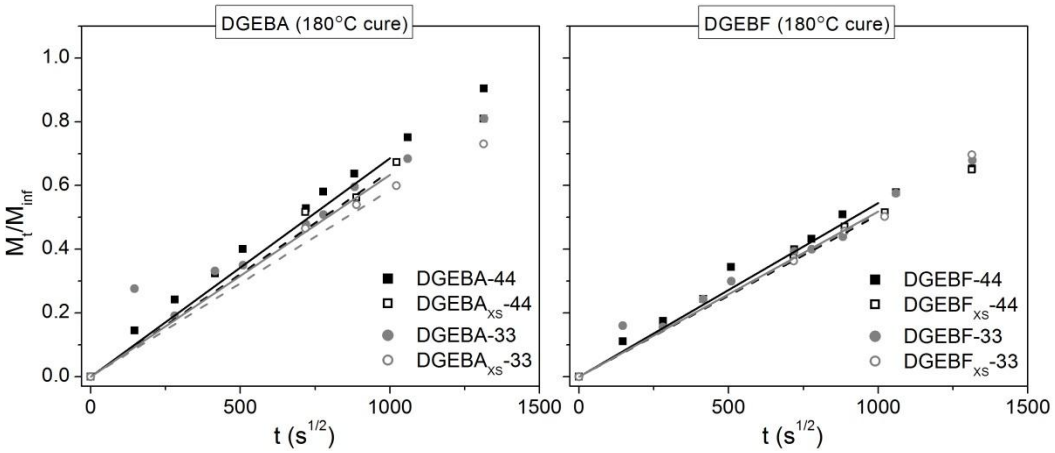

Figure 76. M_t/M_{inf} vs. time $t^{1/2}$ for (a) DGEBA and (b) DGEBF epoxies subjected to one-step cure (180 °C).

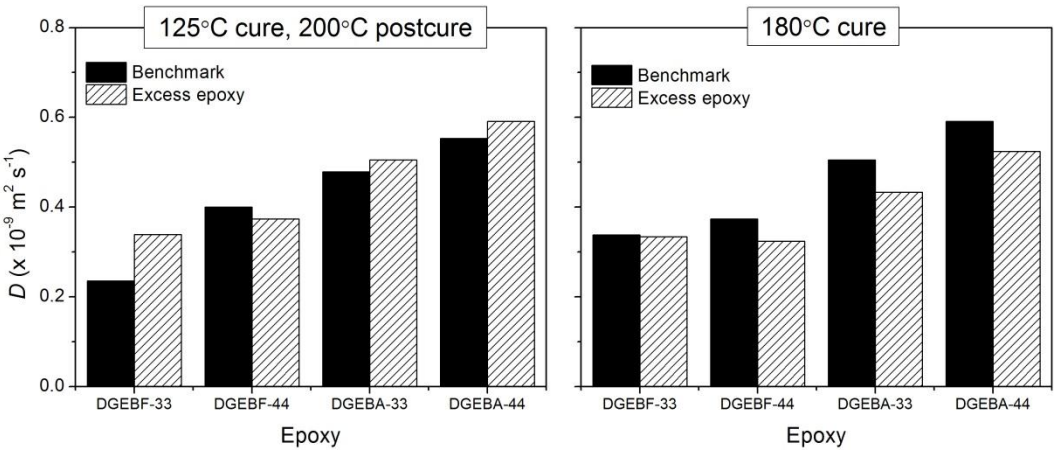

Figure 77. Diffusivity values for (a) epoxies cured at 125 °C/200 °C and (b) epoxies cured at 180 °C.

In other epoxy systems, an exponential correlation has been noted between diffusivity and V_h.[122] The *D*-V_h correlation did not have the same slope for the excess-epoxy materials, as illustrated by Figure 78. Diffusivities were higher in the excess-epoxy materials than in stoichiometric epoxies with similar hole sizes. The increased diffusivities may be due to the lower crosslink density, which could facilitate moisture transport through the material. Etherification crosslinks may also be responsible for the increased diffusivities for excess-epoxy materials. Etherification does not generate a new hydroxyl group. Hydroxyl groups may slow diffusion by forming hydrogen bonds with ingressing water molecules. Therefore a material with a lower hydroxyl concentration may exhibit an increased rate of water diffusion.

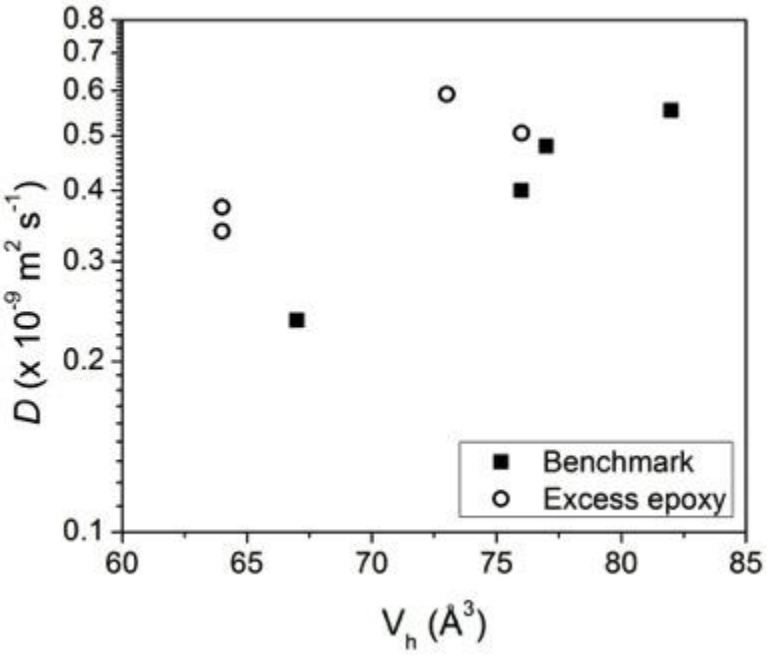

Figure 78. *D* vs. V_h for epoxies subjected to a two-step cure (125C°/200 °C).

MEK Uptake Results

MEK uptake was substantially slowed in most excess-epoxy materials, as compared to their stoichiometric analogues. MEK uptake in the excess-epoxy materials cured at 125 °C/200 °C followed the same general trends as water uptake in those materials. For the DGEBA-based epoxies, uptake rate decreased in the excess-epoxy specimens (Figure 79a). For the DGEBF-based epoxies, uptake rate decreased to approximately the rate of the DGEBF-33 epoxy (Figure 79b). For both epoxies, the difference in uptake rate between 33- and 44-cured epoxy was considerably reduced in the excess-epoxy materials.

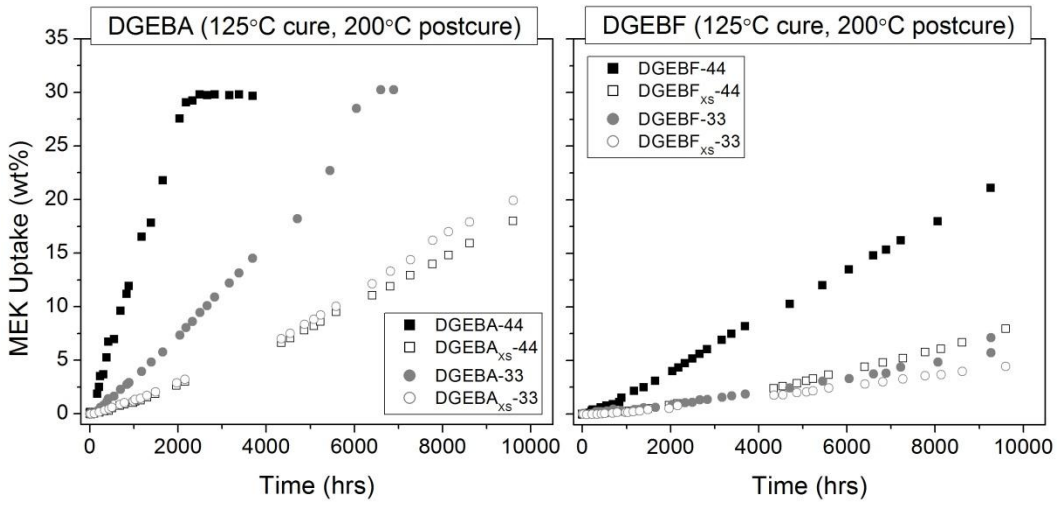

Figure 79. MEK uptake vs. time for (a) DGEBA and (b) DGEBF epoxies subjected to two-step cure (125C°/200 °C).

MEK uptake trends for DGEBA-based epoxies cured at 180 °C were followed the patterns established by preceding results. MEK uptake rate decreased for the excess-epoxy materials (Figure 80a), due to enhanced chain packing in those networks. The gap between DGEBA-33 and DGEBA-44 did not change substantially with excess-epoxy formulation (DGEBA$_{XS}$-33 and DGEBA$_{XS}$-44); the same trend was seen in DMA results for those materials.

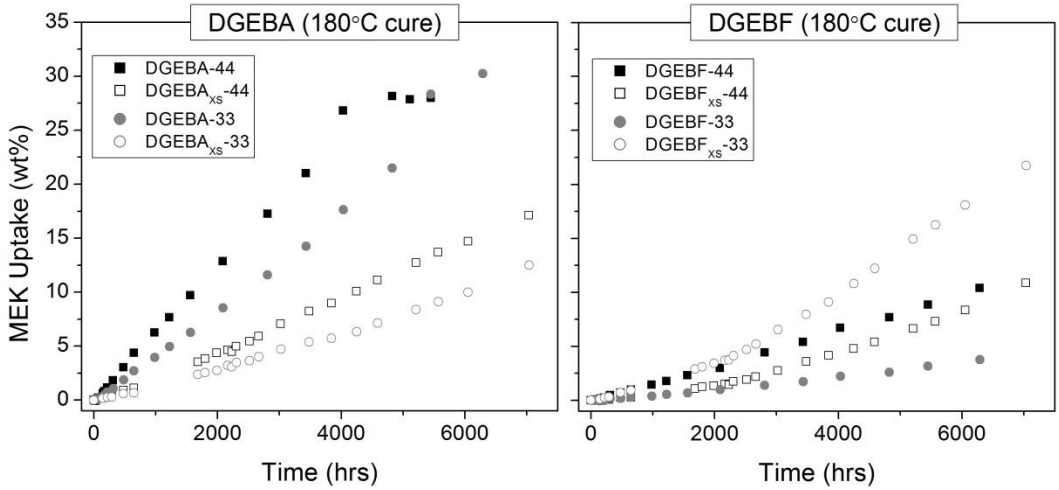

Figure 80. MEK uptake vs. time for (a) DGEBA and (b) DGEBF epoxies subjected to one-step cure (180 °C).

MEK uptake trends were less straightforward for the DGEBF materials cured at 180 °C. In those materials, MEK uptake rate was near-identical for benchmark and excess-epoxy materials until ~2000 h. (Figure 80b). At that time, the uptake curve exhibited a change in slope at ~2000 h that is uncharacteristic of Case II diffusion, and MEK uptake rate became faster for the excess-epoxy materials. The change in diffusion characteristics may be due to the T_g of the $DGEBF_{XS}$ networks. Those networks had the lowest T_g's of any material in this experiment. As a solvent plasticizes the network during Case II diffusion, the T_g of the plasticized region drops considerably.[123] A network with a lower initial T_g will have a lower plasticized T_g. Because the initial T_g of the glassy $DGEBF_{XS}$ networks was low, the T_g onset for plasticized region may have been below 25 °C (the temperature at which fluid absorption was conducted). Thus the diffusion of MEK in $DGEBF_{XS}$-33 and $DGEBF_{XS}$-44 may have shifted from solvent diffusion through a glassy material (pure Case II kinetics) into a regime involving diffusion through rubbery and glassy phases (Case II and Fickian kinetics). A shift in diffusion kinetics near T_g has been demonstrated for other polymer systems.[124,125] After 2000 h, the rubbery region was large enough to influence overall kinetics. Because diffusion through a rubbery material is more facile than diffusion through a glass, MEK uptake rate rose at that point.

Overall, the MEK uptake patterns support the hypothesis that DGEBF-33 represents a "lower limit" for free volume properties and fluid ingress in the epoxy systems under consideration. In some samples MEK uptake rate was reduced to nearly the level exhibited by DGEBF-33, but no epoxy had slower MEK uptake than that

sample. It appears that the DGEBF-33 network assumed the most efficient chain packing achievable in epoxies based on diglycidylbisphenol ethers and DDS curatives. Other networks came close to this degree of packing efficiency as a result of different stoichiometric and cure conditions, but they but did not exceed it.

Conclusions

DGEBA and DGEBF were cured with 33DDS and 44DDS in formulations using 1:1 and excess-epoxy stoichiometries. Curing was conducted in a two-step (125 °C/200 °C) or one-step (180 °C) process. Cure kinetics were followed via near-IR spectroscopy. IR results indicated that etherification occurred in all systems. Etherification was more prevalent in epoxies cured at 125 °C/200 °C due to the high temperature of the postcure. Crosslink density was calculated from the rubbery storage modulus. Crosslink density was reduced in the excess-epoxy formulations, as expected from classical understanding of step-growth networks. The competing effects of etherification, decreased crosslink density, and increased chain packing were responsible for variations in properties exhibited by the materials in this experiment.

Hole sizes were smaller overall for the excess-epoxy materials, and the difference in V_h between 33- and 44-cured materials was reduced. The increasing similarity in the excess-epoxy networks was attributed to increased contributions from etherification crosslinks and the relatively higher fraction of epoxy resin (compared to DDS) in the formulations. The same trend was noted in T_g measurements: T_g decreased in the excess-epoxy materials and the T_g gap between 33- and 44-materials narrowed, as compared to stoichiometric benchmarks. The effect on T_g gap was less pronounced in epoxies cured at

180 °C because those networks were already more similar due to similarities in growth kinetics.

Excess-epoxy treatment improved the fluid resistance of the epoxies under consideration. Equilibrium water uptake decreased by as much as 1.7 percentage points in some samples. The reduction in water uptake was attributed to a decrease in FFV, probably due to enhanced chain packing. The gap in equilibrium uptake for 33- and 44-cured materials narrowed, consistent with the narrowing gap in V_h and T_g.

MEK uptake rate decreased for the excess-epoxy formulations. The measured uptake rates were in line with expectations based on enhanced chain packing and etherification, as seen in the water uptake results. Anomalous results were recorded for the $DGEBF_{XS}$ materials, which exhibited a change in diffusion mechanism and an increase in uptake rate as compared to benchmark materials. The change was attributed to the onset of rubbery diffusion in the plasticized region of those networks.

DMA, water uptake, and MEK uptake data all provided support for the hypothesis that DGEBF-33 represents a lower limit of free volume achievable in the epoxy systems under consideration. T_g, water uptake rate, water diffusivity, and MEK uptake could not be substantially reduced below the threshold set by DGEBF-33.

The analysis of excess-epoxy materials indicated that the excess-epoxy approach is a viable avenue for improving the fluid resistance of these thermosets. Chain packing and etherification affect network architecture in ways that limit fluid diffusion. However, these architectural changes also resulted in losses in T_g that may not be acceptable in some applications.

CHAPTER VI

INVESTIGATION OF PRE-REACTION AND CURE TEMPERATURE ON MULTISCALE DISPERSION IN POSS-EPOXY NANOCOMPOSITES

Abstract

Dispersion of monoamine-functionalizedpolyhedral oligomericsilsesquioxane (POSS) in an epoxy network was improved by pre-reacting the POSS with excess epoxide and employing a high-temperature cure. DGEBA/DDS networks were formulated with 2.5 and 10 weight percent POSS. In some samples, POSS was pre-reacted with DGEBA. The hybrid materials were characterized via SEM, TEM, and DMA. The microscopy and DMA results evinced a multi-scale morphology with POSS-rich glassy domains, nano- and micro-crystallites, and crystallite agglomerations. For a loading level of 2.5 weight percent POSS, the sample with unmodified POSS cured at 125 °C had inorganic crystallites on the order of 1-5 μm and agglomerations on the order of 10-20μm, whereas the sample with pre-reacted POSS cured at 180 °C had near-perfect dispersion with no agglomerations and very few POSS crystallites. The 10 weight percent POSS epoxies also showed improved dispersion with pre-reaction and increasing cure temperature. The dispersion improvements were attributed to the enhanced miscibility of the pre-reacted POSS and the increased rate of POSS reaction into the growing epoxy network at a higher cure temperature.

Results and Discussion

POSS-epoxy nanocomposites were prepared using AI-POSS in a glassy epoxy-amine matrix based on DGEBA and 3,3'-DDS. AI-POSS is reactive and monofunctional, and with perfect dispersion it would be incorporated into the epoxy network as a pendant

group. However, AI-POSS is crystalline and does not dissolve readily in epoxy precursors. Consequently it has a high tendency to aggregate. These aggregates act as nano- or micro-fillers, exhibiting a reinforcing effect on the network.[79] In order to observe the effects of POSS as a pendant group, molecular-level dispersion of the POSS moieties is essential.

In this research, POSS pre-reaction and high-temperature curing were evaluated as methods to improve dispersion of pendant POSS in glassy epoxy networks. For one set of samples, the AI-POSS was pre-reacted with DGEBA before mixing with DGEBA and DDS. For another set of samples, unmodified AI-POSS was mixed directly into epoxy precursors. Each formulation was subjected to two-stage and one-stage curing prescriptions. The two-stage prescription, with a cure at 125 °C followed by a postcure at 200 °C, is a standard laboratory cure process for DGEBA-DDS epoxies. For the one-stage high-temperature cure, 180 °C was used because it is above the expected final T_g of the epoxy networks. POSS loadings of 2.5 and 10 weight percent were used. These levels were selected based on preliminary studies in order to examine two different dispersion scenarios. We hypothesized that near-perfect dispersion was possible with 2.5 weight percent POSS, whereas 10 weight percent POSS would produce a phase-segregated morphology even under optimized conditions.

The products of the POSS pre-reaction were characterized via SEC. The morphology of the resulting nanocomposites was characterized via TEM and SEM, with additional insight into POSS-network interactions provided by DMA results.

SEC Results

AI-POSS was pre-reacted with an excess of DGEBA, yielding a mixture of adducts and unreacted DGEBA. SEC results confirmed that the primary reaction product was an epoxy-POSS-epoxy trimer with a molecular weight of 1500 g/mol, with some higher-MW oligomers (2900 and 4100 g/mol) also present. Some unreacted AI-POSS was present at the end of the reaction. It is possible that POSS-epoxy reactions continued when all the matrix precursors were heated to 100-110 °C without solvent for mixing and degassing. Therefore the final POSS oligomers in the cured epoxy may have had higher molecular weights than indicated by the SEC traces.

SEM Results

POSS dispersion in the epoxy matrix was evaluated via SEM analysis of fractured surfaces. The SEM images of the POSS-modified epoxies showed micron-scale features. Previous authors have identified similar features in POSS-epoxy materials as crystalline POSS particles.[82,84] EDX analysis confirmed that the features were indeed POSS because they had much higher silicon contents than the surrounding epoxy matrix material. These particles will be described hereafter as crystallites and agglomerations. In this report, "crystallite" is used to refer to POSS single crystals embedded in the epoxy matrix, and "agglomeration" is used to refer to clusters of individual POSS crystallites. The observations from all SEM images are listed in Table 17.

Table 17

Observations from SEM Analysis

Sample	Crystallite Size (μm)	Agglomeration Size (μm)	Comments
2.5POSS_125	1-5	10-20	Agglomerates
2.5POSS_180	1-5	10-20	Agglomerates plus some isolated crystallites
10POSS_125	1-5	> 20	Extensive agglomeration
10POSS_180	1-5	> 20	Extensive agglomeration
2.5POSS-PR_125	1-2	5-10	Isolated crystallites plus some agglomerates
2.5POSS-PR_180	1-2	No agglomeration	Isolated crystallites
10POSS-PR_125	1-3	10-20	Agglomerates plus some isolated crystallites
10POSS-PR_180	1-3	5-10	Isolated crystallites plus some agglomerates

Micrographs of the samples with 2.5% unmodified POSS are shown in Figure 81. For the 125 °C sample, the crystallites were 1-5 μm in size and almost completely agglomerated, with agglomerations 10-20 μm in size. For the 180 °C sample, the size of crystallites and agglomerations was approximately the same, but there were some individual crystallites visible in addition to agglomerations.

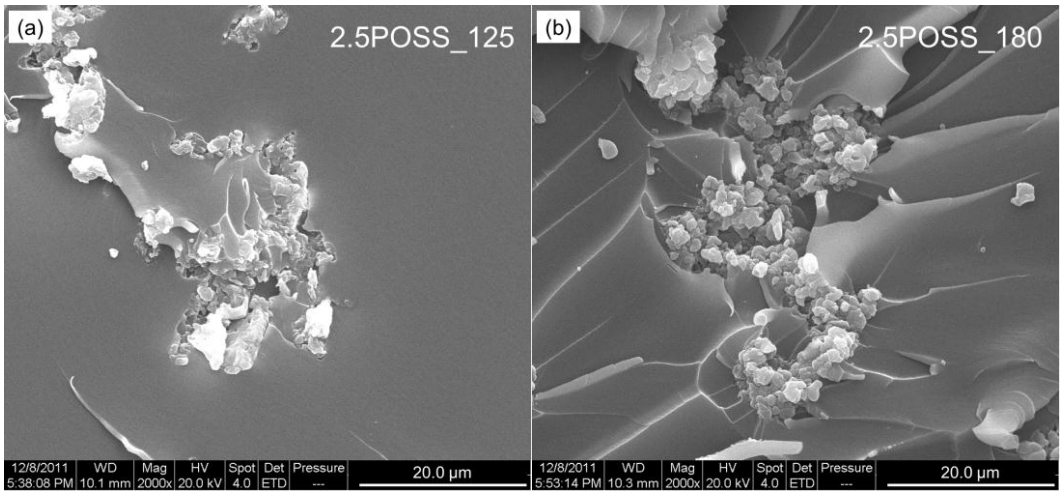

Figure 81. SEM micrographs of (a) 2.5POSS_125 and (b) 2.5POSS_180.

Micrographs of the samples with 2.5% pre-reacted POSS are shown in Figure 82 (2.5POSS-PR_125) and Figure 83 (2.5POSS-PR_180). In both samples, the crystallites were smaller than in the unmodified POSS analogs. The crystallites in the pre-reacted samples were 1-2 µm in size. For the 125 °C sample, the individual POSS crystallites were scattered throughout the matrix with minimal agglomeration. Agglomerations were on the order of 5-10 µm. For the 180 °C sample, agglomeration was even less prevalent, and the crystallites themselves were barely visible. This sample (2.5POSS-PR_180) was the only optically transparent nanocomposite in this study.

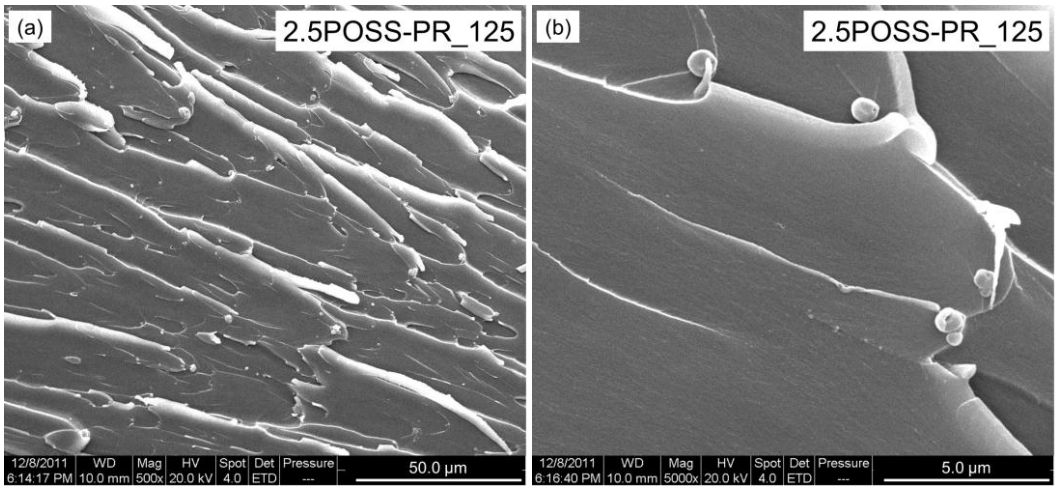

Figure 82. SEM micrographs of 2.5POSS-PR_125.

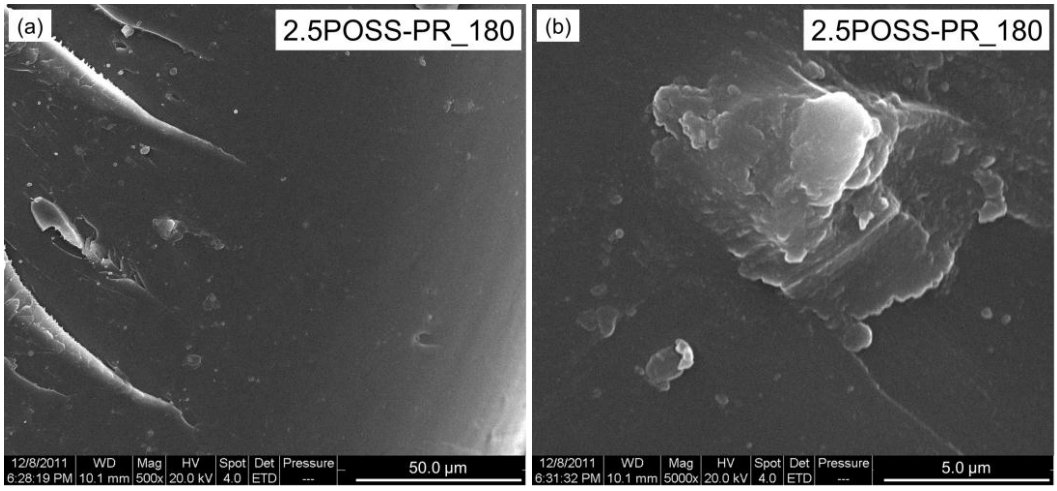

Figure 83. SEM micrographs of 2.5POSS-PR_180.

The epoxies with 10% unmodified POSS (Figure 84) both had fracture surfaces covered in 1-5 µm POSS crystallites, with regions of agglomeration greater than 20 µm in size. These agglomerates were responsible for the development of a fracture surface that was very different than that of the epoxies with less POSS content and therefore fewer POSS agglomerates.

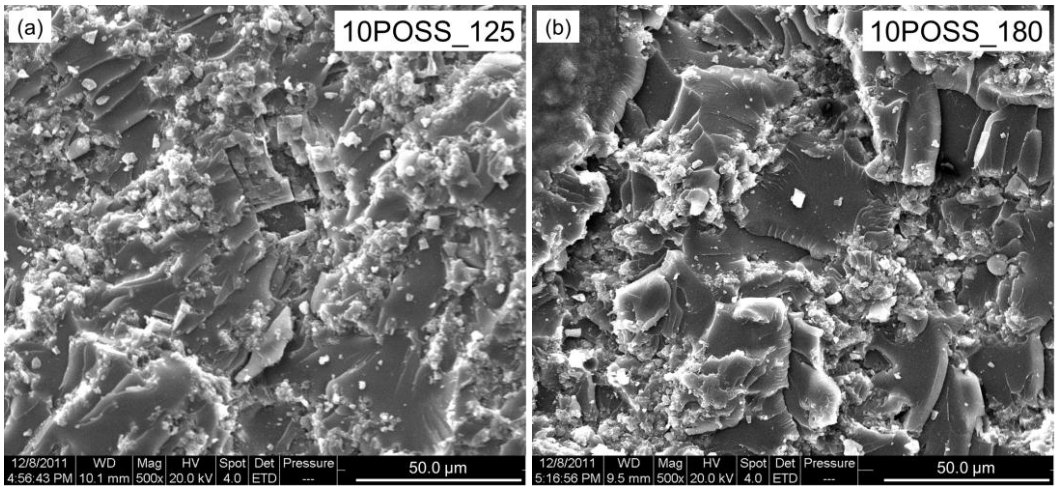

Figure 84. SEM micrographs of (a) 10POSS_125 and (b) 10POSS_180.

Dispersion was greatly improved for the pre-reacted materials. Some distinctions between the 125 °C and 180 °C cures were noted for the epoxies with 10% pre-reacted POSS (Figure 85). The crystallite size (1-3 µm) was slightly smaller than for samples with unmodified POSS. For the 125 °C sample, agglomerations on the order of 10-20 µm were visible in addition to some isolated crystallites. For the 180 °C sample, the agglomerates were smaller in size (5-10 µm) and fewer in number, with more isolated crystallites visible in the specimen.

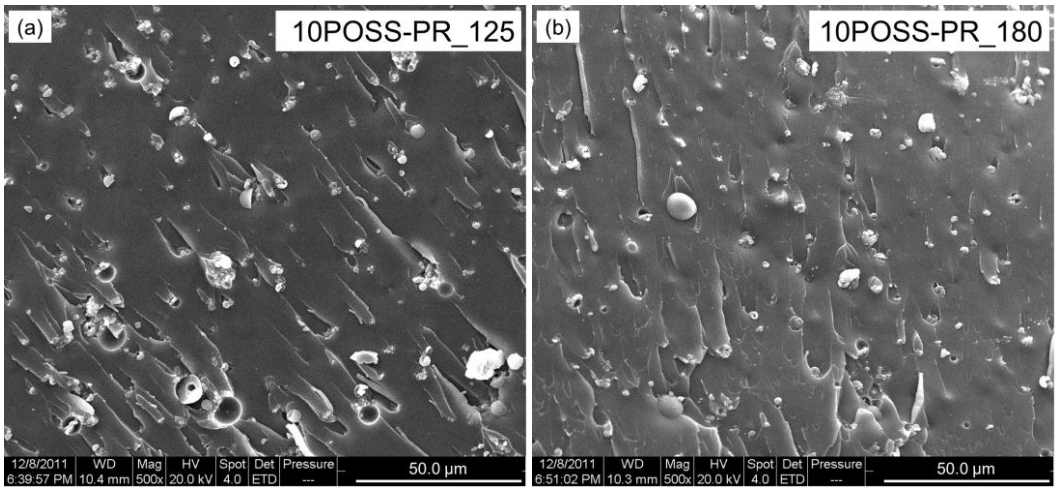

Figure 85. SEM micrographs of (a) 10POSS-PR_125 and (b) 10POSS-PR_180.

Loading level is clearly an important parameter in POSS dispersion in epoxies. The micrographs showed that near-complete dispersion can be achieved in epoxies with 2.5% POSS using a pre-reaction and a high-temperature cure. For 10% POSS, however, agglomeration and crystallization were reduced but not totally eliminated under those conditions.

The curing prescription also played a large role in improving POSS dispersion. Phase segregation and reaction into the network are simultaneous processes. Phase segregation often dominates, in part because the POSS reaction is slow.[86] It was hypothesized that a higher-temperature cure would aid in POSS dispersion by promoting reaction into the growing network in advance of phase segregation. The enhanced chain mobility of the growing epoxy network, as well as the delayed onset of vitrification, may also have improved POSS dispersion into the network at higher tempeatures. The SEM images showed that the shorter cure at 180 °C was much more conducive to dispersion than the longer cure at 125 °C followed by a postcure at 200 °C. For two sets of samples with moderate dispersion (2.5% unmodified POSS and 10% pre-reacted POSS), the 180 °C specimen had less agglomeration and more isolated crystallites than the 125 °C specimen. For the samples with 2.5% pre-reacted POSS, agglomeration was already minimal for the 125 °C cure; employing the 180 °C cure decreased the size and number of crystallites.

TEM Results

Transmission electron microscopy was used to characterize dispersion in the samples with 2.5 weight percent POSS (Figure 86, Figure 87, Figure 88, and Figure 89). All TEM images of the POSS-containing epoxies showed nanoscale features. Features

similar to these have been identified as POSS crystallites in previous research.[73,82] The low-magnification micrographs, shown on the left in these figures, depict microscale aggregates. Microscale aggregates were also seen in the SEM images at similar magnification (Figure 82b and Figure 83b). The high-magnification micrographs, shown on the right in these figures, depict nanoscale aggregates not resolvable via SEM.

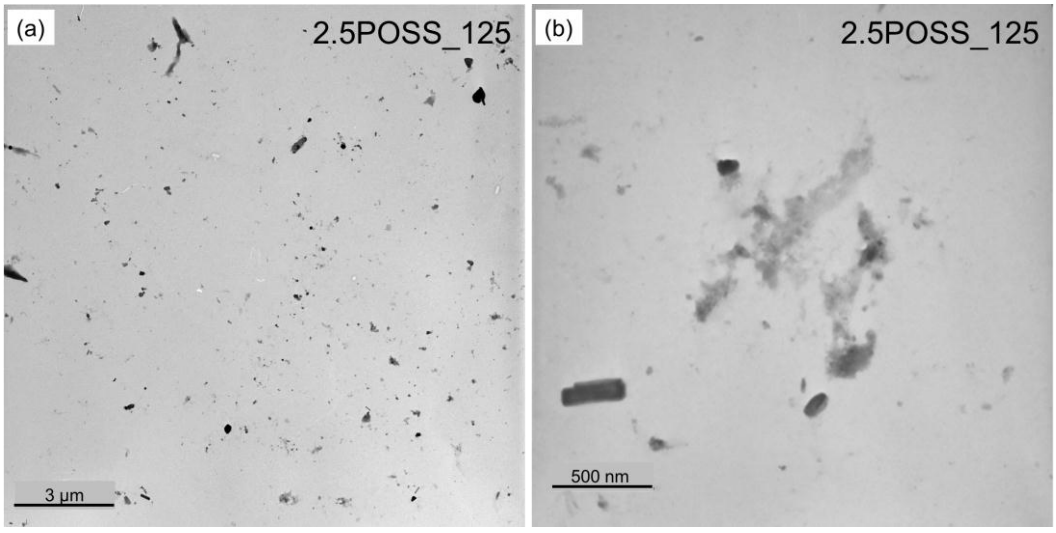

Figure 86. TEM micrographs of 2.5POSS_125.

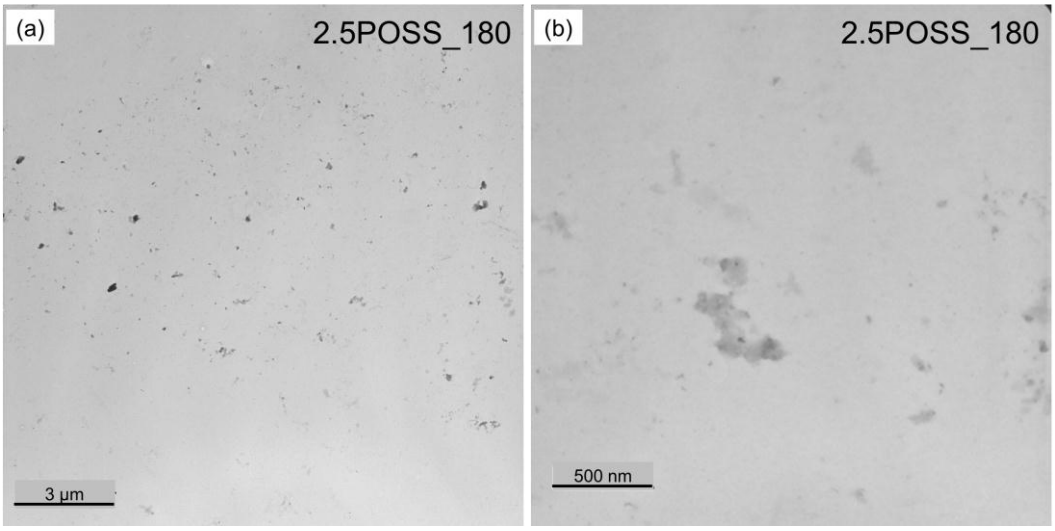

Figure 87. TEM micrographs of 2.5POSS_180.

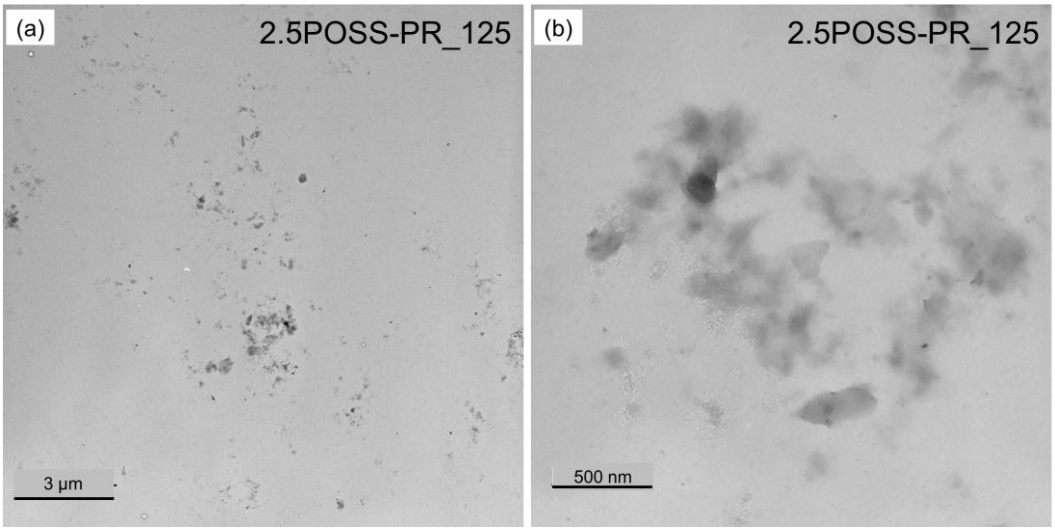

Figure 88. TEM micrographs of 2.5POSS-PR_125.

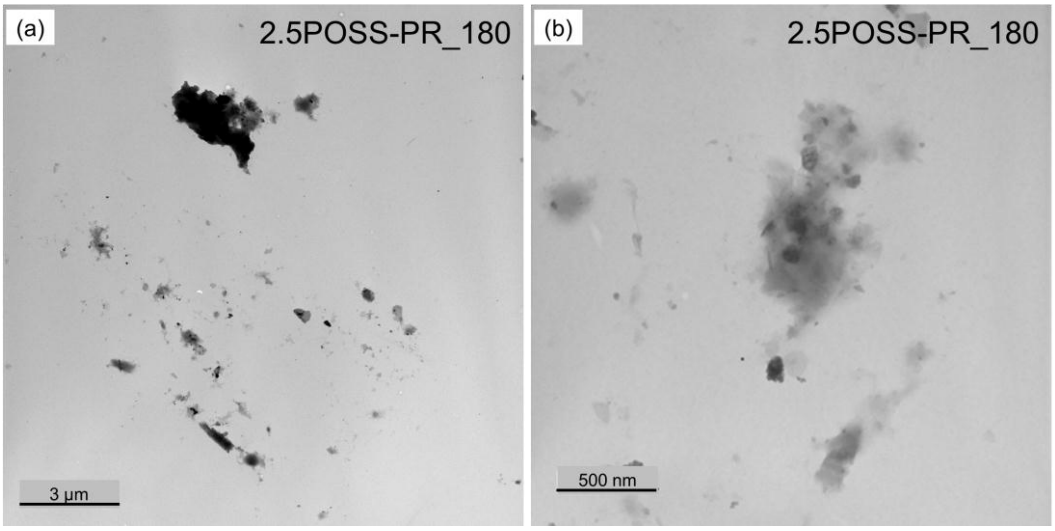

Figure 89. TEM micrographs of 2.5POSS-PR_180.

The high-magnification micrographs were analyzed with ImageJ to obtain particle size distributions. The histograms of the particle size distributions of the samples cured at 125 °C are shown in Figure 90. The sample prepared without pre-reaction had crystallites ranging from 5-150 nm in diameter (Figure 88a). The pre-reacted sample had a similar number of crystallites, but they were almost all less than 50 nm in diameter (Figure 88b). A similar trend was observed for the sample cured at 180 °C. Thus pre-reaction served to

reduce the size of nanocrystallites, though they were not eliminated completely.

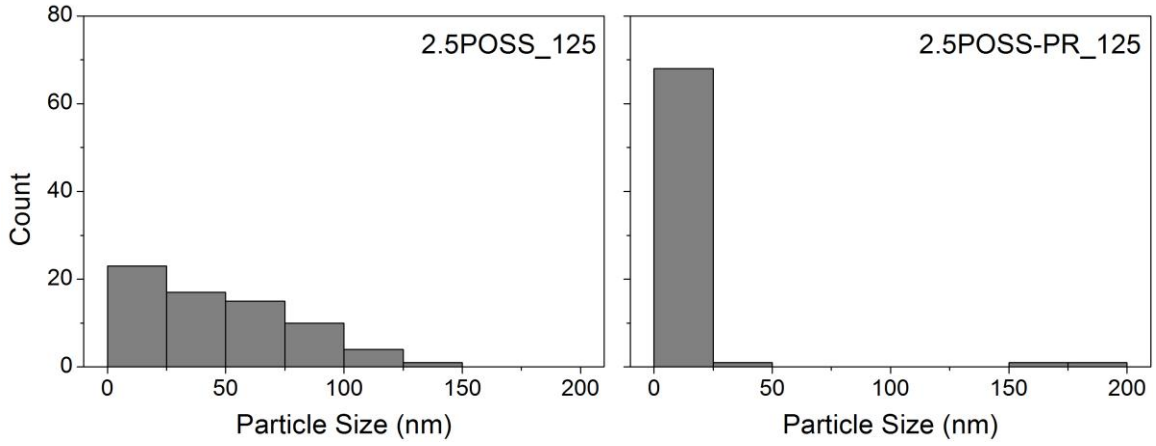

Figure 90. Particle size distribution histograms for 2.5POSS_125 and 2.5POSS-PR_180.

The crystallites resolved by TEM were significantly smaller than the 1-5 μm crystallites resolved by SEM. Thus the TEM images showed that POSS forms both microscale and nanoscale crystallites. The ubiquitous presence of these nanocrystallites indicates that pre-reaction and high-temperature curing may be effective for limiting the growth of micron-scale crystals, but some degree of aggregation is still favored at the nanoscale.

DMA Results

Viscoelastic properties of the POSS epoxies were measured via DMA. DMA is sensitive to molecular-level heterogeneities and can give insight into epoxy network architecture. The glass transition temperatures of the networks, taken as the peak of the alpha relaxation in the tan delta curve, are listed in Table 18. Plots of loss tangent (tan delta) as a function of temperature for the samples with unmodified POSS are shown in Figure 91. The tan delta curves corresponding to 2.5% POSS had low-temperature shoulders (Figure 91a). As the tan delta peak is related to molecular-level motions in the glassy epoxy network, we hypothesize that the tan delta shoulder indicates a POSS-rich

epoxy phase with moderate POSS dispersion in the epoxy. Well-dispersed POSS is believed to plasticize polymers and lower T_g by increasing free volume and reducing interaction between polymer chains.[79,88] POSS is partially crystalline in these samples, as evinced by SEM and TEM images. However, a small amount of POSS was sufficiently well-dispersed to interact directly with the epoxy and plasticize the network.

Table 18

Glass Transition Temperatures for POSS-Modified Epoxies

Sample ID	T_g of Cured Epoxy, from DMA (°C)
DGEBA/DDS_125	178
DGEBA/DDS_180	180
2.5POSS-PR_125	181
2.5POSS-PR_180	176
10POSS-PR_125	177
10POSS-PR_180	175
2.5POSS_125	182
2.5POSS_180	179
10POSS_125	184
10POSS_180	179

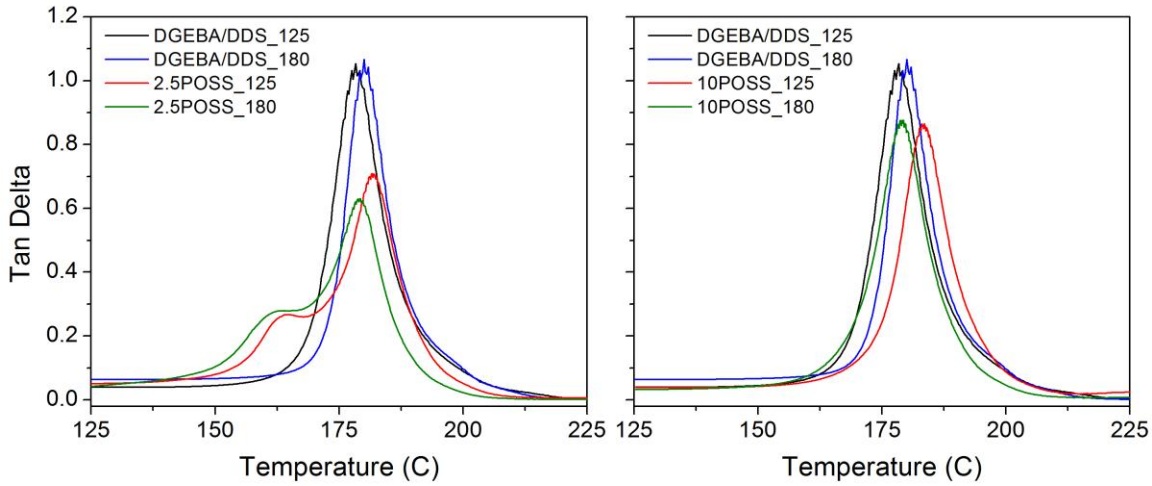

Figure 91. Tan delta curves for samples with 2.5 weight percent unmodified POSS and 10 weight percent unmodified POSS.

The tan delta curves corresponding to 10% POSS were very similar to the tan delta curve for the neat epoxy (Figure 91b). This result has been observed consistently in our laboratory for epoxies with higher loading levels of POSS. The SEM results for those samples indicated extensive POSS crystallization and agglomeration. At higher POSS loadings, when aggregation dominates POSS behavior, the glassy epoxy phase appears to be undisturbed on a molecular level. The lack of a POSS-rich epoxy phase for the samples with 10% POSS may be attributable to modified nucleation and crystallization kinetics for these samples as compared to the materials with 2.5% POSS. With more POSS crystals present initially, there were more nucleation sites to promote crystal growth. Therefore POSS was more likely to become incorporated into the crystalline phase than disperse in the glassy epoxy.

The DMA results for the samples with pre-reacted POSS are shown in Figure 92. The samples for both loading levels displayed a low-temperature tan delta shoulder. The peak broadening in these curves is evidence of increasing heterogeneity in the glassy epoxy network. The shoulders indicate a POSS-rich epoxy phase for all samples, even

with 10 weight percent POSS. The shoulders are evidence of molecular-level dispersion of POSS in the epoxy for all pre-reacted samples.

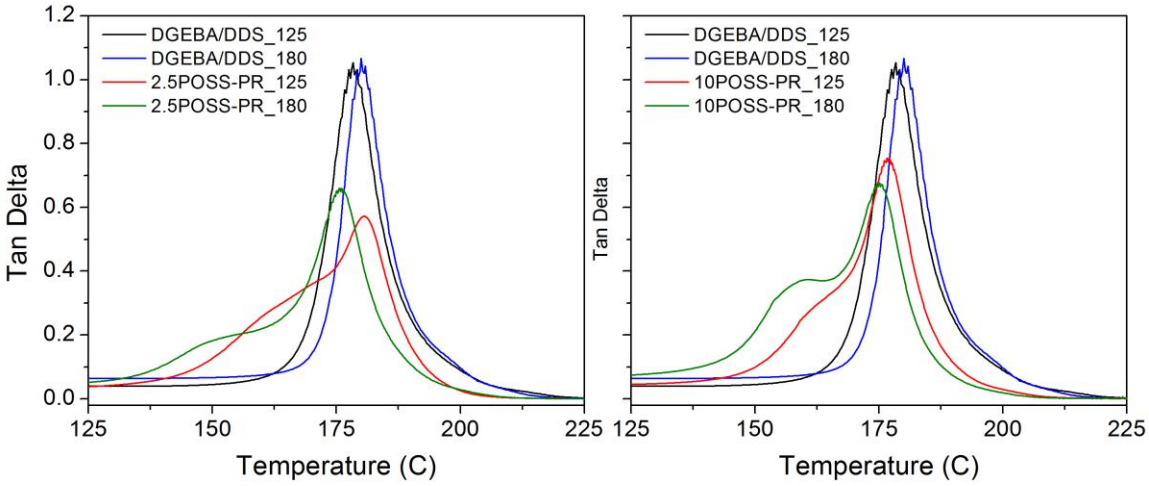

Figure 92. Tan delta curves for samples with 2.5 weight percent pre-reacted POSS and 10 weight percent pre-reacted POSS.

No significant trends were observed for the storage modulus (E'), also obtained via DMA (Figure 93 and Figure 94). The variations in E' across the samples could not be correlated to POSS loading level or pre-reaction state. These variations may be attributable to the complex effects of POSS on bulk material properties. In these epoxies, POSS exists in a variety of dispersion states, giving rise to a variety of POSS-epoxy interactions. These interactions can usually be simplified as plasticizing and reinforcing. Often one interaction is dominant, but the identity of that interaction can vary from sample to sample. The E' values for these epoxies reflected that variability in POSS effect on bulk properties.

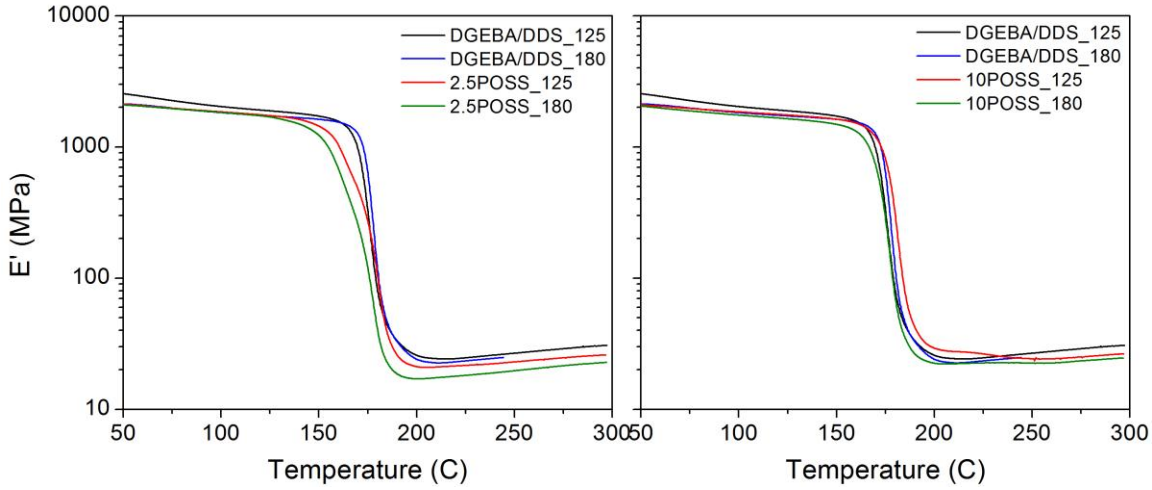

Figure 93. E' vs. temperature for samples with (a) 2.5 weight percent unmodified POSS and (b) 10 weight percent unmodified POSS.

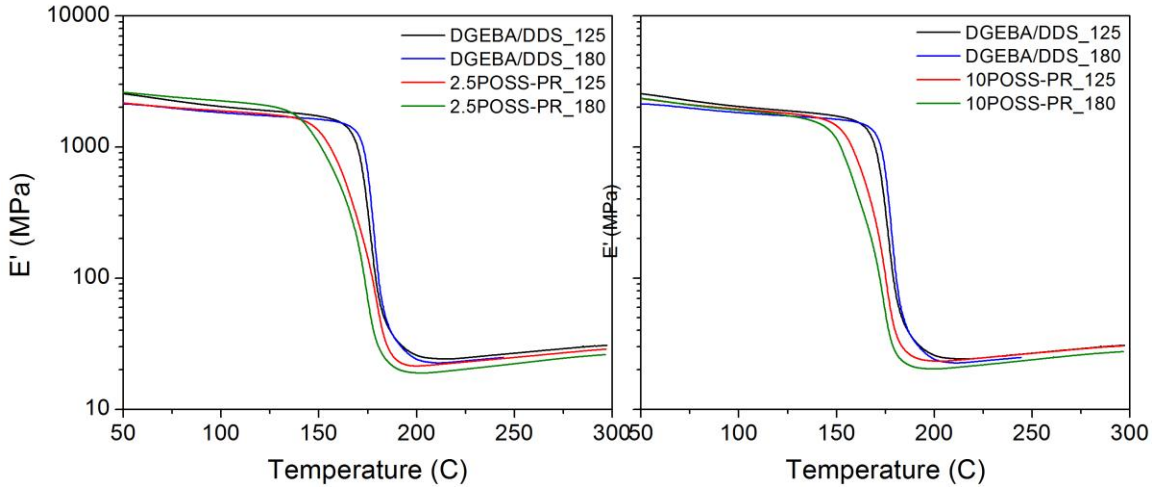

Figure 94. E' vs. temperature for samples with 2.5 weight percent pre-reacted POSS and 10 weight percent pre-reacted POSS.

Conclusions

POSS compounds are a subject of significant interest in polymer research because of their potential for producing hybrid organic-inorganic materials with novel properties. Much of the research on POSS-modified epoxies has focused on multifunctional POSS, which is easily dissolved in epoxy precursors. Multifunctional POSS is incorporated into epoxy networks as a junction point. In contrast, dispersed monofunctional POSS is

tethered to the network as a bulky pendant group. The pendant group has the potential to alter the mechanical properties of the network by increasing free volume and introducing new modes of molecular motion. However, mono-amine POSS compounds are crystalline solids at room temperature and insoluble in epoxy precursors under standard conditions. When mixed and cured into epoxies using standard procedures, they aggregate into micro- or nano-scale crystals.

In this research, two approaches were evaluated for improving the molecular-level dispersion of monofunctional POSS in epoxies. In one approach, AI-POSS was pre-reacted with DGEBA to enhance its solubility in epoxy precursors. In another approach, the epoxies were cured at 180 °C to increase the POSS reaction rate such that incorporation into the epoxy network was competitive with phase segregation.

Mixing monofunctional AI-POSS in a DGEBA/DDS epoxy matrix at loading levels of 2.5 and 10 weight percent produced hybrid nanocomposites. The dispersion of POSS in the cured epoxies was evaluated via SEM and TEM, and viscoelastic properties were measured using DMA. The characterization results showed a spectrum of dispersion states, with a POSS-rich glassy epoxy phase, nanocrystallites (0.1-1 μm), microcrystallites (1-5 μm), and agglomerations of microcrystallites (>5 μm).

The pre-reaction dramatically improved dispersion, as shown by a decrease in the number of microcrystallites and an increase in the prominence of a tan delta shoulder related to the POSS-rich epoxy phase. The high-temperature cure also promoted dispersion, with the samples cured at 180 °C showing fewer agglomerations and more isolated crystallites than the samples cured at 125 °C. The combination of optimal conditions—low POSS loading, POSS pre-reaction, and high-temperature cure—resulted

in an optically transparent nanocomposite with near-molecular-level dispersion of pendant POSS in the epoxy matrix.

CHAPTER VII

STRUCTURE-PROPERTY RELATIONSHIPS IN EPOXIES MODIFIED WITH MONOFUNTIONAL AND PRE-REACTED POSS

Abstract

Pre-reacted $POSS_{trimer}$ and unmodified AI-POSS were incorporated into epoxies based on DGEBF and 3,3'-DDS. Morphology was characterized with SEM. The samples containing unmodified POSS exhibited a bulk epoxy phase with crystalline POSS aggregates. The samples containing $POSS_{trimer}$ exhibited an epoxy-rich phase with dispersed pendant POSS and a POSS-rich phase composed of weakly-bound $POSS_{trimer}$ crystals. The different morphologies impact T_g and crosslink density. For samples with unmodified POSS, T_g and crosslink density initially decreased due to the plasticizing effect of pendant POSS, and then increased due to the fortifying effect of POSS aggregations. For samples with $POSS_{trimer}$, T_g and crosslink density experienced a larger and longer initial decrease due to enhanced plasticization by $POSS_{trimer}$; those properties ultimately increased as POSS aggregation became significant at higher loading levels. Fluid uptake properties were largely unaffected by POSS loading because the uptake-promoting effect of POSS pendants and the uptake-inhibiting effect of POSS aggregates were in direct competition. At longer times, POSS aggregates caused premature cracking in samples exposed to acetone.

Results and Discussion

In POSS-modified epoxies, the nature of POSS-polymer interaction governs material properties, including glass transition temperature (T_g), crosslink density, free volume characteristics, fluid resistance, and mechanical properties. POSS-polymer

interaction is itself a function of dispersion state. The dispersion of unmodified and pre-reacted POSS ($POSS_{trimer}$) in loading levels of 0-2.5 weight percent was characterized via SEM. Properties of the final materials were evaluated via DSC, DMA, compression analysis, and compression testing. The material properties were related to dispersion state in order to develop a deeper understanding of the origins and impacts of POSS-epoxy interactions.

SEM Analysis

The morphologies of POSS-epoxy samples were examined with scanning electron microscopy at various magnifications. Images of epoxies containing unmodified POSS are shown in Figure 95, Figure 96, Figure 97, Figure 98, and Figure 99. Those epoxies exhibited two distinct phases: bulk epoxy (major phase) and crystalline POSS agglomerates (minor phase). The features in the POSS phase were conclusively identified as POSS crystallites in previous research on similar materials.[126]

In the sample with 0.5% POSS (Figure 95), the bulky epoxy phase contained some isolated POSS aggregates <10 μm in diameter while the POSS phase was composed of agglomerated crystallites >10 μm in size.

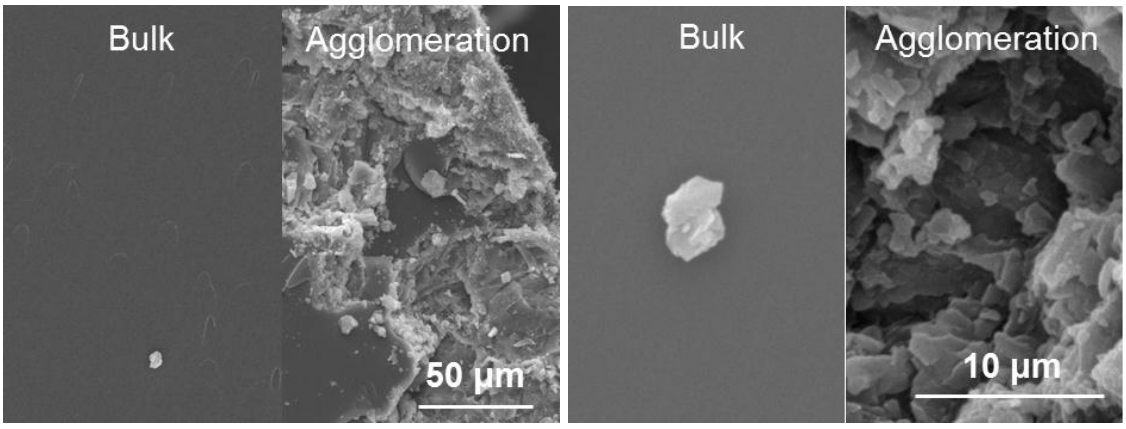

Figure 95. SEM images of 0.5POSS epoxy at low and high magnifications.

The samples with 1.0% POSS (Figure 96) and 1.5% POSS (Figure 97) also exhibited bulk epoxy and crystalline POSS phases. However, the bulky epoxy phase contained more isolated crystallites in these materials than in the 0.5POSS specimen. A preponderance of POSS crystallites appeared in the bulk epoxy phase for the sample with 2.0% POSS (Figure 98). The crystalline phase occupied a slightly greater volume fracture in the 1.0POSS, 1.5POSS, and 2.0POSS specimens, as was expected from the increased POSS content. The size scale of the isolated crystallies (<10 μm) and agglomerations (>10 μm) remained the same for the higher POSS loadings.

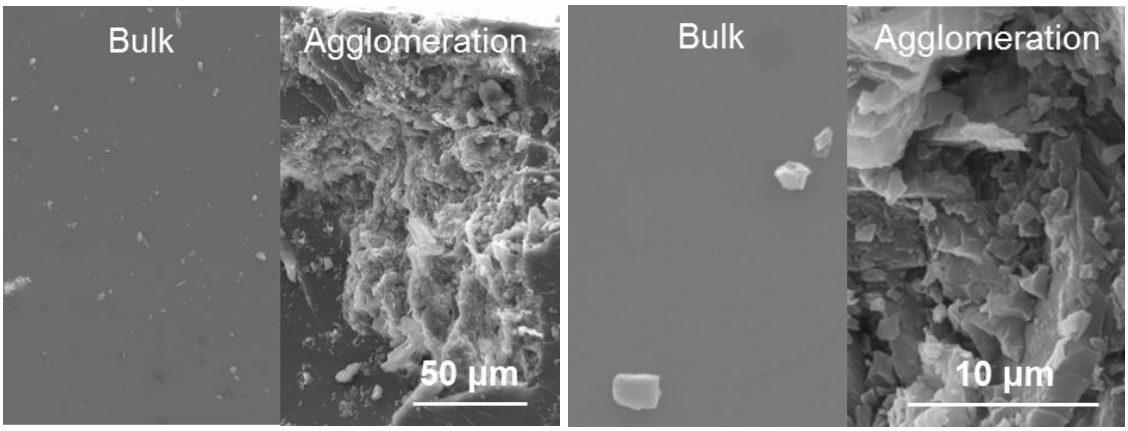

Figure 96. SEM images of 1.0POSS epoxy at low and high magnifications.

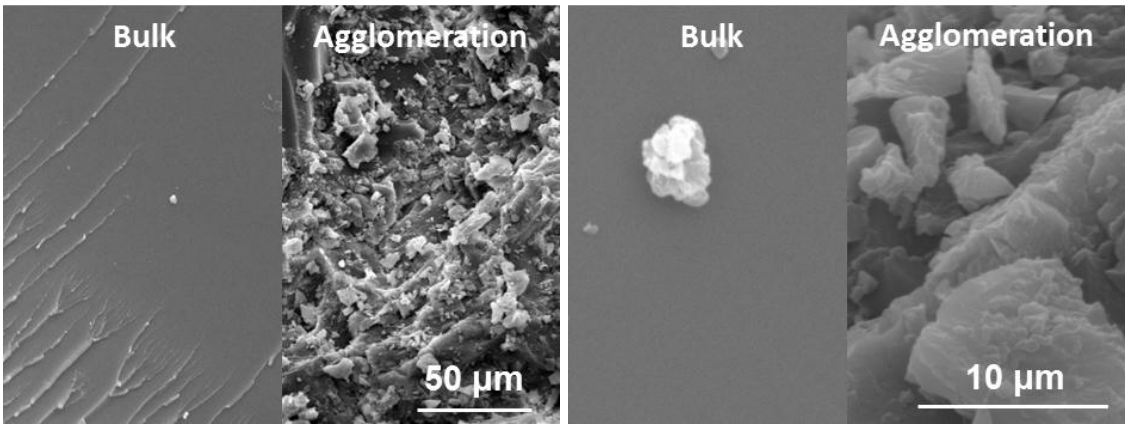

Figure 97. SEM images of 1.5POSS epoxy at low and high magnifications.

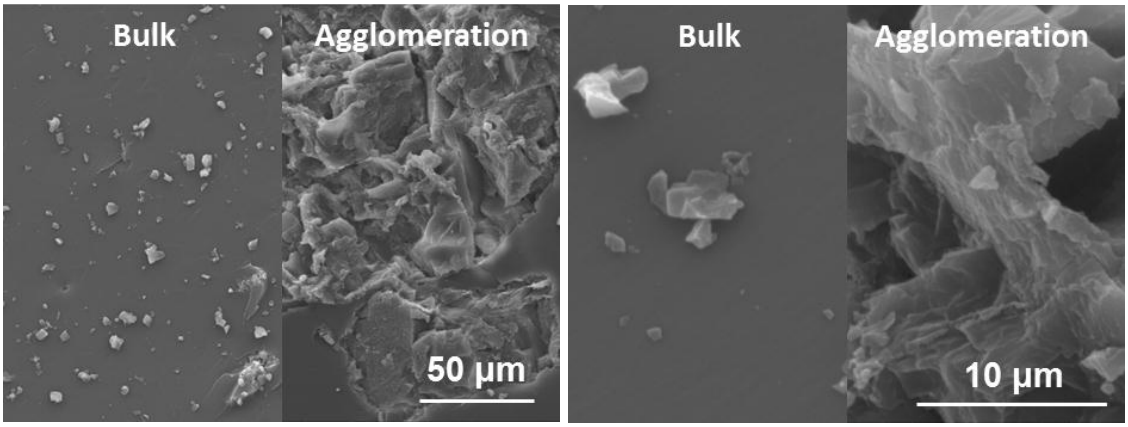

Figure 98. SEM images of 2.0POSS epoxy at low and high magnifications.

The sample containing 2.5% POSS was the first in the series to deviate from the size scales evident at lower loadings. As shown in Figure 99b, the isolated POSS crystallites in the bulk epoxy phase in that material were >10 µm in diameter. At lower concentrations, increasing POSS content increased POSS crystal nucleation rate. The result was an increase in the number of POSS aggregates of the same size in the bulk epoxy. At a concentration of 2.5% POSS, crystal growth rate began to increase, resulting in larger crystallites at that loading level.

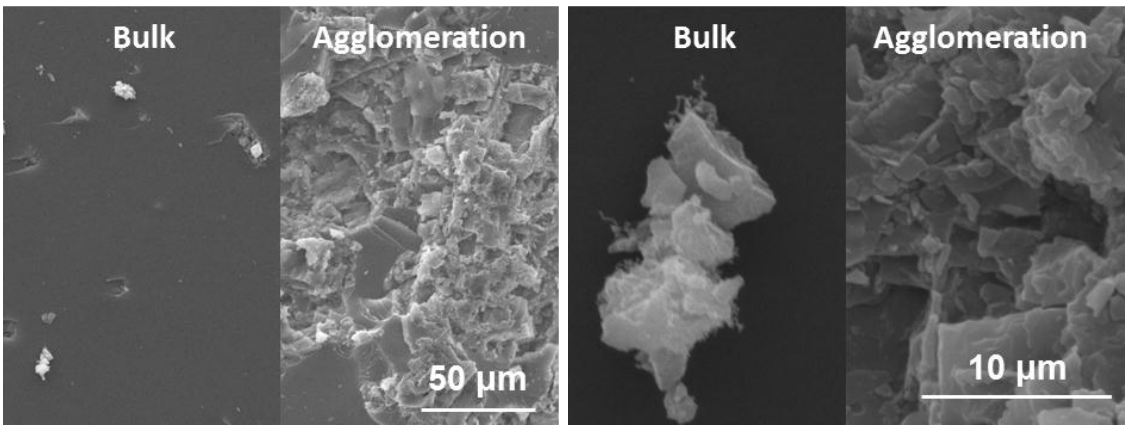

Figure 99. SEM images of 2.5POSS epoxy at low and high magnifications.

The presence of micron-scale aggregates in all epoxies with unmodified POSS suggested that the effect of POSS as a microfiller phase must be considered when

discussing structure-property relationships for those materials. Unmodified AI-POSS is reactive, so it is probable that some POSS reacted with epoxide molecules and became tethered to the network as dispersed pendant groups. This was particularly likely at low concentrations, where fewer POSS crystal nucleation sites were available. The competing effects of dispersed POSS and aggregated POSS will be discussed in relation to material properties later in this chapter.

Morphologies of the samples containing pre-reacted POSS were evaluated in light of slightly different microstructural characteristics than the preceding (unmodified POSS) samples. In the $POSS_{trimer}$ molecule, each POSS moiety was attached to two DGEBF monomer units. As a result, the $POSS_{trimer}$ was expected to form much weaker crystals than unmodified AI-POSS. Therefore aggregates in the $POSS_{trimer}$-containing epoxies were less sharply defined as a crystalline phase than AI-POSS aggregates. It may be appropriate to describe the aggregates in $POSS_{trimer}$ as a "POSS-rich phase" that also incorporates some epoxy. Correspondingly, because pre-reaction has been shown to improve nanoscale or molecular-level dispersion, the bulk epoxy may be considered an "epoxy-rich phase" in which POSS units are tethered to the network backbone or aggregated in nanocrystalline domains not resolvable via SEM.

SEM images of $POSS_{trimer}$ epoxies are shown in Figure 100, Figure 101, Figure 102, Figure 103, and Figure 104. Some evidence of POSS agglomeration persisted for all the $POSS_{trimer}$ samples, in the form of the POSS-rich weakly crystalline phase described above. Dispersion was markedly improved for the samples with pre-reacted POSS. Well-defined crystalline aggregations (like those seen for unmodified POSS) were not visible in any of the specimens. For the sample with 0.5% $POSS_{trimer}$, the only evidence of POSS

aggregation in the material was arcs in the fracture pattern (Figure 100). These arcs are characteristic of crack pinning.[127] Crack pinning occurs when a heterogeneity in the matrix disrupts crack propagation. For this sample, the heterogeneities were assumed to be POSS-rich agglomerates that resisted cracking. Despite the crack pinning, no aggregates were visible at high magnification.

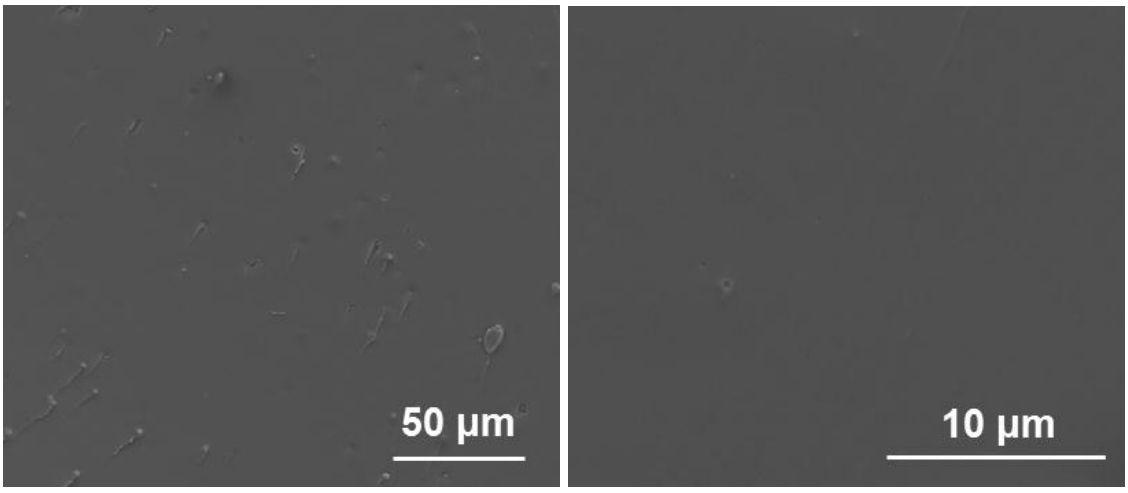

Figure 100. SEM images of 0.5POSS$_{trimer}$ epoxy at low and high magnifications.

When POSS$_{trimer}$ loading was increased to 1.0-1.5 %, some agglomerates were visible in addition to the crack pinning patterns (Figure 101 and Figure 102). These agglomerates were smaller than the crystallites in unmodified POSS (< 5µm) and rounded rather than angular. Both of these characteristics are consistent with a description of the agglomerates as a POSS-rich phase with poorly defined crystals.

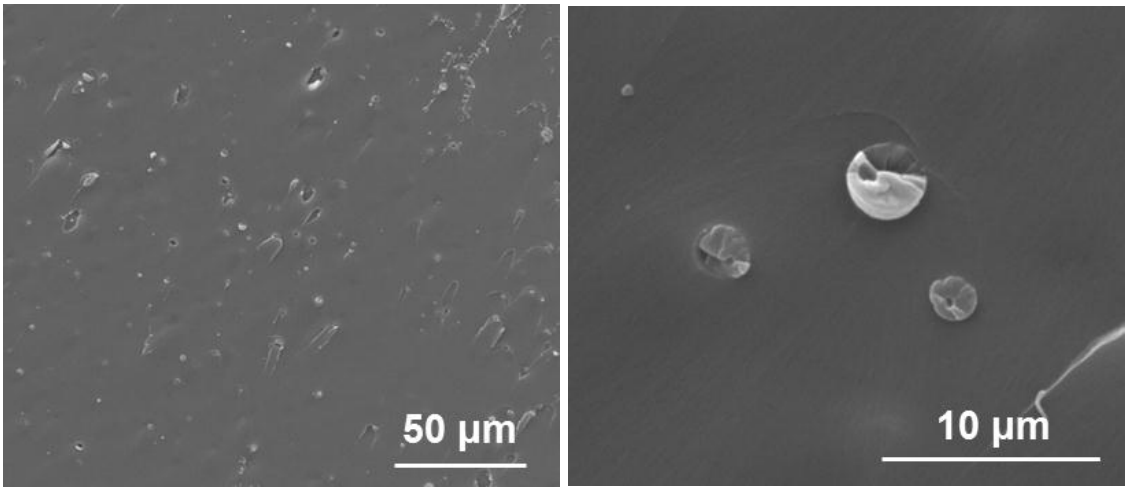

Figure 101. SEM images of 1.0POSS$_{trimer}$ epoxy at low and high magnifications.

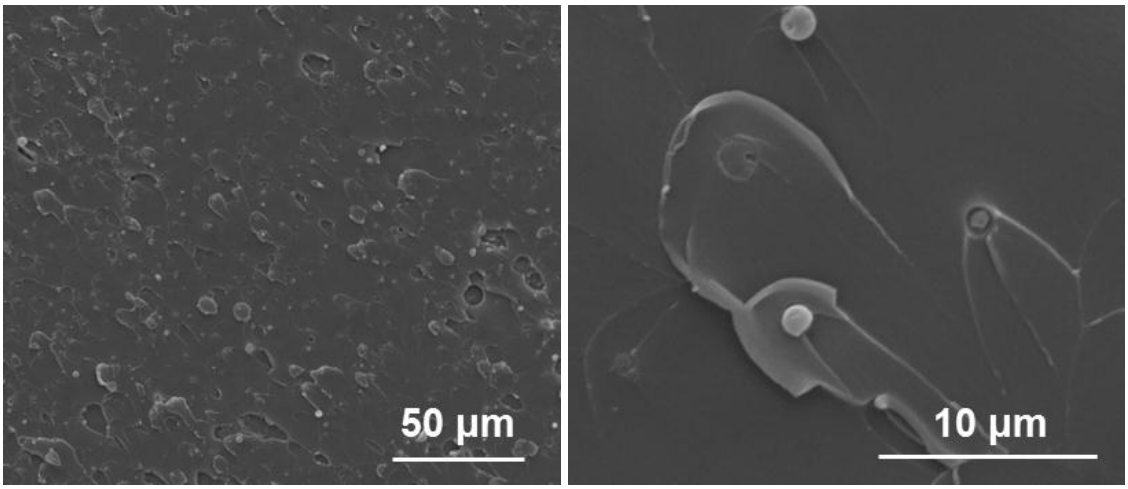

Figure 102. SEM images of 1.5POSS$_{trimer}$ epoxy at low and high magnifications.

Larger and more numerous agglomerates were present in the samples containing 2.0-2.5% POSS$_{trimer}$ (Figure 103 and Figure 104). More agglomerates were visible at low magnification, and some individual agglomerates were close to 10 µm in diameter. The change in agglomerate characteristics indicated that critical thresholds for aggregate nucleation and growth were surpassed at these loading levels.

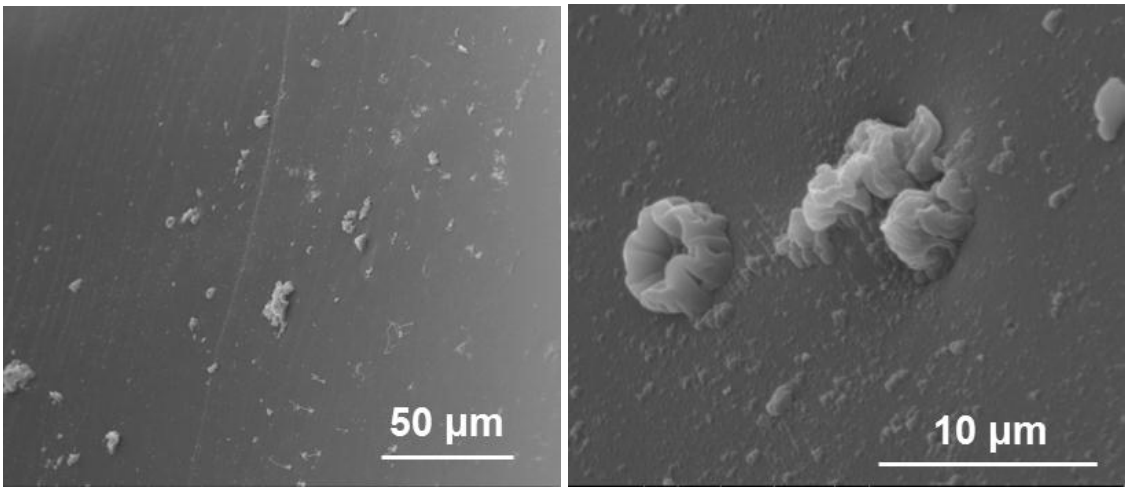

Figure 103. SEM images of 2.0POSS$_{trimer}$ epoxy at low and high magnifications.

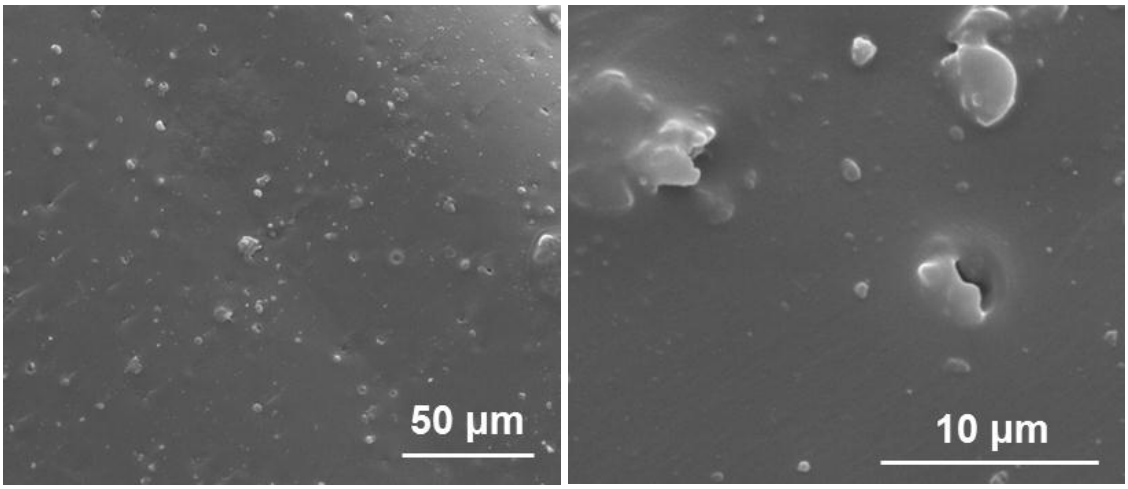

Figure 104. SEM images of 2.5POSS$_{trimer}$ epoxy at low and high magnifications.

Structure-property relationships in the POSS$_{trimer}$ epoxies were predicted to follow different trends than those for unmodified POSS, given the morphological differences. The unmodified POSS materials included crystalline POSS aggregates (which could function as micro-fillers) in addition to some well-dispersed pendant POSS. The POSS$_{trimer}$ materials, on the other hand, contained varying fractions of an epoxy-rich phase with pendant POSS units and a POSS-rich phase with poorly-defined POSS$_{trimer}$ crystals. The different microstructural characteristics of POSS and POSS$_{trimer}$ affected the

thermal and thermomechanical properties of the epoxy in different ways, as seen in DMA and DSC results.

DMA Results

Viscoeleastic properties of the cured epoxies were probed over the -120 °C–300 °C range for all materials in order to evaluate both the beta transition and alpha transitions. The DMA results, including storage modulus (E') and tan delta, are shown in Figure 105 (unmodified POSS) and Figure 106 ($POSS_{trimer}$). As the POSS loadings employed in this experiment were small, they did not have a dramatic impact on viscoelastic properties. However, deeper scrutiny of the tan delta curves revealed subtle differences between epoxies.

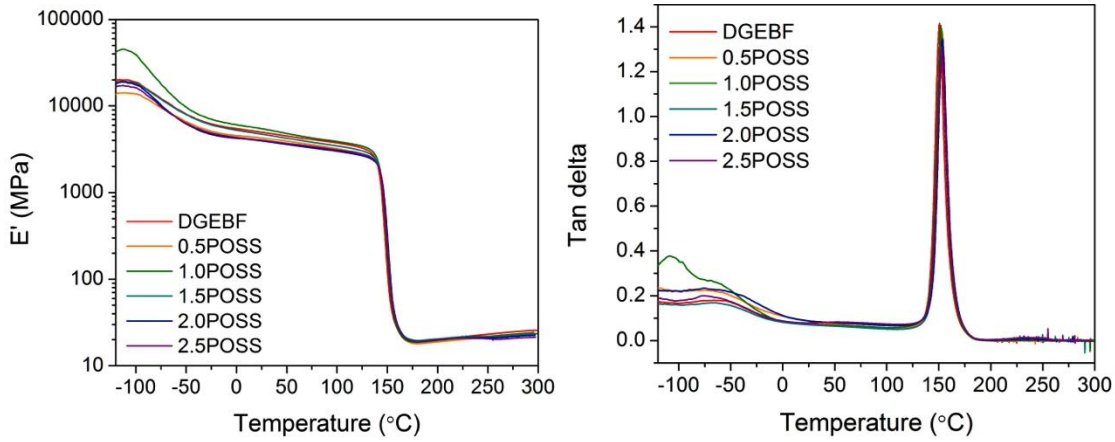

Figure 105. *E*' and tan delta vs. temperature for epoxies with unmodified POSS.

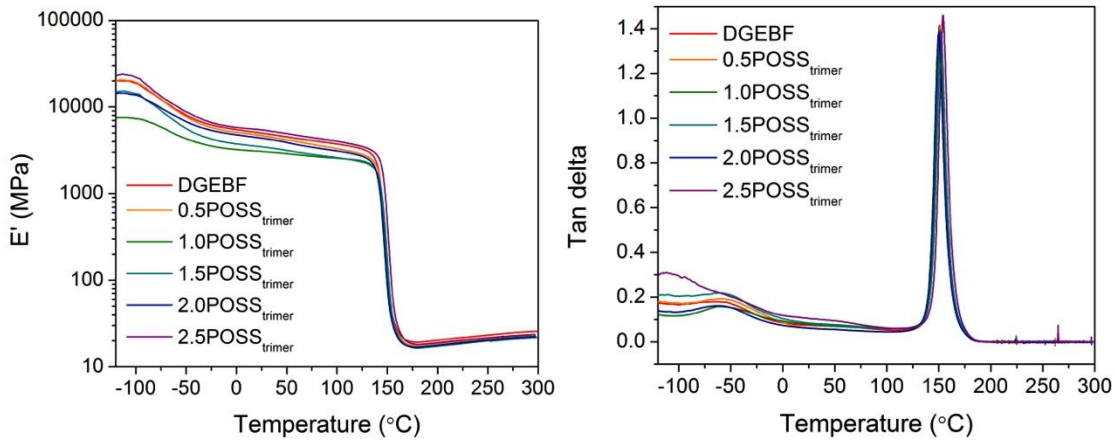

Figure 106. *E*' and tan delta vs. temperature for epoxies with $POSS_{trimer}$.

The beta and alpha transition regions of the tan delta curves for the samples containing unmodified POSS are shown in Figure 107. The beta transition was well-defined at -73 °C in DGEBF. The transition broadened the POSS-modified materials, to the extent that it was not possible to identify a peak center in most specimens. The beta transition in epoxy networks has been attributed to the motion of hydroxypropylether segments.[29,128,129] Peak broadening indicates that those segmental motions are becoming accessible at a wider range of temperatures or that new segmental motions have joined the beta relaxation process.[27,28] POSS may have broadened the beta transition by suppressing some chain motions (shift to higher temperature) and promoting others (shift to lower temperature). Further contributions to the beta peak broadening may have come from the POSS molecule itself, thanks to the aminopropyl and isopropyl groups in the organic corona. Inclusion of POSS also caused the alpha peak to increase from 151 °C for DGEBF to 153 °C for 2.5POSS. This increase was attributed to the "microfiller" effect of the POSS aggregates, which reinforced the epoxy.

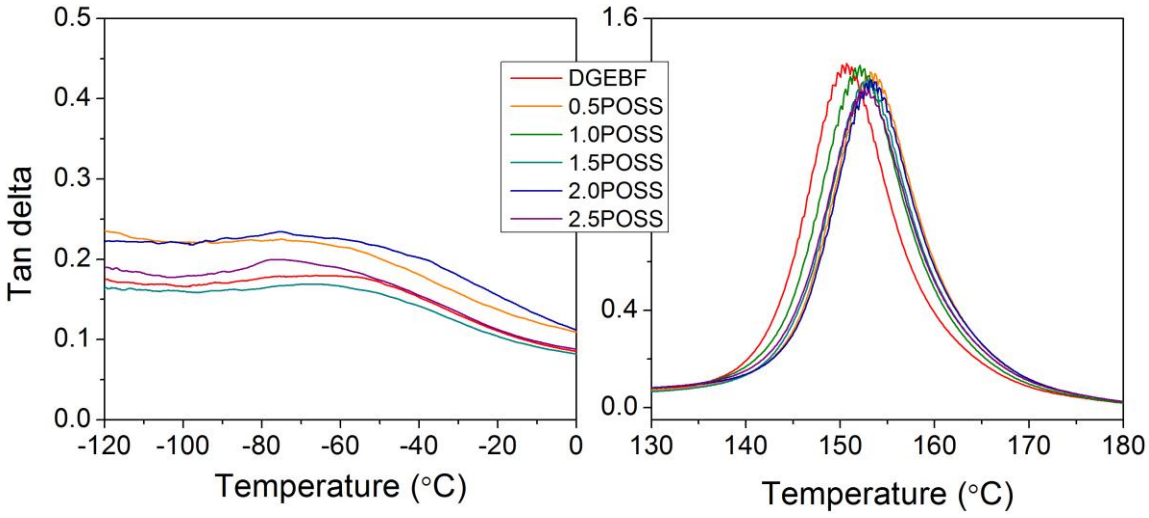

Figure 107. Tan delta vs. temperature for epoxies with unmodified POSS around the (a) beta transition and (b) alpha transition.

The effect of POSS on the beta transition was different in the epoxies modified with $POSS_{trimer}$. The peak shifted from -73 °C (DGEBF) to -60 °C ($2.0POSS_{trimer}$), but its overall shape did not change (Figure 108a). Therefore the beta peak broadening observed for the unmodified POSS epoxies must be attributed to chemical or morphological features that distinguished those samples from the $POSS_{trimer}$ epoxies. The $POSS_{trimer}$ epoxies exhibited weak aggregates and POSS-rich phases, whereas the AI-POSS epoxies were characterized by microscale crystalline agglomerations. It is possible that those agglomerations altered chain motions of epoxy segments in their vicinity, resulting in a change in shape for the beta relaxation of the systems with unmodified POSS.

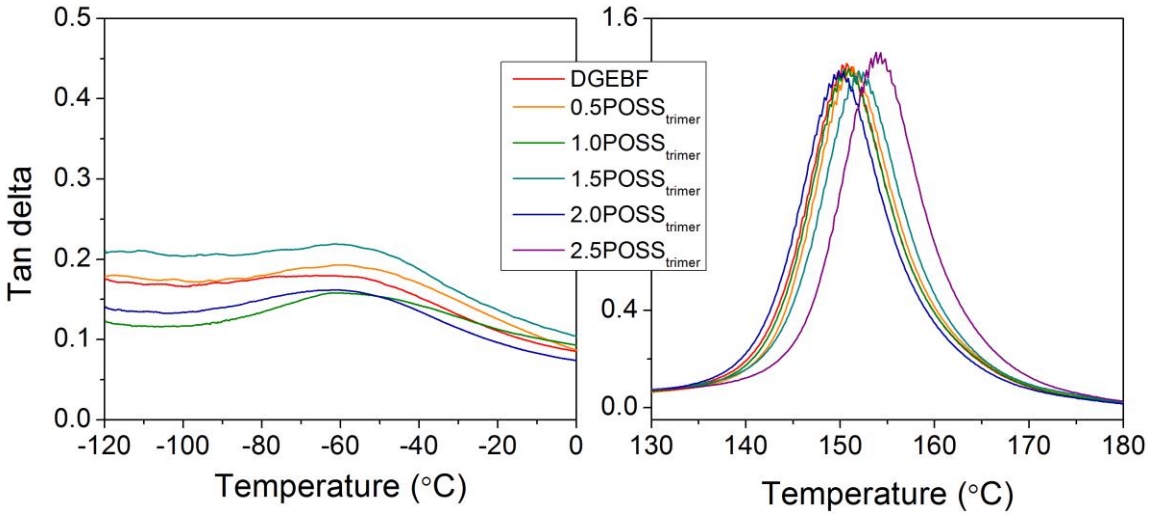

Figure 108. Tan delta vs. temperature for epoxies with $POSS_{trimer}$ around the (a) beta transition and (b) alpha transition.

The alpha relaxation was also affected by the incorporation of $POSS_{trimer}$ (Figure 108b). ThermomechanicalT_g increased from 151 °C for DGEBF to 154 °C for 2.5$POSS_{trimer}$, a similar increase to that observed for unmodified POSS. The increase was attributed to micron-scale POSS agglomerations observed for that loading level. The agglomerations acted as a reinforcing phase, shifting the alpha peak to higher temperatures.

DMA results were used to calculate crosslink density according to the well-known theory of rubber elasticity.[15] Crosslink density as a function of POSS content is shown in Figure 109 for POSS and $POSS_{trimer}$ epoxies. Theoretically crosslink density should decrease with POSS concentration, because replacing tetrafunctional DDS with difunctional AI-POSS (or its $POSS_{trimer}$ analogue) reduces the average functionality of the reactive systems. However, two distinct trends were observed for the two sets of materials. In the POSS epoxies, crosslink density initially dropped from 1704 mol m^{-3} (DGEBF) to 1593 mol m^{-3} (0.5POSS), and then began to rise again, ending at 1686 mol

m^{-3} (2.5POSS). In the $POSS_{trimer}$ epoxies, the decrease in crosslink density was greater and continued over a larger concentration regime, reaching a minimum of 1455 mol m^{-3} for 1.5$POSS_{trimer}$. After that point, crosslink density began to rise again, reaching a final value of 1601 mol m^{-3}.

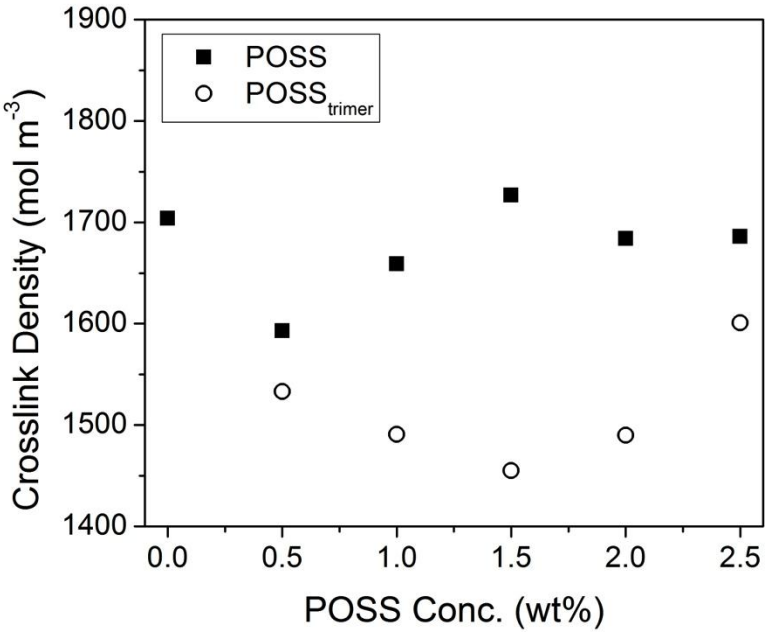

Figure 109. Crosslink density vs. POSS concentration for POSS-modified epoxies.

The different trends in crosslink density can be explained in light of the different POSS aggregation patterns in the epoxies. Crosslink density measurements reflect the extent of chemical and physical crosslinking.[86] Chemical crosslinking is a function of stoichiometry and extent of reaction in the epoxy, while physical crosslinking can develop from nonbonded interactions and reinforcing additives.[14] POSS units have been shown to act as physical crosslinks in a variety of sytems.[79,85,89,130] SEM analysis revealed different dispersion patterns for POSS and $POSS_{trimer}$, with unmodified POSS producing crystalline aggregates and $POSS_{trimer}$ producing a POSS-rich phase. For the unmodified POSS epoxies, crosslink density initially dropped because the functionality of the system

decreased. As POSS loading increased, the physical crosslinking between POSS aggregates offset the decrease in chemical crosslinking due to functionality, and the overall crosslink density increased to near-DGEBF levels.

For the $POSS_{trimer}$ epoxies, aggregates were much weaker. At low POSS loading levels, the aggregates were ill-defined and did not participate in physical crosslinking. Therefore the crosslink density of the system decreased due to decreasing average functionality. After a certain $POSS_{trimer}$ loading level (~2 weight percent) was reached, however, the $POSS_{trimer}$ moieties began to nucleate stronger, larger aggregates. These aggregates acted as physical crosslinkers, producing the increase in crosslink density measured for higher loading levels of $POSS_{trimer}$.

DSC Results

DSC analysis revealed T_g trends similar to those measured for crosslink density. The results are summarized in Figure 110. For the epoxies with unmodified POSS, T_g initially dropped from 153 °C (DGEBF) to 149 °C (0.5POSS), and then rose to ~150 °C for the next three samples. For the $POSS_{trimer}$ epoxies, T_g reached a minimum of 147 °C for 1.5$POSS_{trimer}$ and then rose. Both unmodified POSS and $POSS_{trimer}$ materials finished with a T_g of 149 °C for 2.5 weight percent POSS.

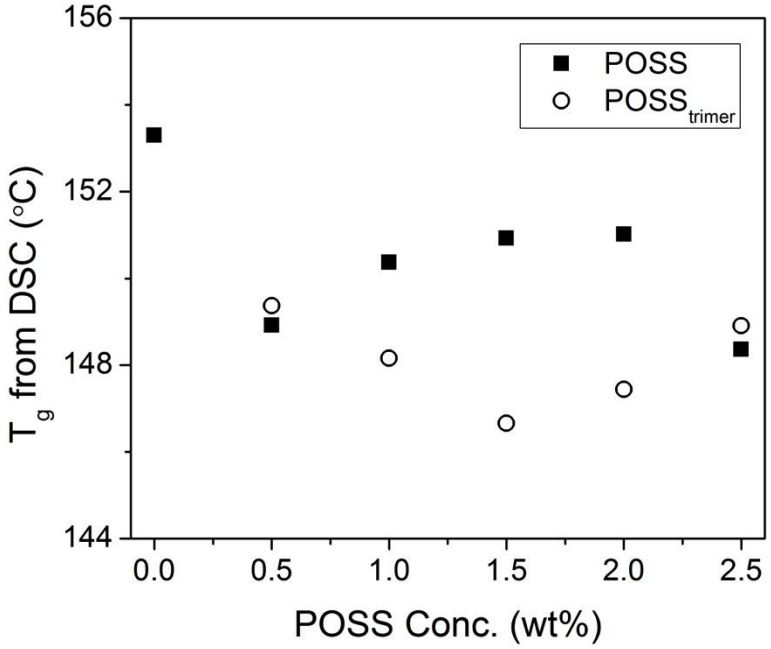

Figure 110. T_g vs. POSS concentration for POSS-modified epoxies.

These trends were explained by the same reasoning applied to crosslink density data, with the additional consideration of plasticization/reinforcing effects. The crosslink density trends reflected changes in average functionality and POSS dispersion state at different POSS concentrations. The glass transition temperature measured by DSC is a function of these factors as well as molecular-level plasticization and antiplasticization interactions. For the samples with unmodified POSS, T_g initially dropped as average functionality decreased. It is possible that plasticization of the epoxy by dispersed pendant POSS also contributed to the decrease in T_g. At higher POSS loading levels, T_g increased as a result of physical crosslinking by POSS aggregates; these aggregates may have also restricted chain motions on the molecular level, thereby delaying the onset of the glass transition. Plasticization was likely more important in the $POSS_{trimer}$ epoxies, which featured improved POSS dispersion and more pendant POSS units tethered to the epoxy network. At lower POSS concentrations, these pendants may have disrupted chain

packing and introduced new free volume, resulting in a decrease in T_g. However, $POSS_{trimer}$ began to aggregate at higher loading levels, resulting in molecular-level and microscale reinforcement and an increase in T_g.

Mechanical Testing

Mechanical properties of the POSS-modified epoxies were evaluated in compression. The stress-strain curves, shown in Figure 111, did not exhibit a substantial change in shape as a result of POSS loading. Slight sample-to-sample differences were more readily apparent in the $POSS_{trimer}$ samples than in the POSS samples. The elastic moduli, yield stresses, and yield strains of the materials are plotted in Figure 112. Clear trends were not observed for modulus or yield strain. Yield strength decreased with POSS loading for both sets of samples.

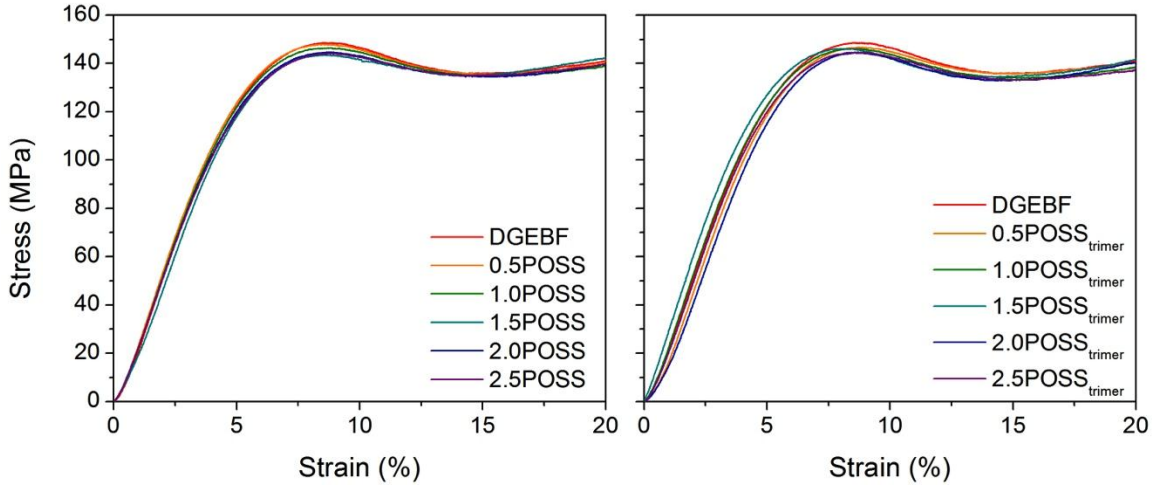

Figure 111. Stress vs. strain curves for epoxies with (a) unmodified POSS and (b) $POSS_{trimer}$.

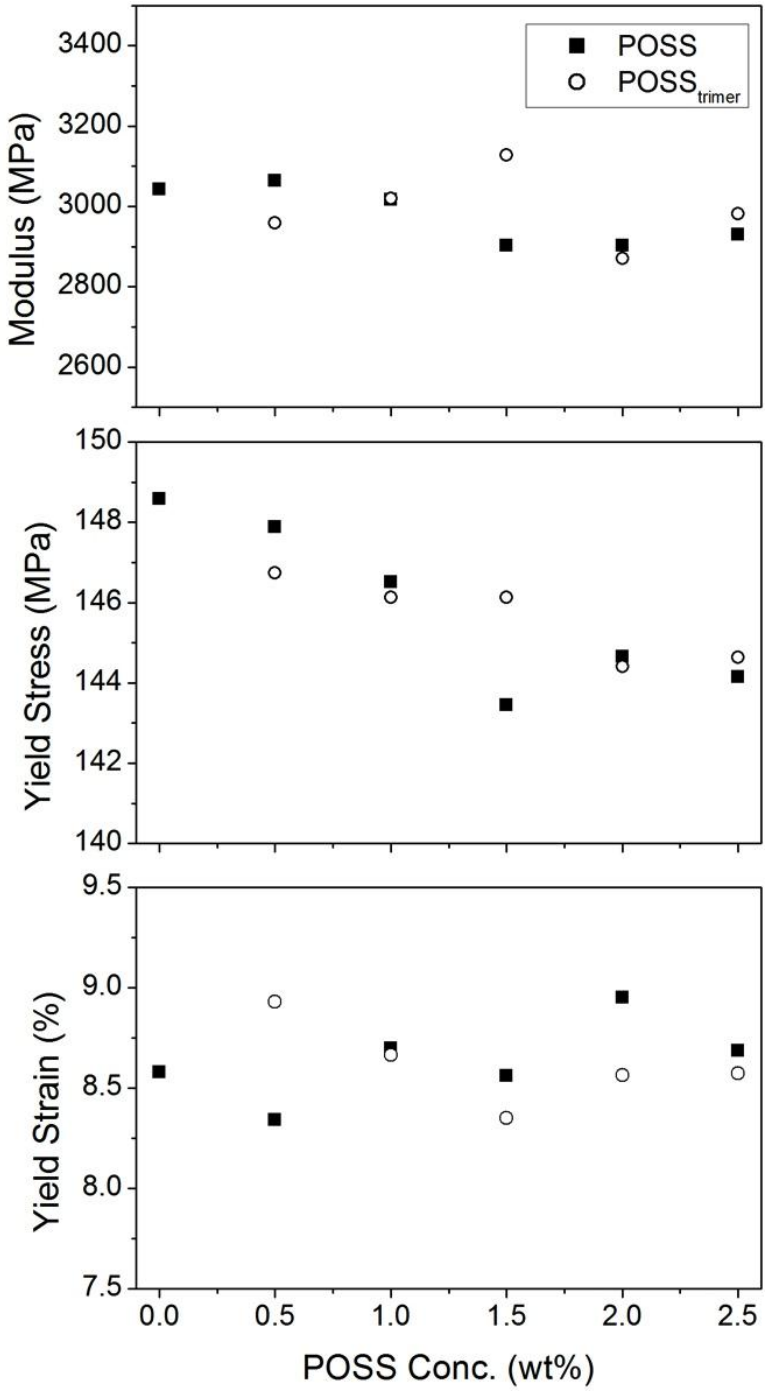

Figure 112. Modulus, yield stress, and yield strain vs. POSS concentration for POSS-modified epoxies.

Mechanical properties did not appear to relate to the morphological and microstructural trends observed via SEM and confirmed in crosslink density and T_g

measurements. The lack of correlation between those tests and mechanical properties may be related to size scale of the phenomena being measured. SEM, DMA, and DSC are techniques that probe materials at the molecular or micron-scale level. Mechanical properties are macroscale properties, and compression is a macroscale test. The compression results suggest that some factors governing stiffness and toughness in the macroscale materials are distinct from the factors governing chain motion at the molecular level. As these materials are phase-segregated, it is probable that variables such as aspect ratio and distribution of aggregates impact mechanical properties in the epoxies with unmodified POSS. Similarly, the exact arrangement and interaction of POSS-rich and epoxy-rich phases in the $POSS_{trimer}$-modified epoxies may exert more influence on mechanical properties than the angstrom-scale events discussed thus far.

SEM analysis demonstrated that using pre-reacted POSS improves researchers' abilities to control POSS dispersion and POSS-epoxy interaction on a molecular- or near-molecular level. However, the compression results indicated that the contributions of those molecular-level alternations to network architecture are overwhelmed by sample-to-sample variations in phase characteristics and distribution. Improved understanding and control of POSS-epoxy interactions at all size scales is necessary to consistently modify macroscale mechanical properties of POSS-epoxy materials.

Fluid Uptake

Fluid sensitivity, like mechanical properties, is a bulk material characteristic governed by network architecture as well as micro- and macroscale material variations. In these materials, POSS was present as a dispersed pendant group and as a microscale crystalline phase. Pendant POSS was expected to increase free volume hole size (V_h) in

the material. Increasing V_h has been shown to increase solvent and water uptake rates in epoxy systems.[16] The POSS aggregates, on the other hand, were composed of a mostly-inorganic crystalline material expected to be impervious to fluid ingress.[131] Therefore fluid ingress is expected to decrease as the relative fraction of POSS aggregates increases. These two potential effects on fluid uptake may have opposed each other in the initial stage of acetone ingress, as shown in Figure 113. At short times, acetone uptake patterns were very similar for all epoxies. This similarity may have been due to the simultaneous effects of molecular-level pendant POSS (increasing uptake) and microscale POSS aggregates (decreasing uptake). Alternatively, the POSS loading levels considered in this experiment may have been too low to impact acetone uptake rate.

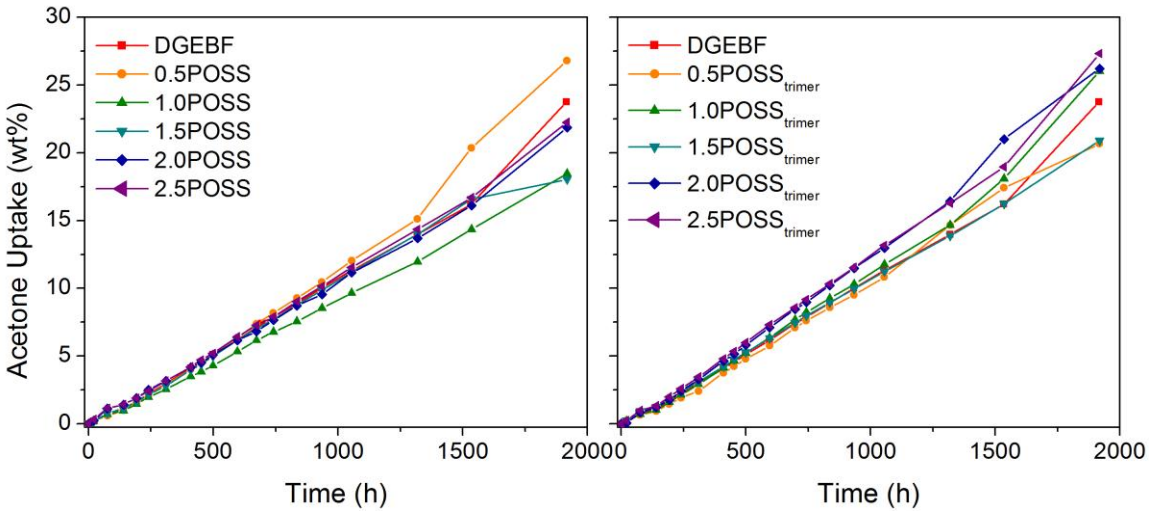

Figure 113. Acetone uptake vs. time for epoxies with (a) unmodified POSS and (b) $POSS_{trimer}$.

At ~1200 h, the acetone uptake patterns began to diverge. At the same time, cracks began to appear in the epoxy samples. Cracks increase absorption rate by providing more surface area and promoting capillary uptake of fluid.[7,132,133] Cracks develop when the osmotic pressure due to swelling exceeds the strength of the material.[63]

Defects and heterogeneities hasten crack development by providing crack initiation sites.[134,135] POSS aggregates in these samples may have promoted crack nucleation as osmotic pressure neared material strength. These results demonstrate the complex dependency of fluid uptake on multiscale material properties. The POSS aggregations did not significantly impact acetone uptake rate early in the experiment (or their contribution was negated by pendant POSS effects). However, the POSS aggregations proved detrimental to fluid resistance at longer times by providing an alternate mechanism for solvent diffusion.

Water uptake results for the POSS-modified epoxies were very similar across all samples and time scales. Equilibrium water uptake and normalized uptake are shown in Figure 114 (POSS) and Figure 115 ($POSS_{trimer}$). Equilibrium uptake did not change significantly with POSS loading level or pre-reaction state. Diffusivity, as calculated from the slope of the M_t/M_{inf} vs. $t^{1/2}$ curve, was also largely unaffected by POSS. The similarity of water uptake results for all samples is likely attributable to the dueling effects discussed above for initial acetone uptake rate. Pendant POSS was expected to increase V_h, thus increasing uptake rate and equilibrium uptake level; POSS aggregates were expected to decrease overall uptake by reducing the volume fraction of epoxy in the material. The simultaneous effect of these two mechanisms on water uptake may have resulted in uptake levels that appeared unchanged from the DGEBF-DDS benchmark. Also, the POSS loading levels may have been too low to alter water diffusion kinetics.

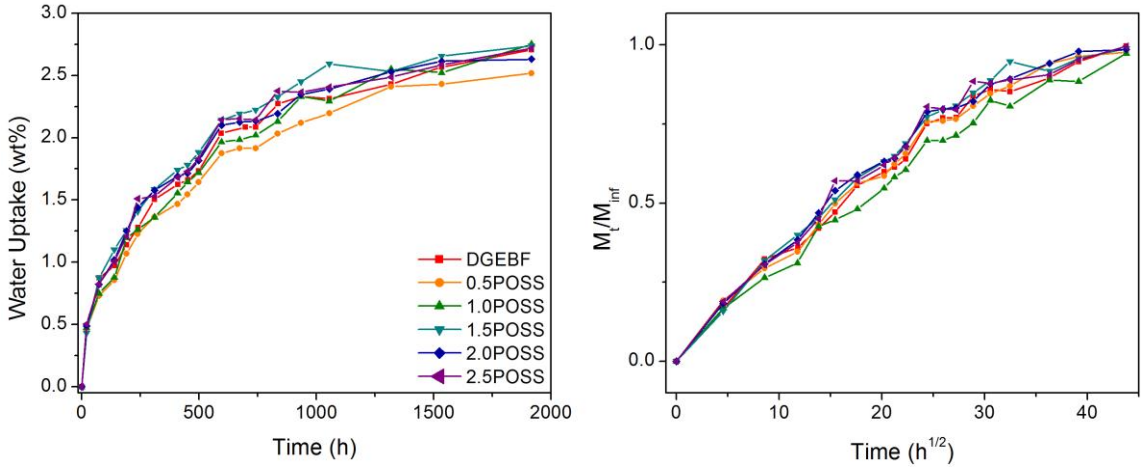

Figure 114. (a) Water uptake vs. time and (b) M_t/M_{inf} vs. $t^{1/2}$ for epoxies with unmodified POSS.

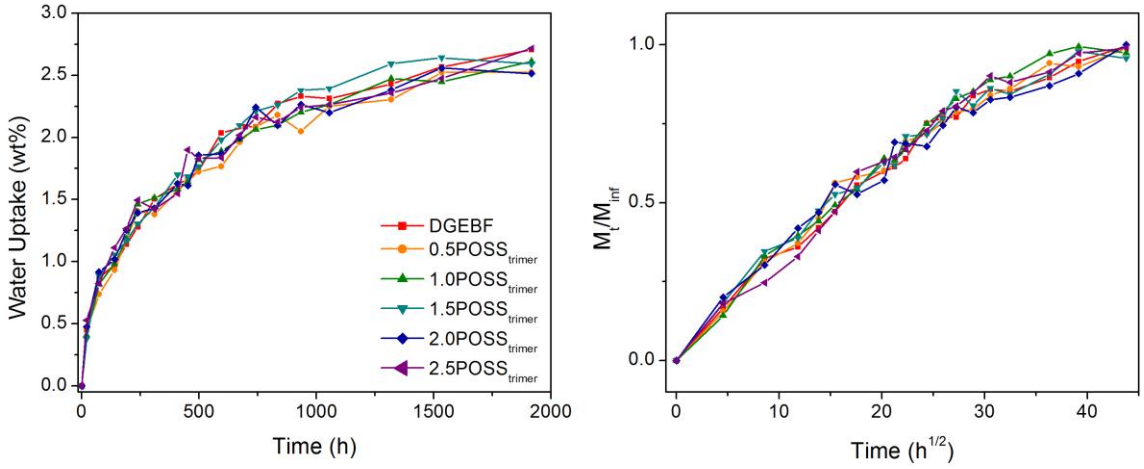

Figure 115. (a) Water uptake vs. time and (b) M_t/M_{inf} vs. $t^{1/2}$ for epoxies with $POSS_{trimer}$.

The effect of POSS on fluid uptake was overall minimal, especially at shorter times. This finding bodes well for the use of POSS-modified epoxies as a high-distortion material. If the distortional properties can be enhanced without degrading fluid resistance, then this class of materials is a strong candidate for further analysis.

Conclusions

Progress towards molecular-level dispersion of pendant POSS in epoxy networks was advanced through the use of a pre-reacted $POSS_{trimer}$ molecule. DGEBF-DDS networks were cured with unmodified POSS and $POSS_{trimer}$ in loading levels of 0.5-2.5

weight percent. SEM revealed distinct morphological trends for the two systems. The epoxies with unmodified POSS were characterized by crystalline POSS aggregations embedded in a bulk epoxy phase. As loading level increased, the number of isolate crystallites in the bulk epoxy increased as well. The epoxies with $POSS_{trimer}$ exhibited weak agglomerations. It was inferred from the structures of the reagents and the SEM images that these materials were composed of a "POSS-rich phase" with weakly aggregated POSS moieties and an "epoxy-rich phase" which also included dispersed pendant POSS tethered to the network.

DMA and DSC results both reflected changes in material properties that could be correlated to the changes in dispersion state. The beta transition broadened for the epoxies with unmodified POSS, indicating a change in molecular-level interactions with the presence of POSS aggregates. Crosslink density (from DMA) and T_g displayed the same trends. Crosslink density and T_g initially decreased and then rose slightly for unmodified POSS epoxies; those properties decreased continuously through several samples for the $POSS_{trimer}$ epoxies before rising again. For unmodified POSS, the initial drop was attributed to decreasing average functionality in the monomers, followed by a reinforcing effect from physical crosslinking of aggregates at all other POSS loadings. For epoxies with $POSS_{trimer}$, crosslink density and T_g underwent a greater decrease because strong aggregates did not form until POSS loadings of 2.0%; after aggregates began to form, crosslink density and T_g did increase. While crosslink density changes were driven by functionality and aggregation, plasticization and antiplasticization mechanisms may have contributed to the changes in T_g.

The impact of POSS incorporation on bulk material properties was examined via compression testing and fluid uptake studies. No overriding trends were apparent in the compression data. The lack of correlation indicated that the molecular-level and microscale effects of POSS on the epoxy network were insignificant compared to macroscale variations in dispersion state, which were neither well understood nor well controlled. For fluid uptake results, the competing effects of pendant POSS and POSS aggregates may have negated each other, resulting in little-to-no change in fluid uptake at shorter times. At longer times, POSS-modified samples soaked in acetone began to crack because the POSS aggregates acted as crack initiation sites.

REFERENCES

[1]Roeseler, B.; Sarh, B.; Kismarton, M. Presented at the 16th International Conference on Composite Materials, Kyoto, July 8-13, 2007.

[2]Niu, M. C. *Composite Airframe Structures*; Conmilit Press: Hong Kong, 1996.

[3]Jang, B. Z. *Advanced Polymer Composites: Principles and Applications*; ASM International: Materials Park, OH, 1994.

[4] Argon, A. S.; Cohen, R. E. *Polymer.* **2003**, *44* (19), 6013-6032.

[5]Tsai, S. W.; Townsley, J. L. In *Proceedings of the 35th International SAMPE Technical Conference*, Dayton, OH, Sept. 28-Oct. 2, 2003.

[6] Chui, C.; Boyce, M. C. *Macromolecules.***1999**, *32* (11), 3795-3808.

[7]Weitsman, Y. J.; Guo, Y. J. *Compos. Sci. Technol.* **2002**, *62*(6), 889-908.

[8]Nogueira, P.; Ramirez ,C.; Torres, A.; Abad, M. J.; Cano, J.; Lopez, J.; Lopez-Bueno, I.; Barral, L. *J. Appl. Polym. Sci*. **2001**, *80* (1), 71-80.

[9]Hinkley, J. A.; Connell, J. W. Resin systems and chemistry: degradation mechanisms and durability. In *Long-term Durability of Polymeric Matrix Composites*; Pochiraji, K.V.; Tandon, G. P., Schoepp.ner, G. A., Eds.; Springer: New York, 2012; pp. 1-38.

[10] Jackson, M. B. Effects of molecular architecture on fluid ingress behavior of glassy polymer networks. Ph.D. Dissertation, University of Southern Mississipp.i, Hattiesburg, MS, 2011.

[11] http://www.merriam-webster.com (accessed Sept. 24, 2012).

[12] Meyer, F.; Sanz, G.; Eceiza, A.; Mondragon, I. *Polymer.* **1995**, *36* (7), 1407-1414.

[13]Sohn, D. W.; Ko, K. J.*Korea Polym. J.* **1999**, *7* (3), 181-188.

[14]Odian, G. *Principles of Polymerization*, 4th ed.; John Wiley & Sons: New York, 2004; pp. 39-197.

[15]Hiemenz, P. C.; Lodge, T. P. *Polymer Chemistry*, 2nd ed.; CRC Press: Boca Raton, 2007.

[16] Jackson, M.; Kaushik, M.; Nazarekno, S.; Ward, S.; Maskell, R.; Wiggins, J. *Polymer.* **2011**, *52*, 4528-4535.

[17]Bellenger, V.; Fontaine, E.; Fleishmann, A.; Saporito, J.; Verdu, J. *Polym. Degrad. Stabil*. **1984**, *9* (4), 195-208.

[18] Li, G.; Zhang, C.; Wang, Y.; Li, P.; Yu, Y.; Jia, X.; Liu, H.; Yang, X.; Xue, Z.; Ryu, S. *Compos. Sci. Tech.* **2008**, *68* (15), 3208-3214.

[19]Bellenger, V.; Dhaoui, W.; Morel, E.; Verdu, J. *J. Appl. Polym. Sci.* **1988**, *35* (3), 563-571.

[20]Grillet, A. C.; Galy, J.; Gerard, J. F.; Pascault, J. P. *Polymer.* **1991**, *32* (10), 1885-1891.

[21]Stutz, H.; Mertes, J. *Polym. Eng. Sci.* **1993**, *31* (8), 2031-2037.

[22]Urbaczewski-Espuche, E.; Galy, J.; Gerard, J. F.; Pascault, J. P.; Sautereau, H. *Polym. Eng. Sci.* **1991**, *31* (22), 1572-1580.

[23] Heinz, S.; Wiggins, J. Presented at the 42nd International SAMPE Technical Conference, Salt Lake City, UT, Oct. 11-14, 2010.

[24]Jeffrey, K.; Pethrick, R. A. *Eur. Polym. J.* **1994**, *30* (2), 153-158.

[25]Varley, R. J.; Lui, W.; Simon, G. P. *J. Appl. Polym. Sci.* **2006**, *99* (6), 3288-3299.

[26]Guenthner, A. J.; Reams, J. T.; Lamison, K. R.; Cambrea, L. R.; Vij, V.; Mabry, J. M. Presented at the 43rd International SAMPE Technical Conference, Ft. Worth, TX, Oct. 17-20, 2011.

[27]Ueberreiter, K.; Kanig, G. *J. Chem. Phys.* **1950**, *18* (4), 399-408.

[28] Mason, P. *Polymer.* **1964**, *5*, 625-635.

[29]Halary, J. L. *High Perform. Polym.* **2000**, *12* (1), 141-153.

[30]VanLandingham, V. R.; Eduljee, R. F. *J. Appl. Polym. Sci.* **1999**, *71*, 699-712

[31]Grave, C.; McEwan, I.; Pethrick, R. A.*J. Appl. Polym. Sci.* **1998**, *69*, 2369-2375.

[32]VanLandingham, V. R.; Eduljee, R. F.; Gillespie, J. W. *J. Appl. Polym. Sci.* **1999**, *71*, 787-798.

[33] Girard-Reydet, E.; Riccardi, C. C.; Sautereau, H.; Pascault, J. P. *Macromolecules.* **1995**, *28* (23), 7599-7607.

[34]Matejka, L. *Macromolecules.* **2000**, *33*, 3611-3619.

[35]Liu, H.; Uhlherr, A.; Varley, R. J.; Bannister, M. K. *J. Polym. Sci. Pol. Chem.* **2004**, *42*, 3143-3156.

[36] Min, B. G.; Stachurksi, Z. H.; Hodgkin, J. H.; Heath, G. R. *Polymer.* **1993**, *34* (17), 3620-3627.

[37]Xu, L.; Fu, J. H.; Schlup, J. R. *Ind. Eng. Chem. Res.* **1996**, *35* (3), 963-972.

[38]Sahagun, C. Molecular network development of a thermosetting epoxy-amine polymer. Ph.D. Dissertation, University of Southern Mississipp.i, Hattiesburg, MS, 2012.

[39]Sbirrazzuoli, N.; Mititelu-Mija, A.; Vincent, L.; Alzina, C. *Thermochim.Acta.* **2006**, *447*, 167-177.

[40]Mijovic, J.; Andjelic, S.; Yee, W. C. F.; Belluci, F.; Nicolais, L. *Macromolecules.* **1995**, *28* (8), 2797-2806.

[41]Mijovic, J.; Andjelic, S.; Fitz, B.; Zurawsky, W.; Mondragon, I.; Belluci, F.; Nicolais, L. *J. Pol. Sci. Pol. Chem.* **1996**, *34*, 379-388.

[42]Mijovic, J. *J. Non-Cryst.Solids.* **1998**, *235-237*, 587-9595.

[43]Eloundou, J. P. *Polymer.* **2002**, *38* (3), 431-438.

[44]Chen, J.; Hojjati, M. *Polym. Eng. Sci.* **2007**, *47* (2), 150-158.

[45]Vyazovkin, S.; Sbirrazuoli, N. *Macromol. Rapid Comm.* **2006**, *27* (18), 1515-1532.

[46]Kandelbauer, A.; Wuzella, G.; Mahendran, A.; Taudes, I.; Widsten, P. *Chem. Eng. J.* **2009**, *152*, 556-565.

[47]Hao, W.; Hu, J.; Chen, L.; Zhang, J.; Xing, L.; Yang, W. *Polym. Testing,* **2011**, *30* (4), 349-355.

[48] Christensen, S. Boeing Research & Technology, The Boeing Company, Seattle, WA. Personal communication, Sept. 2012.

[49]Jonquières, A.; Roizard, D.; Lochon, P. *J. Appl. Polym.Sci.* **1994**, *54*(11), 1673–1684.

[50]Alfrey, T.; Gurnee, E. F.; Lloyd, W. G. *J. Polym. Sci. Pol. Sym.* **1966**, *12*(1), 249-261.

[51]Chin, J. W.; Nguyen, T.; Aouadi, K. *J. Appl. Polym. Sci.* **1998**, *71* (3), 483-492.

[52]Crank, J.*The Mathematics of Diffusion*, 2nd ed.; Clarendon Press: Oxford, 1975.

[53] Soles, C. L.; Chang, F. T.; Bolan, B. A.; Hristov, H. A.; Gidley, D. W.; Yee, A. F. *J. Polym. Sci. Pol. Phys.* **1998**, *36*, 3035-3048.

[54]Mijovic, J.; Zhang, H. *Macromolecules.* **2003**, *36* (4), 1279-1288.

[55]Popineau, S.; Rondeau-Mouro, C.; Sulpice-Gaillet, C.; Shanahan, M. E. R. *Polymer* **2005**, *46* (24), 10733-10740.

[56] Zhou, J.; Lucas, J. P. *Polymer.* **1999**, *40* (20), 5505-5512.

[57]Pethrick, R. A.; Hollins, E. A.; McEwan, I.; Pollock E. A.; Hayward, D. *Polymer.* **1996**, *39*, 275-288.

[58]Mijovic, J.; Zhang, H. *J. Phys. Chem. B.* **2004**, *108* (8), 2557-2563.

[59]Wong, T. C.; Broutman, L. J. *Polym. Eng. Sci.* **1985**, *25* (9), 521-528.

[60]Soles, C. L.; Yee, A. F. *J. Polym. Sci. Pol. Phys.* **2000**, *38*, 792-802.

[61]Diamant, Y.; Marom, G.; Broutman, L. J. *J. Appl. Polym. Sci.* **1981**, *26*, 3015-3025.

[62] Zhou, J.; Lucas, J. P. *Polymer.* **1999**, *40* (20), 5513-5522.

[63] Thomas, N. L.; Windle, A. H. *Polymer.* **1981,** *22* (5), 627-639.

[64]Sahlin, J. J.; Pepp.as, N. A. *Ind. Eng. Chem. Res.* **1991**, *30* (1), 211-217.

[65]Crank, J. *J. Polym. Sci.* **1953**, *11* (2), 151-168.

[66]Liu, H.; Li, J.; Hu, Y. *Fluid Phase Equilbr.* **1999**, *158-160* (1), 1035-1044.

[67]Thomas, N. L.; Windle, A. H. *Polymer.* **1982**, *23* (4), 529-542.

[68]Gall, T. P.; Lasky, R. C.; Kramer, E. J. *Polymer.* **1990**, *31* (8), 1491-1499.

[69]Hui, C. Y.; Wu, K. C.; Lasky, R. C.; Kramer, E. J. *J. Appl. Phys.* **1987**, *61* (11), 5129-5137.

[70] Ramesh, N.; Davis, K. P.; Zielinski, J. M.; Danner, R. P.; Duda, J. L. *J. Polym. Sci. Pol. Phys.* **2011**, *49* (23), 1629-1644.

[71]Tricklebank, S. B.; Nanis, L.; Bockris, J. *J. Phys. Chem.* **1964**, *68* (1), 58-63.

[72]Shantarovich, V. P.; Kevdina, I. B.; Yampolskii, Y. P.; Alentiev, A. Y. *Macromolecules.* **2000**, *33* (20), 7453-7466.

[73]Matejka, L.; Strachota, A.; Plestil, J.; Whelan, P.; Steinhart, M.; Slouf, M. *Macromolecules.* **2004**, *37*(25), 9449–9456.

[74]Strachota, A,; Kroutilova, I.; Kovarova, J.; Matejka, L. *Macromolecules.* **2004**, *37* (25), 9457–9464.

[75]Constantin, F.; Garea, S. A.; Sandu, T.; Horia, I. *Int. J. Polym. Anal. Ch.* **2010**, *15*(2), 119-128.

[76]Ni, Y.; Zheng, S.; Nie, K. *Polymer.* **2004**, *45*(16), 5557-5568.

[77]Liu, Y.; Zheng, S.; Nie, K. *Polymer.* **2005**, *46*(25), 12016-12025.

[78]Wang, Y. Z.; Tsai, H. S.; Ji, Z. Y.; Chen, W. Y. *J. Mater. Sci.* **2007**, *42*(17), 7611-7616.

[79]Bocek, J.; Matejka, L.; Mentlik, V.; Trnka, P.; Slouf, M. *Eur. Polym. J.* **2011**, *47*(5), 861-872.

[80]Liu, Y. L.; Chang, G. P.; Hsu, K. Y.; Chang, F. C. *J. Polym. Sci. Pol. Chem.* **2006**, *44*(12), 3825-3835.

[81]Lee, A.; Lichtenhan, J. D. *Macromolecules.* **1998**, *31*(15), 4970-4974.

[82]Xu, Y.; Ma, Y.; Deng, Y.; Yang, C.; Chen, J.; Dai, L. *Mater. Chem. Phys.* **2011**, 125(1), 174-183.

[83]Liu, Y. L.; Chang, G. P. *J. Polym. Sci. Pol. Chem.* **2006**, *44*(6), 1869-1876.

[84]Zucchi, I. A.; Galante, M. J.; Williams, R. J. J.; Franchini, E.; Galy, J.; Gerard, J. F. *Macromolecules.* **2007**, *40*(4), 1274-1282.

[85]Matejka, L.; Murias, P.; Plestil, J. *Eur. Polym. J.* **2012**, *48* (2), 260-274.

[86]Strachota, A.; Whelan, P.; Kriz, J.; Brus, J.; Urbanova, M.; Slouf, M.; Matejka, L. *Polymer.* **2007**, *48*, 3041-3058.

[87]Sanchez-Soto, M.; Schiraldi, D. A.; Illescas, S. *Eur. Polym. J.* **2009**, *45* (2), 341-352.

[88]Iyer, S.; Schiraldi, D. A. *Macromolecules.* **2007**, *40* (14), 4942-4952.

[89]Perrin, F. X.; Chaoui, N.; Margaillan, A. *Thermochim.Acta.* **2009**, *491*, 97-102.

[90]Guenthner, A.; Lamison, K.; Lubin, L.; Mabry, J. Presented at the 243rd ACS National Meeting, San Diego, CA, March 25-29, 2012.

[91]Milliman, H. W.; Boris, D.; Schiraldi, D. A. *Macromolecules.* **2012**, *45* (4), 1931-1936.

[92]Yaping, Z.; Aibo, Z.; Qinghua, C.; Jiaoxia, Z.; Rongchang, N. *Mater. Sci. Eng. A.* **2006**, *435-436,* 145-49.

[93]Cho, J.; Daniel, I. M.; Dikin, D. A. *Compos. Part A-Appl. Sci.* **2008**, *39*, 1844-50.

[94]Handge, U. A.; Hedicke-Hochstotter, K.; Alstadt, V. *Polymer.* **2010**, *51* (12), 2690-2699.

[95]Kourkoutsaki, T.; Logakis, E.; Kroutilova, I.; Matejka, L.; Nedbal, J.; Pissis, P. *J. Appl. Polym. Sci.* **2009**, *113* (4), 2569-2582.

[96]Gnanasekaran, D.; Madhavan, K.; Reddy, B. S. R. *J. Sci. Ind. Res.* **2009**, *68*, 437-464.

[97]Phillips, S. H.; Haddad, T. S.; Tomczak, S. J. *Current Opin. Solid St. M.* **2004**, *8*, 21-29.

[98] Lee, K. M.; Knight, P. T.; Chung, T.; Mather, P. T. *Macromolecules.* **2008**, *41* (13), 4730-4738.

[99]Tao, S. J. *J. Chem. Phys.***1972**, *56* (11), 5499.

[100]Eldrup, M.; Lightbody, D.; Sherwood, J. N. *Chem. Phys.***1981**, *63* (1), 51-58.

[101]Zoller, P.; Walsh, C. J. *Standard pressure-volume-temperature data for polymers*. Lancaster: Technomic, 1995.

[102]Simha, R.; Somcynski, T. *Macromolecules***1969**, *2* (4), 342-350.

[103]Utracki, L.; Simha, R. *Macromol. Theor. Simul.* **2001**, *10* (1), 17-24.

[104]Dlubek, G.; Pionteck, M.; Hassan, E. M.; Krause-Rehberg, R. *J. Polym. Sci. Pol. Phys.* **2007**, *45* (18), 2519-2534.

[105]Dyakonov, T.; Mann, P. J.; Chen, Y.; Stevenson, W. T. K. *Polym. Degrad. Stabil.* **1996**, *54* (1), 67-83.

[106]Budrugeac, P.; Segal, E. *Polym. Degrad. Stabil.* **2008**, *93* (6), 1073-1080.

[107]Kao, K. C. *Dielectric Phenomena in Solids.* Elsevier: Amsterdam, 2004; pp. 1-40.

[108]Hedvig, P. *Dielectric Spectroscopy of Polymers*. John Wiley & Sons: New York, 1977; pp. 13-68.

[109]Vassilikou-Dova, A.; Kalogeras, I. M. Dielectric Analysis (DEA). In *Thermal Analysis of Polymers*; Menczel, J. D.; Prime, R. B., Eds.; John Wiley & Sons: New York, 2009; pp. 497-614.

[110]Hedvig, P. *Dielectric Spectroscopy of Polymers*. John Wiley & Sons: New York, 1977; pp. 312-355.

[111] Fournier, J.; Williams, G.; Duch, C.; Aldrige, G. A. *Macromolecules.* **1996**, *29* (22), 7097-7107.

[112]Eloundou, J. P.; Gerard, J. F.; Pascault, J. P.; Boiteux, G.; Seytre, G. *Angew. Makromol. Chem.* **1998**, *263*, 57-70.

[113]Mangion, M. B. M.; Johari, G. P. *J. Polym. Sci. Pol. Phys.* **1991**, *29* (9), 1127-1135.

[114]Vyazovkin, S.; Sbirrazzuoli, N. *Macromolecules.* **1996**, *29* (6), 1867-1873.

[115]Safarpour, M. A.; Omrani, A.; Afsra, S.; Zare-Hossein-Abadi, D. *Polym. Adv. Tech.***2011**, *22* (5), 718-723.

[116]Lee, J. Y.; Shim, M. J.; Kim, S. W. *Thermchim. Acta.* **2001**, *371*, 45-51.

[117] Cole, K. C. *Macromolecules.* **1991**, *24* (11), 3093-3097.

[118] Wise, C. W.; Cook, W. D.; Goodwin, A. A. *Polymer.* **1997**, *38* (13), 3251-3261.

[119]Altaweel, A. M. A. M.; Ravikumar, H. B.; Ranganathaiah, C. *Phys. Status Solidi. C.* **2009,** *6* (11), 2401-2403.

[120]Loos AC, Springer GS. *Environmental effects on composite materials*. Technomic: Westport, 1981.

[121]Wu, L.; Hoa, S. V.; Ton-That, M. *J. Appl. Polym. Sci.* **2006**, *99*, 580-588.

[122] Frank, K.; Childers, C.; Dutta, D.; Gidley, D.; Jackson, M.; Ward, S.; Maskell, R.; Wiggins, J. *Polymer.* **2012**, accepted for publication.

[123]Nicolais, L.; Drioli, E.; Hopfenberg, H. B.; Tidone, D. *Polymer.* **1977**, *18* (11), 1137-1142.

[124]Ercken, M.; Adriaensens, P.; Reggers, G.; Carleer, R.; Vanderzande, D.; Gelan, J. *Macromolecules.* **1996**, *29* (17), 5671-5677.

[125]Doppers, L. M.; Sammonm, C.; Breen, C.; Yarwood, J. *Polymer.* **2006**, *47* (8), 2714-2722.

[126] Frank, K. L.; Exley, S. E.; Thornell, T. L.; Morgan, S. E.; Wiggins, J. S. *Polymer.* **2012**, *53* (21), 4643-4651.

[127]Wetzel, B.; Rosso, P.; Haupert, F.; Friedrich, K. *Eng. Frac. Mech.* **2006**, *73*, 2375-2398.

[128]Heux, L.; Halary, J. L.; Laupretre, F.; Monnerie, L. *Polymer.* **1997**, *38* (8), 1737-1778.

[129]Chateauminois, A.; Sauvant, V.; Halary, J. L. *Polymer Int.* **2003**, *52*, 507-513.

[130]Strachota, A.; Kroutilova, I.; Kovarova, J.; Matejka, L. *Macromolecules.* **2004**, *37* (25), 9457-9464.

[131] Lee, W. E. *Ceramic Microstructures*, Chapman & Hall: London, 1994; pp. 67-123.

[132]Weitsman, Y. J. *Compos. Part A-App. S.* **2006**, *37* (4), 617-623.

[133]Weitsman, Y. J. *Fluid Effects in Polymers and Composites*, Springer: New York, 2012: pp. 13-28.

[134] Miller, E. *Introduction to Plastics and Composites*. Marcel Dekker: New York, 1996; pp. 250-314.

[135]Callister, W. D. *Fundamentals of Materials Science and Engineering*, 2nd ed., John Wiley & Sons: New York, 2005; pp. 282-356.